Partialdehydrierung von Ethylbenzol zu Styrol an Kohlenstoffmaterialien

Vorgelegt von
Diplom-Ingenieur
Maximova, Nadejda
aus Russland

Von der Fakultät II - Mathematik und Naturwissenschaften
Institut für Chemie
Der Technischen Universität Berlin
Zur Erlangung des akademischen Grades
Doktor der Ingenieurwissenschaften
Dr. Ing.
genehmigte Dissertation

Promotionsausschuß:
Vorsitzender: Prof. Dr. M. Lerch
Berichter: Prof. Dr. R.Schlögl
Berichter: Prof. Dr. R. Schomäcker

Tag der wissenschaftlichen Aussprache: 20. Dezember 2002

Berlin 2002

D 83

Contents

Contents……..3

Chapter 1. Introduction……...5

1.1. Industrial Styrene Production from Ethylbenzene over Potassium Promoted Iron Oxide Catalyst…….5

1.2. Alternative Styrene Production Processes……..8

1.3. Oxidative Dehydrogenation of Ethylbenzene to Styrene with Carbon Materials as Catalysts…….…..….10

1.4. Carbon Materials as Catalysts……..….11

Chapter 2. Experimental Methods……..….15

2.1. Set-up for the Reaction Performance……16

2.2. Characterization Techniques…….21

2.2.1. Microscopic Methods (TEM, SEM)……21

2.2.2. Spectroscopic Methods (XPS, EDX, Raman- and IR-spectroscopy)……..22

2.2.3. Additional Methods (XRD, TG/DTA, BET surface area)……..24

Chapter 3. Experimental Design with Response Surface Model……...……26

Chapter 4. Oxidative Dehydrogenation of Ethylbenzene to Styrene over Carbon Materials: Catalytic Study and Characterization…….……41

4.1. Carbon Black, Graphite and Nanofilaments…….41

4.2. Nanotubes and Nanofilaments……..52

4.3. Onion-Like Carbon……...……67

4.4. Ultra-Dispersed Diamond……77

4.4.1. Catalytic activity of sp^3-hybridized carbon in ODH of EB to ST……..…77

4.4.2. Experiments with OLC and UDD samples pretreated in helium, hydrogen and oxygen ……85

Chapter 5. Reaction Mechanism and Kinetics of the Oxidative Dehydrogenation of Ethylbenzene to Styrene……...…..…94

5.1. Surface Functional Groups……94

5.2. Reaction Kinetics…….……..99

5.3. Model of the Reaction Mechanism……..……105

Conclusions…….…….…114

Appendix:…….……..117

Abbreviations:……..117

Kurzzusammenfassung:……..…..…….…..119

Danksagung:…….…….120

Lebenslauf:…….……...120

Publikationsliste:…….…..……...121

1. Introduction

Heterogeneous catalysis plays an important role not only in the modern chemical industry, but also in car manufacturing and food industries. A fundamental understanding of the reaction mechanisms in selective catalytic reactions, *i.e.* catalytic oxidation, hydrogenation, dehydrogenation of aliphatic and aromatic hydrocarbons, directly affects the development of chemical processes and catalysts. The interest in the development of chemical processes and catalysts is stimulated by the high economical profit, which can be reached.

1.1. Industrial Styrene Production Processes

Styrene (ST) is used as a starting monomer for polystyrene, ABA resin, and synthetic rubber manufacturing. Nowadays, the production of ST monomer from ethylbenzene (EB) is one of the ten largest production processes in the chemical industry. Recently, the annual styrene production reached 23 mio tons per year [1]. Figure 1.1 shows the reaction (1) of the direct dehydrogenation (DH) of EB to ST performed in industry [2].

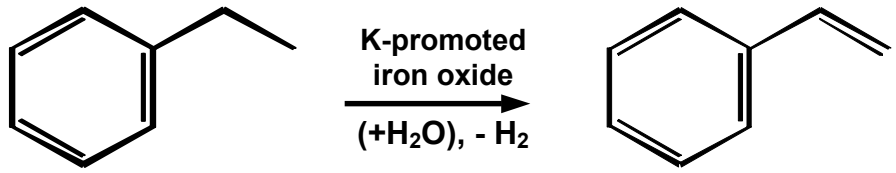

(1.1)

Fig. 1.1. Synthesis of styrene

The process is realized at high temperatures between 600 and 700°C mainly at atmospheric pressure with an excess of overheated (~700°C) steam, *i.e.* the steam to EB ratio is 10:1. It is catalysed by a hematite catalyst promoted mainly by potassium

(10%) and other compounds (Al_2O_3, Cr_2O_3, V, Ce, W, Mo), which increase the catalyst selectivity and enhance the stability of the catalyst structure [3]. The DH reaction of EB to ST is equilibrium limited and strongly endothermic (ΔH=129.4 kJ/mol). It can be run either adiabatically or isothermally over a fixed bed reactor, in which the reactants are passed over the catalyst bed employing radial or axial flow. The industrial process is highly energy consuming because of the excess of steam used and the endothermic reaction. The application of steam in the process is proposed to (i) shift the equilibrium of the reaction, (ii) limit the build up of the carbonaceous deposits by their gasification, and (iii) keep the iron oxide in an appropriate oxidation state [4] by diminishing the partial pressures of the products. Still, side reactions, mainly benzene (1%) and toluene (2%) formations (Eq. 2 and 3, respectively), also take place in the presence of water [5]:

$$C_6H_5C_2H_5 \longrightarrow C_6H_6 + C_2H_4 \quad (1.2)$$

$$C_6H_5C_2H_5 + H_2 \longrightarrow C_6H_5CH_3 + CH_4 \quad (1.3)$$

Water molecules from steam react with ethene formed according to (Eq. 1.2) and methane formed according to (Eq. 1.3) to yield CO and H_2:

$$2H_2O+C_2H_4 \longrightarrow 2CO+4H_2 \quad (1.4)$$

$$H_2O+CH_4 \rightarrow CO+3H_2 \quad (1.5)$$

CO also reacts with H_2O from steam under the formation of CO_2 and H_2:

$$CO + H_2O \longrightarrow CO_2+H_2 \quad (1.6)$$

Steam also reacts with coke deposits via gasification to yield CO and H_2:

$$C + H_2O \longrightarrow CO + H_2 \quad (1.7)$$

The reversibility of the dehydrogenation process thermodynamically hinders maximum yields of ST. The technical EB conversion is limited below 60% to keep an acceptable high selectivity to ST. The limited ST yields and the low EB conversions achieved per pass through the reactor lead to the necessity of a reactant recycle.

For ST polymerisation applications, ST has to be purified to more than 99.8%. The separation of non-reacted EB and co-products from ST is costly due to the close boiling points, especially for EB and ST, with 136° and 145°C, respectively.

The K-Fe catalyst slowly deactivates with operation and typically needs to be replaced every 1-2 year. In view of the scale of the reactors used, this is an expensive operation and, consequently, much research has been dedicated to understand and prevent the deactivation mechanisms involved. From a survey of the literature, four reasons for deactivation are generally brought forward, *i.e.* build up of carbonaceous deposits, loss or redistribution of the potassium promoter, change in oxidation state of the Fe-oxide, and physical degradation of catalyst. Many of these features are interrelated and take place concurrently. In summary, the deactivation of the potassium promoted iron oxide catalyst is a very complex process.

A steady state layer of coke is always present during typical styrene synthesis conditions [6]. Coke gasification is in equilibrium with coke build up [7]. Menon [8] has classified coke on catalysts into four general types: harmful, harmless, invisible and beneficial. Coke is certainly not only a deactivating black layer. The exact role of coke on catalyst surfaces in itself is still controversial.

The number of problems of the styrene production via dehydrogenation of EB in the presence of steam leads to the strong incentive to develop alternative technologies.

1.2. Alternative Styrene Production Processes

To overcome the above mentioned drawbacks of DH of EB in the presence of steam some alternative routs were proposed. The equilibrium of the DH of EB can be shifted to ST formation using an oxidizing agent reacting selectively with hydrogen. Oxidative dehydrogenation (ODH) produces water rather than hydrogen and as a result the reaction is exothermic [9]. Several alternative processes have been proposed:

- Oxidative dehydrogenation in the presence of oxygen

$$C_6H_5CH_2CH_3 + ½\ O_2 \rightleftharpoons C_6H_5CH = CH_2 + H_2O, \quad (1.8)$$

which allows one to realize an exothermic reaction (ΔH^0_{298} = -116 kJ/mol) and to operate at low temperatures, but the partial combustion of the hydrocarbons, EB and ST leads to ST selectivities not exceeding 90% [10];

- Dehydrogenation, followed by oxidation of hydrogen

$$C_6H_5CH_2CH_3 \rightleftharpoons C_6H_5CH{=}CH_2 + H_2 \quad (1.9)$$

$$H_2 + 1/2O_2 \longrightarrow H_2O, \quad (1.10)$$

which allows one to reach an EB conversion of approximately 80%, by removing the H_2 from the reaction. But it is necessary in this process to mechanically separate the hot aromatics from the oxygen to escape explosion [11];

- Oxidative dehydrogenation by CO_2

$C_6H_5CH_2CH_3 + CO_2 \rightleftharpoons C_6H_5CH{=}CH_2 + CO + H_2$ (1.11)

which shifts the equilibrium to lower temperatures. The realization of such a process leads to a decrease of the amount of energy required and to an increase of the styrene yield. But, CO_2 blocks the active centres of the catalyst, which leads to quick catalyst deactivation [12];

- Membrane catalysis allows one to immediately remove the H_2 in the reaction which leads to an increase of the EB conversion. Nevertheless, the realization of an industrial membrane process is complicate and requires certain developments not achieved yet [13].

Among the alternatives proposed, the ODH of EB to ST in the presence of O_2 is one of the most elegant and promising reactions. The ODH of EB to ST allows one to realize an exothermic reaction due to water formation as the secondary product. The thermodynamic equilibrium proposes EB conversions as high as 90% at much lower temperatures than in the dehydrogenation reaction.

1.3. Oxidative Dehydrogenation of Ethylbenzene to Styrene with Carbon Materials as Catalysts

During the last three decades, a group of catalysts was reported, such as aluminas and various metal oxides [14-17] and phosphates [18-21] that showed activities and selectivities in the ODH of EB to ST comparable to the iron catalyst. Evidence was gradually accumulated that the active sites were not located on the initial catalyst surface, but on a carbonaceous overlayer. This carbonaceous overlayer is initially deposited on the surface, and it is one reason why the catalysts exhibited induction periods in their activities. Later, active carbon itself, in particular activated carbon, was shown to be an active catalyst for the ODH reaction [22-24]. It was found that the ODH of EB to ST could be performed over carbon materials at lower temperatures (350-400°C) than those normally used with mixed oxide catalysts (450-550°C).

Activated carbon was mainly studied as a promising catalyst for the ODH of EB to ST [22-26]. However, a commercialization of the activated carbon as catalysts for ODH of EB to ST is not possible, because its low stability in an oxidative atmosphere hindered the potential use of activated carbons.

Accordingly, carbon catalysts, if to be used in industrial applications, should be further improved to achieve high catalytic activity and selectivity, and stability during long time of operation. The underlying hypothesis of this thesis is that the nature and microstructure of the carbon material are determining a high and stable catalyst efficiency.

1.4. Carbon materials as catalysts

Carbon materials are used mainly as supports for the active phase in heterogeneous catalysis. Several reactions were referred to as being catalysed by activated carbon, such as ODH of EB to ST [22-26], oxidative reactions with oxygen and halogens such as the oxidation of SO_2 to H_2SO_4 and the production of $COCl_2$ from CO and Cl_2 [27], NO reduction [28], dehydration and dehydrogenation of 2-propanol [29] and ethanol [30], oxidative dehydrogenation and dehydrogenation of methanol, propanol and propanal [31], H_2SO_3 oxidation [32], oxidative dehydrogenation of cyclohexanol [33], and isoborneol oxidation [34], among others.

Carbon assumes a large variety of forms because of its unique position in the periodic table. The various bonding states of carbon are related to certain structural arrangements. Sp^1-hybridization gives rise to carbon chain structures, sp^2-hybridization to planar carbon structures, and sp^3-hybridization to tetrahedral carbon structures.

Since the discovery of fullerenes [35] and carbon nanotubes [36], great interest is paid to new families of non-planar sp^2-hybridized carbon nanostructures, *i.e.* polyhedra, onions, nanotubes, nanofilaments, etc. These nanostructures are formed because a graphene layer (defined as a single 2D layer of 3D graphite) of finite size has many edge atoms with dangling bonds, and these dangling bonds correspond to high-energy states. Therefore, the total energy of a small number of carbon atoms (30-100) is reduced by eliminating these dangling bonds even at the expense of increasing the strain energy, thereby promoting the formation of closed cage clusters, such as fullerens and carbon nanotubes [37]. The structural eccentricity and high stability of these new carbon nanostructures at high temperatures and in severe environments

predict their potential applications in catalysis. An extensive experimental research was performed to produce new carbon nanostructures in large scales, and to decrease the costs for such materials. At present, the production of nanocarbon materials has been successfully improved, but this work is still in progress [38-40].

It was proposed that carbon nanostructures, i.e. carbon nanotubes, nanofilaments, and onions, could be active and stable catalysts for certain reactions. The use of carbon nanostructures as catalysts for the oxidative dehydrogenation of ethylbenzene to styrene is proposed in the present thesis and is outlined in greater detail below. The main goal of the present work was to study the influence of the carbon nature on the ODH performance by investigating and comparing carbon materials of different structure. The following carbon materials were chosen for the present study: carbon black, graphite, multi-walled nanotubes (MWNT´s), nanofilaments (CNF´s), onion-like carbon (OLC), and ultra-dispersed diamonds (UDD). Time on stream experiments of ODH of EB over these carbon materials were performed to investigate their different stability during reaction in dependence on their nature. The different carbons were characterized before and after catalytic tests by numerous bulk and surface sensitive techniques in order to develop a structure-function relationship for nanocarbons as catalysts in the oxidative dehydrogenation reaction. The structure-activity relationship developed in this thesis allows one to propose a reaction mechanism for the ODH of EB to ST over carbon materials and to define a carbon catalyst with an optimum structure for high activity, selectivity and stability in this reaction.

References

[1] NOVA Chemical Corporation Supplemental Financial and Product Information (2000) 10.

[2] James D.H., Castor W.M. in *Ullmann's Encycl*. 5. Ausg. 25 (Ind.Chem. 1994) 329-344.

[3] Kearby K.K. in Catalysis (Ed.: O.Emmet), Vol. III, 469, Reinhold, New York, 1955.

[4] Holmlid L., Menon P.G. Appl. Catal. A: General 212, 1 (2001) 247.

[5] Lee E.H. Catal. Rev. 8 (1973) 285.

[6] Herzog B.D., Rase H.F. Ind. Eng. Chem. Prod. Res. Dev. 23 (1984) 187.

[7] Devoldere K.R., Froment G.F. Ind. Eng. Chem. Prod. Res. Dev. 38 (1999) 2626.

[8] Menon P.G. J. Mol. Catal. 59 (1990) 207.

[9] Cavani F., Trifiro F. Appl. Catal. A: General 133 (1995) 219.

[10] Vrieland G.E., Menon P.G. Appl. Catal **77** (1991) 1.

[11] Romatier J., Bentham M., Foley T., Valentine J.A. Proc. Dewitt Petrochem. Rev., Houston, Texas, 1992, p. K1.

[12] Mimura N., Takahara I., Saito M., Hattori T., Ohkuma K., Ando M. Cat. Today 45 (1998) 61.

[13] Wu J.C.S., Liu P.K.T. Ind. Eng. Chem. Res. 31 (1992) 322.

[14] Zhyznevskiy V., Tsybukh R., Gumenetskiy V. React. Kinet. Catal. Lett. 71, 2 (2000) 209.

[15] Cracium R., Dulamita N. Ind. Eng. Chem. Res. 38 (1999) 1357.

[16] Ogranowski W., Hanuza J., Kepinski L. Appl. Catal. A: General 171, 1 (1998) 145.

[17] Ogranowski W., Hanuza J., Drulis H., Mista W., Macalik L. Appl. Catal. A: General 136, 1 (1996) 143.

[18] Castro Luna A.E., Becerra A.M. React. Kinet. Catal. Lett. 63, 2 (1998) 335.

[19] Vrieland G.E. J. Catal. 111 (1988) 1.

[20] Vrieland G.E. J. Catal. 111 (1988) 14.

[21] Dziewiecki Z., Jagiello M., Makowski A. Reactive & Functional Polymers 33 (1997) 185.

[22] Alkhazov T.G. Kinet. Katal. 13 (1972) 509.

[23] Pereira M.F.R., Orfao J.J.M., Figueiredo J.L. Appl. Catal. A: General 184 (1999) 153.

[24] Pereira M.F.R., Orfao J.J.M., Figueiredo J.L. Appl. Catal. A: General 196 (2000) 43.

[25] Pereira M.F.R., Orfao J.J.M., Figueiredo J.L. Appl. Catal. A: General 218 (2001) 307.

[26] Guerrero-Ruiz A., Rodriguez-Ramos I. Carbon 32 (1994) 23.

[27] Boehm H.P., Mair G., Stoehr T. Rincón A.R., Tereczki B. Fuel 63 (1984) 1061.

[28] Yang J., Mestl G., Herein D., Schloegl R., Find J. Carbon 38 (2000) 715.

[29] Szymanski G., Rychlicki G. Carbon 31 (1993) 247.

[30] Szymanski G., Rychlicki G., Terzyk A.P. Carbon 32 (1994) 265.

[31] Grunewald G.C., Drago R.S. J. Am. Chem. Soc. 113 (1991) 1636.

[32] Stöhr B., Boehm H.P., Schlögl R. Carbon 36 (1991) 707.

[33] Silva I.F., Vital J., Ramos A.M., Valente H., Botelho do Rego A.M., Reis M.J. Carbon 36 (1998) 1159.

[34] Valente H., Vital J., Silva I.F., Ramos A.M., Botelho do Rego A.M., Reis M.J. Extended abstracts, in: Proceedings of the 23rd Biennial Conference on Carbon, Penn State University, 1997, p.216.

[35] Kroto H., Heath J., O'Brien S., Curl R., Smalley R. Nature 318 (1985) 162.

[36] Iijima S. Nature 354 (1991) 56.

[37] Nanostructured Carbon for Advanced Applications. Ed. Benedek G., Milani P., Ralchenko V.G. NATO Science Series. II. Mathematics, Physics and Chemistry, Vol. 24, 368.

[38] Huong P. V., Ajayan R., Cavagnat R., Stephan O. Physical Reviews B 51 (1995) 10048.

[39] Saito Y. Carbon 33 (1995) 979.

[40] Ivanov V., Fonseca A., Nagy J.B., Lucas A.A., Lambin P., Bernaerts D., Zhang X.B. Carbon 33 (1995) 1727.

Chapter 2. Experimental Methods

The goal of a catalytic reaction study is to achieve detailed knowledge about the various processes taking place inside the reactor and on the catalyst surface during the reaction. Being a multidiscipline science, catalysis attracts a large number of methods and techniques during the process of catalyst development. Model systems, being one of the classical catalytic studies, allow one to conduct reactions on the surface of well-defined single crystals under UHV conditions and to use a large spectrum of powerful analytical tools to study the catalyst surface under these model reaction conditions. Yet, it is impossible to extract the full information from the model systems necessary to understand the catalytic behavior of real systems not only because of the complexity of the latter but also due to the impossibility to achieve the correct reactor conditions. It is obvious that investigations of more complex systems, which mimic closer the composition of real catalysts and the operations of the catalyst under industrial conditions are of paramount importance. Modern research in the field of catalysis is based on the establishment of empirical relations between behavior of the catalyst during the reaction at different reaction conditions and the catalyst composition, structure, and texture, which can be studied *ex situ*. It is apparent that the study of the catalytic activity under determined reaction conditions with a combination of useful methods for catalyst characterization prior and subsequent to the reaction could maximize useful information about reaction pathways, active sites of reaction, and the reaction mechanisms. In an optimum case, the catalyst / reaction characterization is *in situ* in the operating reactor.

In this chapter, it is described how the ODH of EB to ST over bulk catalysts was performed. A critical assessment is provided of the methods applied for the

comparative characterizations before and after ODH catalysis over the differently structured carbon catalysts to find evidences of key aspects of the reaction mechanism.

2.1. Set-up for the catalytic reaction tests

The catalytic tests are carried out in the set-up, which is shown schematically in Figure 2.1. The reactor allows one to perform catalytic tests with full control of all reaction parameters, and to conduct the process in the presence of He as the carrier gas, steam, O_2, CO, CO_2 or mixtures of these gases. The gaseous reactants are led to the reactor by mass flow controllers (Bronkhorst). The EB is evaporated in the saturator maintained at 35°C in flowing He to achieve a EB partial pressure of 2160 Pa, subsequently mixed with additional gases, and passed to the reactor. All gas lines are either separately heated or inside a heated compartment to escape EB and ST adsorption. The catalytic tests were performed in quartz tubular flow reactors (30 cm length, 4.0 mm i.d.) placed inside of an electrical heating oven, which was controlled by an Eurotherm PID temperature controller. The catalyst particles mixed with quartz chips were held in the isothermal oven zone between two quartz wool plugs. Quartz chips are further used in order to minimize the dead volume of the reactor upstream the catalyst bed. The choice of the reaction parameters is described in the following chapter. The hydrocarbon products are analysed every 25 min by an on-line gas chromatograph “Varian 3800” equipped with two columns. The first one is a 5% SP-1200/1.75% Bentone 34 packed column, which is connected to the FID detector and is used for the analysis of hydrocarbons. The second one is a Carboxen 1010 PLOT

column, which is connected to a TCD detector and is used for the simultaneous analysis of the permanent gases.

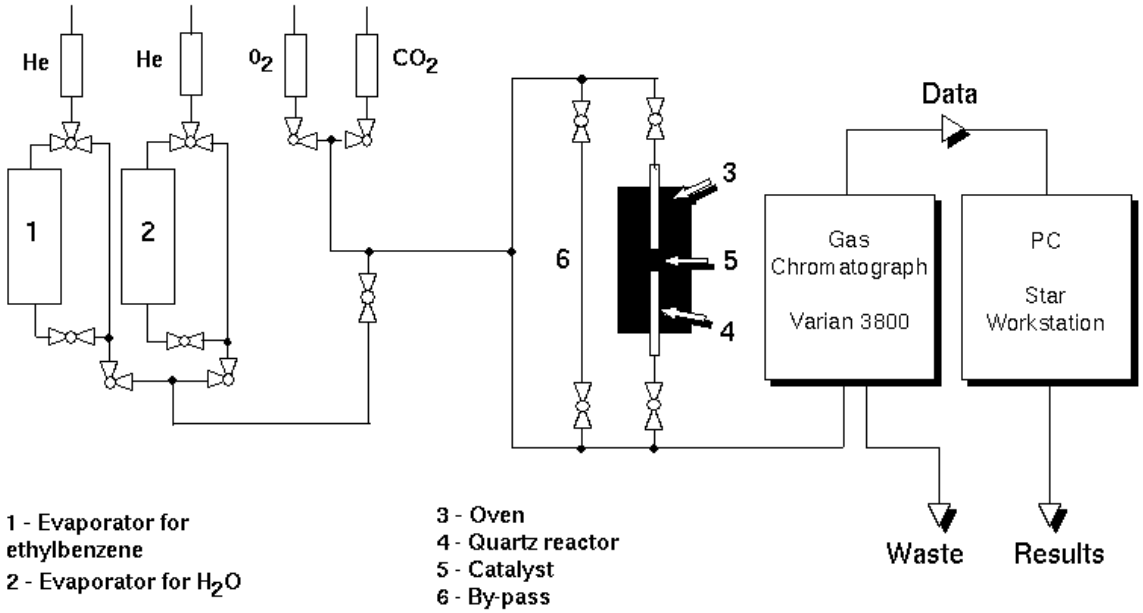

Figure 2.1. Scheme of the reactor set-up used for the catalytic experiments.

The parameters of the catalytic performance were defined by the following equations:

$$\text{EB conversion: } X = \frac{F_{EBin} - F_{EBout}}{F_{EBin}} \times 100\% \quad (2.1)$$

$$\text{Selectivity to ST: } S_{ST} = \frac{F_{ST}}{F_{EBin} - F_{EBout}} \times 100\% \quad (2.2)$$

$$\text{ST yields: } R_{ST} = \frac{F_{ST}}{F_{EBin}} \times 100\% \quad (2.3)$$

with "F" being the concentrations in moles of the different gases and the subscripts, "in" and "out", the respective concentrations in moles of the feed and outlet. The relative yields of by-products were calculated by the same way. The experimental errors estimated for the different products did not exceed 5%.

The specific catalytic conversions over the carbon catalysts with time on stream were calculated by the following equation:

$$X_s = \frac{\left(F_{EBin} - F_{EBout}\right)/F_{EBin}}{C \times S} \tag{2.4}$$

with C being the weight of the catalyst in grams, and S the BET surface area in m^2/g of the catalyst measured after reaction.

The specific catalytic selectivities of the tested carbon materials with time on stream were calculated analogously by the following equation:

$$S_s = \frac{F_{ST}/\left(F_{EBin} - F_{EBout}\right)}{C \times S} \tag{2.5}$$

The specific catalytic yields over the different carbon materials with time on stream were calculated analogously by the following expression:

$$R_s = \frac{F_{ST}/F_{EBin}}{C \times S} \tag{2.6}$$

The specific reaction rates of ODH of EB to ST over carbon materials were calculated according to the following equation:

$$W = \frac{F_{EBin} - F_{EBout}}{\tau \times S} \tag{2.7}$$

with τ being a contact time and S is the BET surface area in g/m^2 of the catalyst measured after reaction.

The carbon balance was calculated from the sum of the reaction products to obtain information about possible carbon deposition or oxidation taking place during the course of the experiment of ODH of EB. The experimental error in the carbon balance did not exceed 5%.

Tests for a possible contribution of homogenous, gas-phase reactions were done by comparing the EB conversions obtained with (i) the empty reactor, (ii) the reactor filled with a quartz plug, and (iii) the reactor filled with both quartz plugs and

chips. Only very low EB conversions up to 2% were detected in such catalytic tests in the temperature range up to 600°C.

If the rates of heat and mass transfer to the carbon catalyst are less than the rate of reaction on the catalyst surface, diffusion processes determine the reaction kinetics. To exclude such diffusion limited reactor conditions, a series of experiments was performed. The influence of diffusion through the porosity of carbon materials was studied over high surface area graphite, HSAG 300, at 520°C with an EB to O_2 ratio 1:1. The contact time was chosen to be constant ($V_{catalyst}$/Flow rate), but the linear gas flow rates were changed, and catalyst amounts were proportionally increased. Fig. 2.2 shows the conversions, selectivities and styrene yields obtained in these tests. The differences in the catalytic performances were below 5%, *i.e.* within the experimental error. Accordingly, it was concluded that diffusion limitations are negligible under these reactor conditions for the carbon material with similar or lower porosity. However, these tests cannot exclude diffusion limitations for carbon materials with more porous structures. Therefore, graphite HSAG 300 was used in those measurements in which it was necessary to fully exclude diffusion limitation (experimental design, etc.). In the experiments performed with other carbon materials, the diffusion limitation was minimized by the low concentrations of the reactants in the stream.

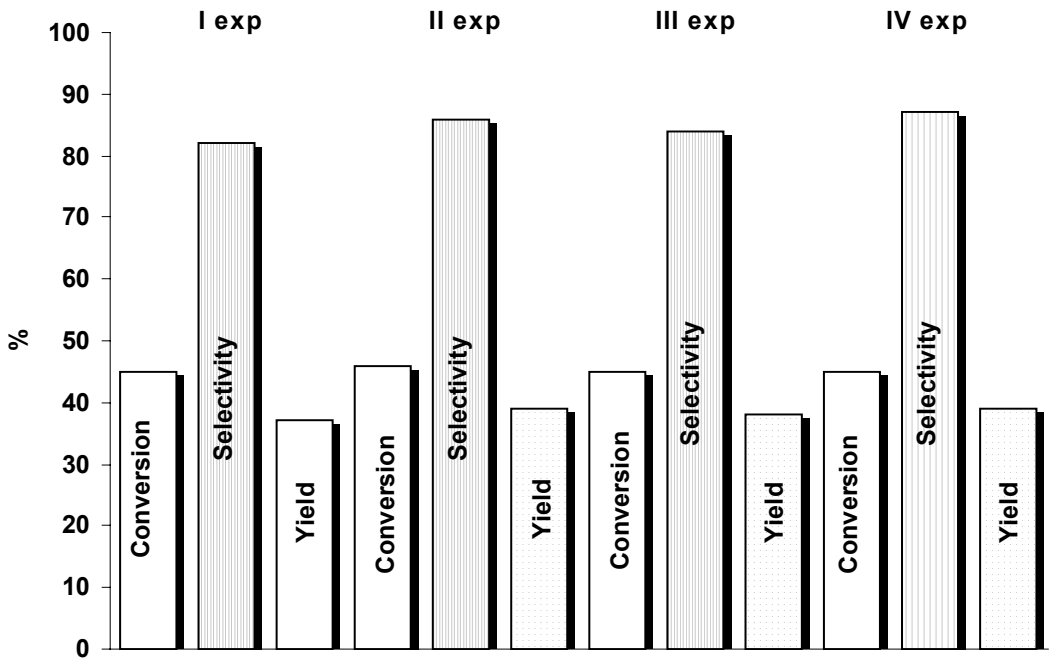

Figure 2.2. Diffusion limitation experiments over graphite HSAG 300 at 520°C showing the EB conversions, ST selectivities and ST yields for different catalyst loadings and higher flow rates.

2.2. Characterization Techniques

2.2.1. Microscopic Methods (TEM, SEM)

Transmission electron microscopy (TEM) is very important for the determination of the real structure of catalysts. The TEM technique uniquely provides information on the size, shape and structure of carbon materials used in the present study. Information about changes of the catalyst surface and structure during the reaction can also be obtained by comparing the TEM data of the fresh and used samples.

The catalysts used in the present study were examined in a Phillips CM200 FEG field-emission gun electron microscope operated at an accelerating voltage of 200 kV equipped with an energy dispersive X-ray analysis (EDX) (DX-4) and electron energy loss spectroscopy (EELS) detectors (Gatan 100) for elemental analysis. The samples were prepared by suspending the solid powder in ethanol under ultrasonic vibration. One drop of the thus prepared suspension was brought onto holey carbon films on copper grids.

The morphologies of the catalysts were monitored as a function of time on stream in the ODH of EB to ST by scanning electron microscopy (SEM) using a Hitachi S-4000 apparatus operated at 15 kV and 25 kV acceleration voltages, which is also equipped with EDX (DX-4).

2.2.2. Spectroscopic Methods (XPS, Raman- and IR-spectroscopy)

X-ray photoelectron spectroscopy (XPS) is an analytical tool invaluable for the identification of the chemical composition of the near-surface region of catalyst materials. XPS was used in the present work to study the formation of oxygen-carbon species on the surfaces of the different carbon nanostructures. XPS has to be performed *ex-situ*, which may lead to some problems, *e.g.* the adsorption of water during the transport of the samples through air. To receive information about the changes of the carbon surfaces during the reaction, the C1s and O1s spectra of the carbon samples before and after catalysis were compared.

XP spectra were recorded on a modified Leybold Heraeus spectrometer (LHS12 MCD) with Mg K_α radiation (1253.6 eV) and a power of 240 W. The bandpass energy was set to 50 eV. X-ray satellites and Shirley backgrounds were subtracted. The peak areas were normalized with the theoretical cross-sections to obtain the relative surface compositions. The C1s and O1s peaks were fitted by combined convoluted Gauss Lorentz functions.

Laser Raman spectroscopy (LRS) is an important technique for the structural characterization of carbon materials because of its sensitivity to crystalline, amorphous, glassy, or molecular species. The Raman spectra were recorded with a LabRam spectrometer (Dilor). A He/Ne laser at 632.8 nm was used as the excitation source. The characterization of the samples was conducted in the wave number interval from 950 to 2000 cm^{-1} with the spectral slit width set at 500 μm giving a spectral resolution of 5 cm^{-1}.

Infra-red (IR) spectroscopy is one of the primary tools to identify the nature of species adsorbed on the carbon surface and to clarify their interaction with the substrate. IR-spectra were obtained using a Fourier transform spectrometer (BOMEM

MB-102). The samples were prepared as suspensions by pressing in alkali metals halides (KBr). Not all carbon samples could be successfully studied by IR spectroscopy, because sp^2-hybridized carbon materials are black for IR transmission.

2.2.3. Additional Methods (XRD, TG/DTA, BET surface area)

X-ray diffraction (XRD) is invaluable in the determination of the phase composition of catalytic materials. In the present study, XRD was used to determine the bulk catalyst phases and their changes during the reaction. X-ray diffraction patterns were recorded with a STOE STADI P diffractometer using Cu K_α radiation and a HOPG-secondary monochromator. The samples were scanned in the range $10° < 2\theta < 80°$ over several hours. XRD also allows one to determine the degree of crystallinity of catalysts.

Thermogravimetric analysis (TGA) was performed on a Netzsch STA 449C balance. Temperature programmed oxidation (TPO) was applied in order to study the oxidation of carbon materials. TPO was conducted passing a 20 % (v/v) O_2/He mixture over the samples heated with a linear heating rate of 10 $K \cdot min^{-1}$. The TGA apparatus was coupled to a QMS200 mass spectrometer (Thermostar, Pfeiffer Vacuum) for the determination of the evolved gaseous oxidation products as a function of temperature. This technique allows one to investigate, which reactions may take place in an oxidative atmosphere at high temperatures, and certain oxygenated species present on the carbon surface may be proposed from the data.

The specific surface area was measured by the dynamic BET method on a Quantachrome apparatus from Quantasorb (USA). The specific BET surface area of the catalysts was determined by N_2-adsorption at 77 K. The microporosity of carbon materials was calculated with the use of the t-method of Lippens and de Boer [4].

References

[1] Catalysis from A to Z. A Concise Encyclopedia. Ed. by Cornils B., Herrmann W.A., Schlögl R., Wong Ch.-H. WILEY-VCH, Weinheim, 2000.

[2] Niemandtsverdriet J.W. Spectroscopy in Catalyis. Sec. Ed. WILEY-VCH, Weinheim, 2000.

[3] Handbook of Heterogeneous Catalysis. Ed. by Ertl G., Knözinger H., Weitkamp J. Vol. 2. WILEY-VCH, Weinheim, 1997.

[4] Lippens B.C., De Boer J.H. J. Catal. 4 (1965) 319.

Chapter 3. Experimental Design by the Response Surface Method

Reliable ODH experiments of EB to ST require the precise determination of the conditions under which each tested catalyst develops its activity maximum. Several parameters have to be tested in order to determine the optimum performance in the reaction of ODH of EB to ST. These parameters are (1) reaction temperature, (2) concentration of EB in the feed, (3) linear feed velocity, (4) amount of catalyst, (5) oxygen to EB ratio in the feed, and (6) time on stream. All parameters listed above affect the reaction, either independently or dependent on each other. Due to these important reaction parameters and their possible interactions, the optimisation of the catalytic activity requires a large number of experiments. For example, to determine three experimental parameters with 3 variables, it is necessary to perform $3^3 = 27$ experiments to screen the effects of all parameters. Such a screening of the experimental parameters with the theoretically lowest possible number of experiments can be done by experimental design. The experimental design develops a model, in our case a regression model, to study the relationships between all variable parameters. The final aim of the regression analysis is to predict the performance of the catalyst at optimum reaction conditions using the mathematical expression which relates to responses of variations of the reaction parameters.

An experimental design by building a response surface model was constructed to find the optimum conditions for ODH of EB to ST with the different carbon catalysts. The design was conducted with the three following reaction parameters, i.e. (i) reaction temperature (T), (ii) contact time between EB and the catalyst (τ_C), and (iii) oxygen to EB ratio in the feed (O).

The contact time (τ_C) is described by the following equation:

$$\tau_C = \frac{V_C}{V_{EB}}, \text{min}, \qquad (3.1)$$

where V_C is a volume of the catalyst in ml; V_{EB} is the velocity of the EB flow through the volume of the catalyst, ml/min.

As seen from the equation (3.1), the contact time of the EB and the catalyst, τ_C, can be varied by varying (i) the catalyst volume (amount), (ii) the linear feed velocity, or (iii) the partial pressure of EB in the feed by the temperature of the EB evaporator. In our case, the contact time can not be successfully varied by neither the feed velocity nor the EB pressure, because of the low oxygen percent in the feed (~0.1-0.2 vol. %) due to the limitation of the mass-flow controllers. Due to this limitation and to decrease the number of variable factors, the concentration of EB in the feed and the total flow rate were chosen to be constant. Under these conditions, the contact time was varied by the variation of the catalyst amount (m, g). The choice of a constant EB concentration in the feed and a total flow rate allows one to vary the oxygen to EB ratio by regulating the oxygen content in the feed (O, vol. %). Three levels (variables) were chosen, *i.e.* (1), (0) and (-1), for every factor to screen their effect on catalysis. Synthetic graphite (HSAG-300, Timcal Ltd) and carbon black (Tunnel Black, Degussa) with high BET specific surface areas (300 and 328 m^2/g, respectively), and carbon nanofilaments (CNF's) were used with the range of variables as listed in Table 3.1, a, b.

The Box-Behnken Plan [1] is very convenient for a design with three factors and three variables allowing one to build the response surface model by performing only 13 experiments (Tab. 3.2). The design also uses three replicates for one experiment (points 13-15) to determine the experimental error (Tab. 3.2).

Every experiment was performed with a fresh catalyst to obtain results independent of time on stream, and was conducted during 20 hours to reach a stable performance for each point of the experimental design. The experiments were randomly conducted, as it is required to minimize the experimental error. All values used for the calculation of the catalytic performances were chosen after the same time on stream (10 hours) for better comparability.

Table 3.1, a.

The range of the three parameters for the experimental design with graphite.

Factors/Variables	**T,°C**	**m, g**	**O, %**
-1	450	0.02	0.25
0	500	0.04	0.5
1	550	0.06	0.75

Table 3.1, b.

The range of the three parameters for the experimental design with carbon black.

Factors/Variables	**T,°C**	**m, g**	**O, %**
-1	450	0.02	0.2
0	500	0.035	0.4
1	550	0.05	0.6

Table 3.2.

The experiments according to the Box-Behnken Plan.

Experiment number	**T,°C**	**m**, g	**O, %**
1	-1	-1	0
2	1	-1	0
3	-1	1	0
4	1	1	0
5	-1	0	-1
6	1	0	-1
7	-1	0	1
8	1	0	1
9	0	-1	-1
10	0	1	-1
11	0	-1	1
12	0	1	1
13	0	0	0
14	0	0	0
15	0	0	0

The results obtained from the experiments done according to the Box-Behnken Plan were calculated according to the Eq. 2.1-2.3 described in Chapter 2.

The calculated results are collected in Table 3.3 a, b for graphite and carbon black, respectively. The effect of every parameter on the catalytic performance was calculated by the software “Statistica 5.5”. This software allows one to perform all necessary estimations, to determine the level of significance of all effects, to calculate the regression coefficients, and to build a 3d response surface model.

Table 3.3, a.

EB conversion, selectivity to ST and ST yield calculated for the Box-Behnken Plan experiments performed with graphite.

Experiment number	Conversion, %	Selectivity to ST, %	ST yield, %
1	33	78	42
2	46	83	38
3	22	96	21
4	38	86	33
5	48	86	41
6	78	69	53
7	48	85	40
8	76	77	58
9	54	83	45
10	75	76	57
11	49	78	38
12	48	86	41
13	68	80	54
14	69	79	55
15	63	79	50

Table 3.3, b.

EB conversion, selectivity to ST and ST yield calculated for Box-Behnken Plan experiments performed with carbon black.

Experiment number	Conversion, %	Selectivity to ST, %	ST yield, %
1	43	86	37
2	45	83	37
3	79	78	62
4	96	51	48
5	70	83	58
6	85	69	59
7	76	76	57
8	87	60	52
9	79	74	58
10	93	65	61
11	78	67	52
12	94	54	50
13	86	66	57
14	91	59	53
15	94	60	56

Tables 3.4, a, b show the effects (Effects) of every parameter, standard errors (Std. Error), the *t* - values with 8 degrees of freedom (T(8)), the probabilities (p), and the confidence limits (Cnf. Limt). In case of the graphite catalyst, the standard errors estimated for the square effects were less than for the linear effects. In case of carbon black (Tab. 3.4, a, b), the standard errors were less for the linear effects than for the square effects, which means that all parameters chosen had a linear influence for graphite and a square influence for carbon black. The reason for this different parameter influence on the two different carbon catalysts is not clear yet, but it is

suggested to be related to the different microstructures (*e.g.* sp^3- and sp^2-carbon) and degrees of crystallinity for graphite and carbon black.

The confidence limits showed the interval of significance of the corresponding regression coefficients. A regression coefficient is significant if the confidence interval does not include zero. The significant linear and square effects are marked by asterisks in Tab. 3.4. In the chosen parameter regime, the third parameter O, oxygen content in the feed, seems to have a negative effect or was less important on both the linear and square effects and hence may be disregarded for the regression (Tab. 3.4, a, b). This observation clearly indicates that the oxygen concentration in the feed, which had to be used due to the mass flow controllers, was to high for a determination of the real reaction order in O_2. In addition, it can be assumed that the EB selectivities, which can be reached for optimised O_2 partial pressures, should still be higher than those found in this study.

From the analysis of the obtained p values, the probability of the factor T (temperature) is comparable to zero within the experimental error for significant effects. The estimated effects for carbon black were similar to those of graphite. The difference to graphite was found in the importance of the linear effect of the m factor, while the square effect was not important (Tab. 3.4, b).

Tables 3.5, a and b show the regression coefficients as calculated for graphite and carbon black, respectively.

Table 3.4, a.

Effect of the parameters and their interactions for graphite.

Parameter	Effect	Std. Error	T(8)	p	-95, % Cnf. Limt	+95, % Cnf. Limt
Mean/Inter.	42,0000*	2.046974*	20,51809*	0.00000*	37.2797*	46.72033*
(1) T (L)	10.2500	5.014043	2.04426	0.075175	-1.3124	21.81240
T (S)	8.7500*	3.690236*	2.37112*	0.045167*	0.2403*	17.25970*
(2) m (L)	-2.0000	5.014043	-0.39888	0.700417	-13.5624	9.56240
m (S)	11.5000*	3.690236*	3.11633*	0.014308*	2.9903*	20.00970*
(3) O (L)	-4.7500	5.014043	-0.94734	0.371199	-16.3124	6.81240
O (S)	-3.7500	3.690236	-1.01620	0.339281	-12.2597	4.75970

Table 3.4, b.

Effect of the parameters and its interaction for carbon black.

Parameter	Effect	Std. Error	T(8)	p	-95, % Cnf. Limt	+95, % Cnf. Limt
Mean/Inter	90.2667*	4.583083*	19.69562*	0.00000*	79.6981*	100.8353*
(1) T (L)	11.3750	5.613108	2.02651	0.077275	-1.5688	24.3188
T (Q)	-30.8917*	8.262271*	-3.73888*	0.005714*	-49.9445*	-118388*
(2) m (L)	29.2000*	5.613108*	5.20211*	0.000820*	16.2562*	42.1438*
m (Q)	-17.8417	8.262271	-2.15941	0.062847	-36.8945	1.2112
(3) O (L)	1.5750	5.613108	0.28059	0.786142	-11.3688	14.5188
O (Q)	8.9083	8.262271	1.07819	0.312381	-10.1445	27.9612

Table 3.5, a.

Regression coefficients for graphite.

Parameter	Regress. Coeff.t	Std. Error	T(8)	p	-95, % Cnf. Limt	+95, % Cnf. Limt
Mean/Inter.	53,00*	4.09*	12.95*	0.001*	43.56*	62.44*
(1) T (L)	5.13	2.51	2.04	0.075	-0.66	10.911
T (Q)	-8.75*	3.69*	-2.37*	0.045*	-17.26*	-0.24*
(2) m (L)	-1.00	2.51	-0.40	0.700	-6.78	4.78
m (Q)	-11.50*	3.69*	-3.12*	0.014*	-20.01*	-2.99*
(3) O (L)	-2.38	2.51	-0.95	0.371	-8.16	3.41
O (Q)	3.75	3.69	1.02	0.339	-4.76	12.26

Table 3.5, b.

Regression coefficients for carbon black.

Parameter	Regress. Coeff.t	Std. Error	T(8)	p	-95, % Cnf. Limt	+95, % Cnf. Limt
Mean/Inter.	90.2667*	4.583083*	19.69562*	0.0000*	79.6981*	100.8353*
(1) T (L)	5.6875	2.806554	2.02651	0.077275	-0.7844	12.1594
T (Q)	-15.4458*	4.131135*	-3.73888*	0.005714*	-24.9722*	-5.9194*
(2) m (L)	14.6000*	2.806554*	5.20211*	0.000820*	8.1281*	21.0719*
m (Q)	-8.9208	4.131135	-2.15941	0.062847	-18.4472	0.6056
(3) O (L)	0.7875	2.806554	0.28059	0.786142	-5.6844	7.2594
O (Q)	4.4542	4.131135	1.07819	0.312381	-5.0722	13.9806

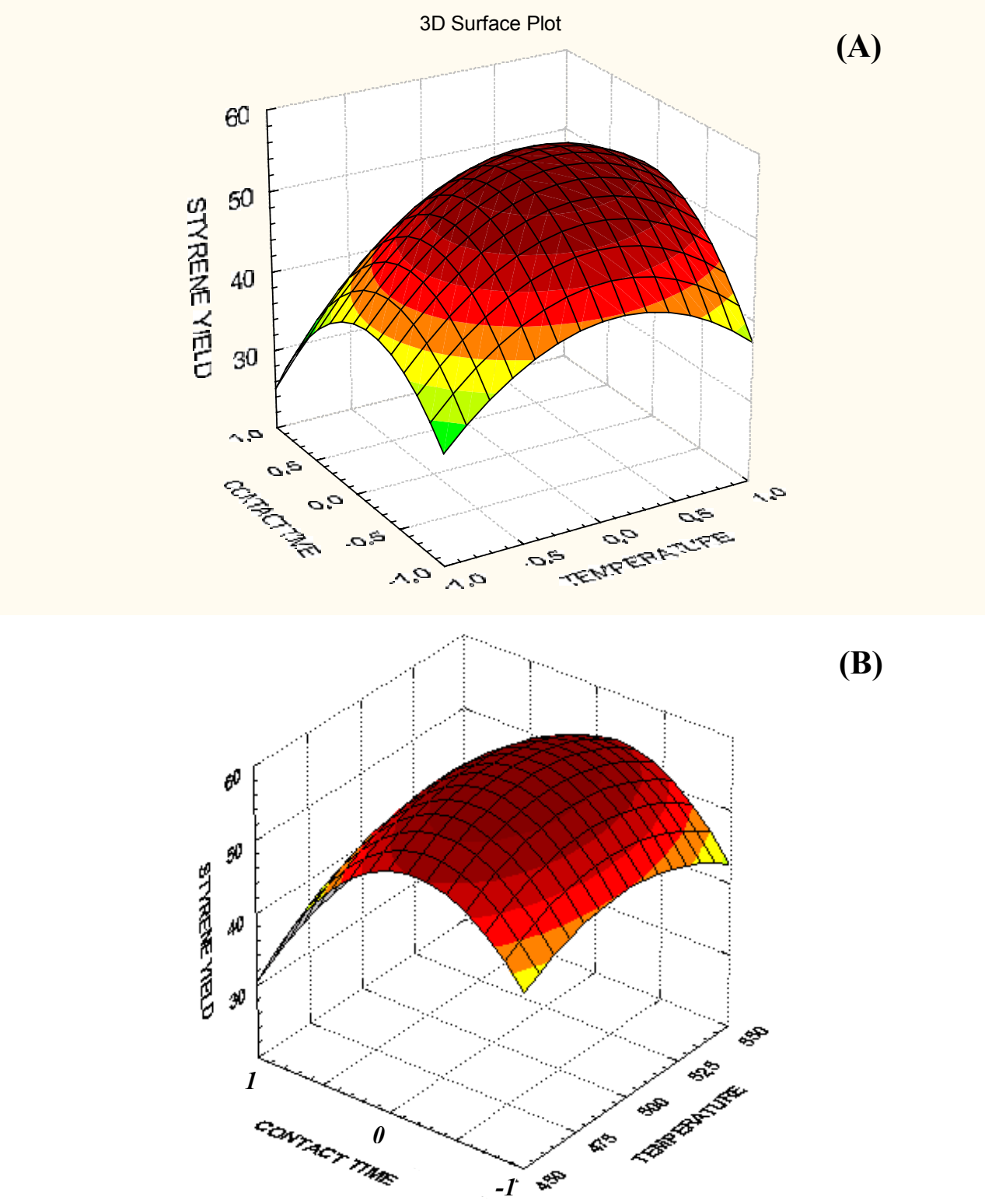

Figure 3.1. The response surface model obtained for the ST yield over graphite (A) and carbon black (B) as a function of temperature (T) and the oxygen to EB ratio in the feed (O).

In case of graphite, the following mathematical model for the ST yield, *r*, was obtained from the calculated regression coefficients (Table 3.5, a):

$$r = 53.00 + 5.13T - 8.75T^2 - 11.5m^2 \quad (3.5)$$

The other coefficients and parameters were not important for the catalyst performance according to Tab. 3.4,a and, thus, were not included in the above equation.

The *t*-value was calculated according to the following equation:

$$|t| = \frac{|\overline{T} - \mu_0|}{s/\sqrt{n}}, \quad (3.6)$$

where $\overline{T}$ is the regression coefficient; *s* - the standard error; *n* – the degree of freedom for *s*; μ_0 - comparison. In our case, the degree of freedom is n = 1 and $\mu_0 = 0$.

With the *t*-value, the equation (1) was written:

$$r = 53.00 + 5.13 \cdot \left(\frac{T - 500}{50}\right) - 8.75 \cdot \left(\frac{T - 500}{50}\right)^2 - 11.5 \cdot \left(\frac{m - 0.04}{0.02}\right)^2 \quad (3.7)$$

and after simplification:

$$r = -919.3 + 2300 \cdot m - 28750 \cdot m^2 + 360T - 0.35T^2 \quad (3.8)$$

The equation (3.8) describes the ST yield, *r*, as a function of contact time τ_C measured as m and temperature T, *i.e.* it contains 2 undetermined parameters - m and T. The dependence of the ST yield, *r*, on temperature, T, shows a maximum as obtained from the experimental results (Fig. 3.1, A). This implies that the first derivative of equation (3.8) in respect to T is 0 at this point. The dependence of the ST yield, *r*, from m also shows a maximum. Again, the first derivative of the equation (3.8) with respect to m is 0 at the maximum point. Accordingly, a system of two equations with two undetermined parameters can be established:

$$\begin{cases} \dfrac{\partial r}{\partial T} = (-919.3 + 2300 \cdot m - 28750 \cdot m^2 + 360T - 0.35T^2)'_T = 360 - 2 \times 0.35T = 0 & (3.5) \\ \dfrac{\partial r}{\partial m} = (-919.3 + 2300 \cdot m - 28750 \cdot m^2 + 360T - 0.35T^2)'_m = 2300 - 2 \times 28750 \cdot m = 0 & (3.6) \end{cases}$$

The solution of these equations yields the following estimates for the optimum reaction parameters:

$$\begin{cases} T = 515\,^{\circ}\mathrm{C} \\ m = 0.04 \end{cases}$$

These estimated parameters imply that the optimum reaction conditions should be obtained at a temperature of T=515°C, and for a catalyst amount of 0.04 g in case of graphite.

The same calculations were done for the case of carbon black. In Fig. 3.1, B, a maximum is shown for the dependence of the ST yield, *r*, on temperature, T, and catalyst amount, m. This maximum is broader and more flat for carbon black than the maximum of the styrene yield for graphite (Fig. 3.1, A). This difference again seems to reflect the more amorphous structure of carbon black. The optimum reaction conditions were found for a temperature of T=510°C, and for a catalyst amount of 0.06 g. These numbers reflect the higher reactivity of the ill-defined carbon black, *i.e.* the lower optimum reaction temperature, on one side, and its smaller number of active centers *i.e.* bigger catalyst amount necessary, on the other. The oxygen content in the feed is an insignificant parameter in the chosen region for both graphite and carbon black, which certainly is not correct and only arises from the fact the used mass flow controllers limited the O_2 partial pressures. It can be expected that the optimum O_2 partial pressure is much lower.

CNF's (Applied Science Ltd, Ohio, USA) was the third material used for an experimental design. According to the two important reaction parameters found in the

first two experimental designs with graphite and carbon black, an optimisation of only these two factors could be applied, *i.e.* the contact time by variation of the catalyst amount and the temperature.

The Simplex experimental design with two variable parameters was applied to optimise the reaction ODH of EB to ST over CNF's. First, three direct sets of experimental parameters were chosen in the region close to the optimum as found in the previous experimental designs (Fig. 3.2).

The three points (1, 2 and 3) represent an experimental triangle, in which point 1 (in the first triangle) showed the worst result of the measured reaction parameters, *e.g.* conversion, yield and selectivity. Then the next triangle was built by rejecting the worst point and calculating a new experimental point opposite to the worst point. The procedure was repeated up to the 6^{th} experimental step, after which the general direction of the progression axis was changed. After the 7^{th} experiment, the general direction of the progression axis was changed again and returned back parallel to the first direction. After the measurements of the 8^{th} experiment, it was found that the triangle of points 4, 7 and 8 contained three more successive simplexes. Hence, it was concluded that the highest point of these last three simplexes was the reaction optimum. This was the parameter set of point number 7 (Fig. 4.2).

The optimum reaction conditions found for CNF´s were a reaction temperature of T = 495°C, and a catalyst amount of 0.04 g. From the results summarized in Tab. 3.6 it is evident that the CNF´s are more active than graphite and carbon black as reflected by the lower reaction temperature. The number of active sites on CNF´s and graphite per unit weight, on the other hand seem to be comparable.

Table 3.6.

The optimum conditions for ODH of EB to ST over carbon materials determined by experimental design.

Sample	Temperature, °C	Catalyst amount, g
Graphite	515	0.04
Carbon black	510	0.06
CNF's	495	0.04

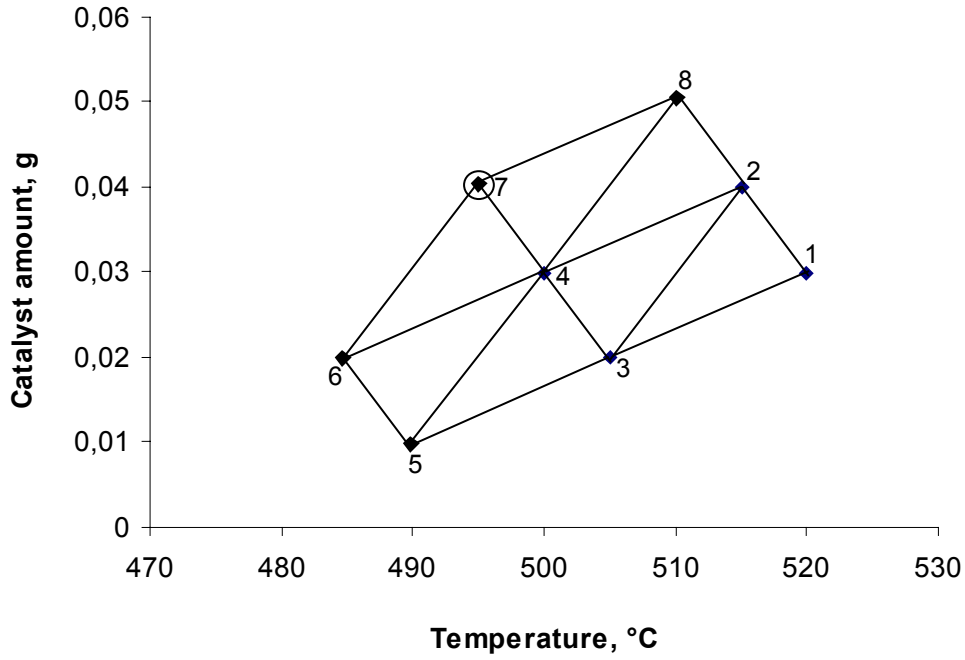

Figure 3.2. Simplex experimental design performed for CNF´s. Each point is a set of reaction parameters. The set point 7 (marked by the circle) was identified as reaction optimum.

References

[1] Data Handling in Science and Technology. V. 20A. Ad. Ed. B.G.M. Vandeginste, S.C. Rutan: Handbook of Chemometrics and Qualimetrics: Part A. Ed. D.L.Massart, B.G.M. Vandeginste, L.M.C. Buydens, S. De Jong, P.J. Lewi, J. Smeyers-Verbeke. Elsevier. 1997.

Chapter 4. Oxidative Dehydrogenation of Ethylbenzene to Styrene over Carbon Materials: Catalytic Study and Characterisation

4.1. Carbon Black, Graphite and Nanofilaments

The catalytic properties of carbon black (Lamp Black, Degussa, Düsseldorf, Germany), graphite (HSAG 300, Timcal, Bodio, Switzerland), and multi-walled carbon nanofilaments (CNF´s, Applied Science, Cedarville, Ohio) were compared in order to determine which carbon structure exhibits the higher activity and stability and to give a basis for a structure-activity relationship. The evolutions of the catalytic properties of these carbon materials were determined with time on stream in the ODH of EB under identical experimental conditions that allowed quantitative comparison.

Figure 4.1.1 displays the evolutions of conversion, selectivity and styrene yield obtained over carbon black, graphite and CNF´s in the ODH of EB at 550°C with time on stream on a mass referenced basis. The higher temperature as compared to the reaction optimum determined by experimental design was selected in order to enhance catalyst activation or deactivation processes, which in turn allows catalytic experiments in reasonable laboratory time periods.

Carbon black shows a high performance in the very beginning of the reaction with an initial EB conversion of 96%, a selectivity to ST of 53%, and a ST yield of 51%. Initially, the benzene yield was higher than 2%, the ethene and toluene yields were both less than 1%, and the yields of CO and CO_2 were both at about 20%. But, the formation of all products decreased with time on stream due to the combustion of carbon black. It was also accompanied by a dramatic decrease of the EB conversion

and, expectedly, an increase of selectivity to ST (Fig. 4.1.1). In the beginning of the reaction, the carbon balance was about 70% indicating a deposition of carbon from the EB source on the catalyst. With time on stream, the carbon balance increased and reached 110% after 6 hours on stream. Hence, the catalytic behavior of carbon black proves its instability and combustion during reaction, which renders its useless for the catalytic ODH reaction.

In the case of high surface area graphite, a quick increase of the initial ST yield from 37% to 48% and its subsequent decrease to 44% were observed during a stabilisation period of about 2 hours (Fig. 4.1.1). Then, the steady state was reached accompanied with an EB conversion of 52% and selectivity to ST of 84% (Fig. 4.1.1). The total formation of ethene, benzene and toluene was not higher than 5% during the experiment. The amounts of CO and CO_2, being 4-6%, were stable with time on stream. During first 5 hours, the carbon balance decreased from 126% to 100%, indicating the catalyst combustion. The following slow decrease of the carbon balance to 85% indicates that carbon combustion switched to carbon deposition with time on stream.

As seen from the catalytic behaviour of high surface area graphite, its activity was completely different from that of carbon black under the same reaction conditions, which renders it a possible candidate for an active and selective ST catalyst.

In the contrary to carbon black and graphite, an initial activation period of about 3 hours was observed over CNF´s. In the beginning of the reaction, the ST yield was 26% (Fig. 4.1.1) accompanied mainly with benzene (0.2%), toluene (0.2%), CO (2%), and CO_2 (9%) formations. After the induction period of 2 hours, a steady state was observed over the CNF´s with an EB conversion of 64%, a selectivity to ST of

74%, and a ST yield of 54%. Thus, the ST yield increased 2 times during this induction period. In the same time, the benzene and toluene yields also increased to 4% and 1.5%, respectively, while the CO yield decreased negligibly, and the CO_2 yield increased to 10.5%. These changes already hint changes of the catalyst nature.

The carbon balance, being 90% in the beginning and pointing to carbon deposition, increased quickly to 120%, which indicates carbon combustion. After this induction period, the carbon balance again decreased to 80% becoming stable at this level. This too small balance proves carbon deposition from the EB source on the catalyst. These combined results suggest a complex reaction network of carbon deposition, carbon combustion and oxidative EB dehydrodenation with its parallel reactions to toluene or benzene.

According to the obtained catalytic results, the time on stream activity of CNF´s was completely different from those of high surface area graphite and carbon black. Graphite and CNF´s were stable toward combustion in the contrary to carbon black. At the steady state of the reaction, CNF´s showed higher EB conversions and ST yields, but lower selectivities to ST formation on a mass referenced basis in comparison to graphite (Fig. 4.1.1).

A comparison of the specific EB consumption rate, specific selectivities to ST and specific ST yields of the three investigated carbon materials after 7h operation is shown in Table 4.1.1. Carbon black exhibits the highest activity, selectivity to ST and ST yield after 7 hours of reaction as already mentioned, but it combusts under the reaction conditions. Although the specific activity of CNF´s is lower than that of graphite, CNF´s exhibit a 41% higher selectivity to ST formation and a 37% higher specific ST yield as compared to graphite. Hence, the superiority of the nanofilaments in comparison to other tested forms of carbon is evident for this catalysed reaction.

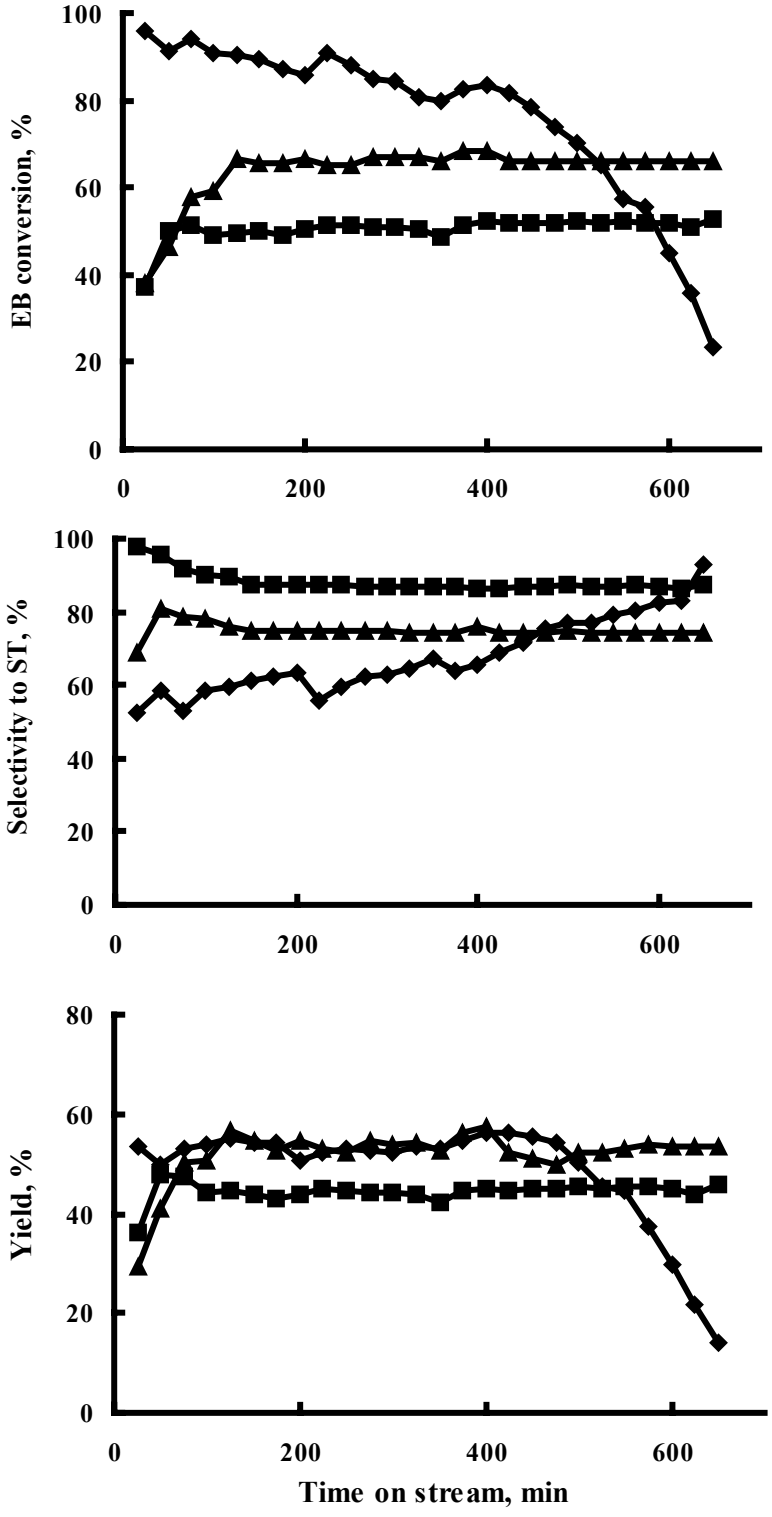

Fig. 4.1.1. Comparison of the conversions, selectivities and styrene yields over carbon black (♦), graphite (■) and nanofilaments (▲) with time on stream in the ODH of EB at 550°C.

Table 4.1.1

Comparison of the specific activities, selectivities and yields of styrene of carbon black*, graphite and nanofilaments after 7h reaction.

Catalyst	**Carbon black***	**Graphite**	**CNF's**
Specific EB consumption rate, 10^{-7} mol·m^{-2}·s^{-1}	(14.40)	3.66	3.03
Specific selectivity, 10^{-7} mol·m^{-2}·s^{-1}	(9.39)	2.94	4.97
Specific yield, 10^{-7} mol·m^{-2}·s^{-1}	(9.32)	2.93	4.67

* Values in parentheses indicate that carbon black quantitatively combusts under the reaction conditions.

Comparisons of the initial stage weight losses of carbon black, graphite and CNF´s after 12 hours on stream in the ODH of EB to ST at 550°C and also the specific surface areas of the samples before and after the reaction are presented in Table 4.1.2. The amorphous carbon black burned off as proven by the weight loss and the reduction of the specific surface area, and hence its catalytic activity decreased with time on stream. The change of the specific nature of the graphite surface can also be correlated with its weight loss and a significant loss of the specific surface area under reaction conditions (Tab. 4.1.2). The high activities of carbon black and high surface area graphite in the beginning of reaction and the absence of activation periods in the catalytic tests presumably arise from the high reactivities of the fresh surfaces with abundant defects.

The initial catalytic activity of CNF´s was low and seemed to be due to peculiarities of their fresh surface. Their activity increased about two times during the induction period, which probably indicates the formation of functional groups on the CNF's surface. Simultaneously the BET surface area increased about two times after the reaction. Both observations most probably are related with the detected carbon

deposition during reaction. Accordingly, the weight loss of CNF´s during reaction was lower in comparison to the other carbons tested (Tab. 4.1.2). This shows their high resistance toward total combustion which renders them ideal for catalysis.

Table 4.1.2.

Comparison of initial stage weight losses of the samples after 12 hours on stream, and the specific surface areas of samples before and after the ODH of EB over carbon black, graphite and CNF´s.

Sample	Activity during the initial stage	Weight loss after 12 h on stream, %	BET before reaction, m^2/g	BET after reaction, m^2/g
Carbon black	Decreasing	100	26	19
Graphite	Stabilization	25	267	69
CNF´s	Increasing	15	26	47

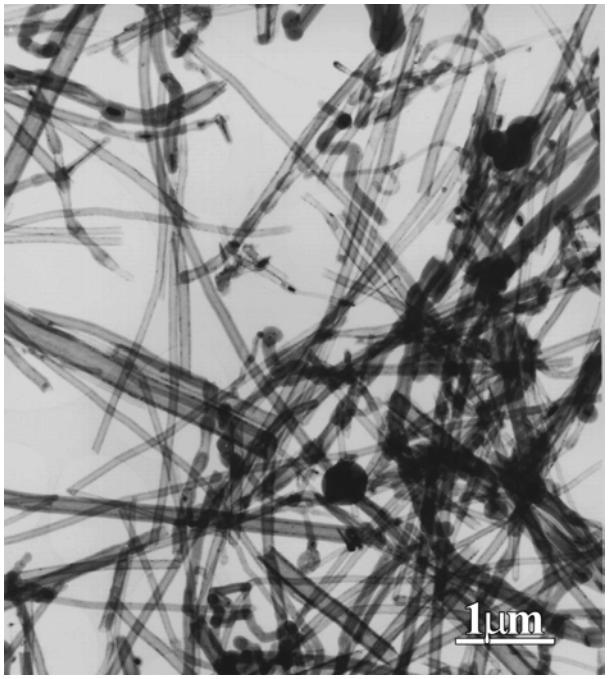

Figure 4.1.2. Representative HREM image of carbon nanofilaments before the reaction.

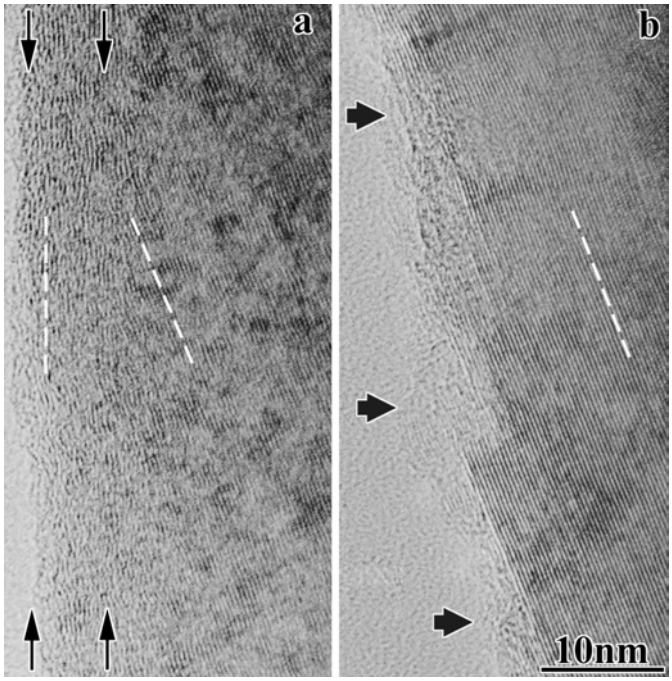

Figure 4.1.3. HREM image of the wall of a carbon nanofilament: (a) before the reaction and (b) after 20 hours on stream.

Because of their high catalytic performance and structural peculiarities, the CNF´s were characterized before and after the reaction in detail by TEM and XPS techniques. A representative HREM image of the CNF sample is shown in Fig. 4.1.2. CNF´s and chain-like filaments were observed with diameters in the range of 50 – 500 nm and a length from 100 nm to a few microns. A systematic HREM study revealed that the walls of the CNF's consisted of two layers as shown in Fig. 4.1.3, a. The filaments are built up first by an inner layer of conical graphite layers. The angle of the inclination of the graphite layers to the nanofilament axis is about 26° and their interplane distance is 0.348 nm, which is similar to that of graphite. The second outer nanofilament shell is formed by amorphous carbon layers, which are oriented parallel to the tube axis. The average distance between the layers was determined to be about 0.388 nm.

In Fig. 4.1.3, b, the wall of a carbon nanofilament is shown after 20 hours time on stream. The HREM images indicate that the outer second shell of more amorphous carbon layers has disappeared, but the wall of the nanofilament was covered by amorphous carbon, especially at the step edges between the conical graphene sheets. It is suggested that this amorphous material was deposited during the reaction in line with the unclosed carbon balance (*vide supra*). In addition, the ends of the inner conical layer seem to be partially oxidized.

These observations shed some light on the role of amorphous and graphene-like carbons in the ODH. The CNF´s were initially completely covered by a shell of amorphous carbon. After reaction, this shell has been burned off. Hence, high catalytic activity only developed after this amorphous shell was removed and the graphene layers were accessible to the gas phase. In addition, HRTEM and the carbon balance proved carbon deposition during reaction. It is proposed that this deposited carbon is comparable to polystyrene and is preferentially combusted. This preferential combustion lowers the actual oxygen partial pressure in the reactor and thus inhibits complete EB combustion. Additionally, it removes this soft coke from the active catalytic centers and prevents catalyst deactivation.

Systematic HREM observations showed the absence of Fe particles uncovered by carbon layers. Carbon combustion during the reaction did not lead to uncovered Fe particles. This observation hints that Fe particles did not take part in the reaction.

The C1s XP spectra of the carbon nanofilaments before and after the reaction are shown in Fig. 4.1.4. The major C1s signal with a binding energy of 284.8 eV is assigned to graphitic sp^2 carbon. The asymmetry of the peak toward lower binding energies is characteristic for the presence of oxygenated surface groups, *e.g.*

carbonyls, quinones, hydroxyls [1]. A detailed deconvolution of all the contributions was not attempted due to the arbitrariness of such a multisignal deconvolution. However, XPS still proved the presence of at least two different carbon species on the surface of the fresh sample (Fig. 4.1.4, a, and inset). The second species had a binding energy of about 286 eV and is attributed to carbon atoms oxygen containing surface groups, *c.g.* -OH. After reaction (Fig. 4.1.4, b), the signal intensity of these groups has strongly decreased relative to that of the graphitic carbon. This indicates their preferential burn-off during the reaction.

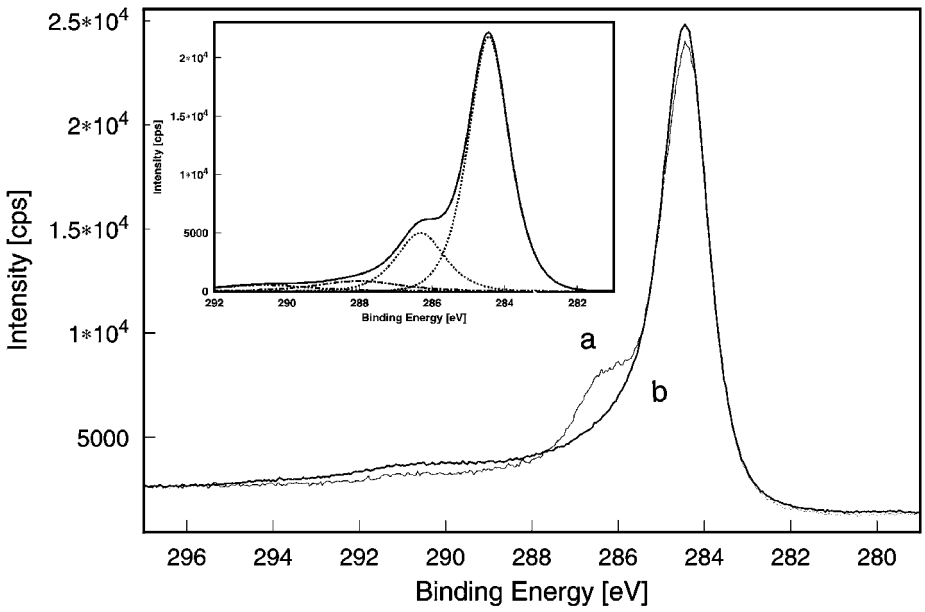

Figure 4.1.4. Carbon 1s core level spectra of carbon nanofilaments: (a) and inset before the reaction, (b) after the reaction.

Fig. 4.1.5 displays the O1s XP spectra recorded of the nanofilaments prior and subsequent to the catalytic reaction. The decrease of the oxygen content was also confirmed by the O1s XP signals. Oxygen-containing functional groups could be observed before the reaction (Fig. 4.1.5, a). After the reaction (Fig. 4.1.5, b), only a weak O1s signal was detected at 533.6 eV, which indicates a decrease of the concentration of C-O functional surface groups. This result seems to imply that the C-

O species do not actively take part in the catalytic ODH. It is suggested that the catalytic ODH reaction takes place at some other active surface sites on the graphene-like layers of the nanofilaments.

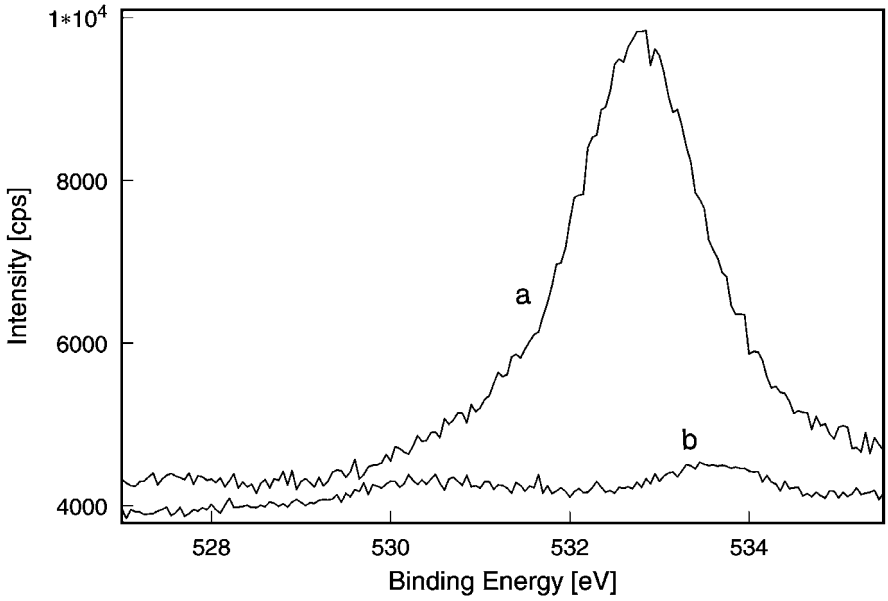

Figure 4.1.5. Oxygen 1s core level spectra of carbon nanofilaments. (a) before the reaction and (b) after the reaction.

Graphite and CNF´s showed a higher resistance toward oxidation in comparison to carbon black. Despite the higher specific activity of $3.66 \cdot 10^{-7}$ mol/m^2 shown by graphite (Tab. 4.1.1), a higher specific selectivity and specific yield of $4.97 \cdot 10^{-7}$ mol/m^2 and $4.67 \cdot 10^{-7}$ mol/m^2, respectively, were detected over CNF´s. This is explained by the general interrelation between activity and selectivity: the higher the conversion, the lower is the selectivity.

The rigid graphitic structure has the capacity to form surface groups with the labile hydrogen abstracted from EB, which favours the production of styrene [2]. The radius of curvature of the basic structural element of CNF´s and the high aspect ratio provide a high density of functional surface groups on the CNF´s for the ST formation

under reaction conditions. It is suggested that this structural peculiarity of CNF's is the reason for their high catalytic performance [3].

4.2. Nanotubes and Nanofilaments

The main goal of the studies described in this chapter was the determination of a structure-activity relationship for nanofilaments and nanotubes used as catalysts in the ODH of EB to ST. These nanocarbons of comparable particle shapes and comparable sizes differentiate themselves by details in the ordering of their carbon layers. Depending on this graphene layer ordering, the surfaces of these nanocarbons undergo different degrees of oxidation under reaction conditions, after which they exhibit different ratios of basal and prismatic planes exposed to the reaction mixture. These structural peculiarities already hint a structure-activity relationship for such carbon materials, which, if proven, might provide further insight into the fundamental reaction mechanism.

Two types of carbon filaments and two types of carbon nanotubes were used, prepared by different ways:

(i) commercially available multi-walled carbon nanofilaments (CNF´s) supplied by Applied Science Inc. (Cedarville, USA);

(ii) bamboo-like nanofilaments (BNF´s) prepared by decomposing hydrocarbons over iron nanoparticles embedded in silica by thermal CVD at 750°C and 600 Torr, supplied by Nanolab (Boston, USA);

(iii) multiwalled carbon nanotubes (MWNT´s) obtained via catalytic decomposition of ethane supplied by Prof. M. Ledoux (Strasbourg, France);

(iv) multiwalled carbon nanotubes (MWNT´s-A) synthesized using the arc-discharge graphite evaporation technique supplied by the Institute of Inorganic Chemistry of the Siberian Branch of the Russian Academy of Science (Novosibirsk, Russia).

The schematic nano-structures, the size parameters, and the specific BET surface areas of the carbon nanofilaments and nanotubes are summarized in Table 4.2.1. CNF´s consist mainly of hollow carbon filaments with relatively large mean diameters of about 100 nm and mean lengths of several microns. Small amounts of bamboo-like nanofilaments and Fe particles covered by several graphite layers were observed too (Fig. 4.2.2). The typical structure of the CNF sample is shown in Fig. 4.2.2 and 4.2.3 and described in detail in the previous chapter.

BNF´s consist of parabolically curved carbon layers stacked regularly along their tube axis in bamboo-like manner (Fig. 4.2.1). The walls of BNF´s are built up by ~10 tortuous graphene layers. The diameters of BNF´s varied from 10 to 50 nm. Such filaments were several microns long (Tab. 4.2.1).

The MWNT´s are hollow and built up by cylindrical, slightly amorphitized graphene layers oriented parallel to the tube axis. Fig. 4.2.2 shows a representative TEM image of the MWNT´s prepared by catalytic decomposition of ethane/H_2 over a Fe/SiO_2 catalyst at 750°C. The purification procedures applied after preparation yielded a pure nanotube sample. The nanotubes usually are curved, their ends are open (Fig. 4.2.2).

Table 4.2.1.

Structures and sizes of carbon nanofilaments and nanotubes used.

Sample	**Scheme of carbon layers**	**Mean length, nm**	**Mean diameter, nm**	**BET, m^2/g**
CNF´s	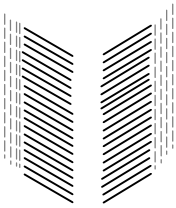	Several micrometers	100	33
BNF´s	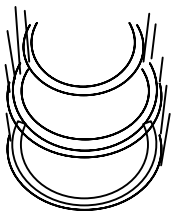	Several micrometers	30	105
MWNT´s (ethane decomposition)	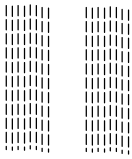	Several micrometers	25	240
MWNT´s-A (arc-discharge)	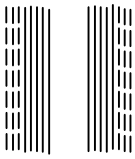	≤ 1 μm	35	28

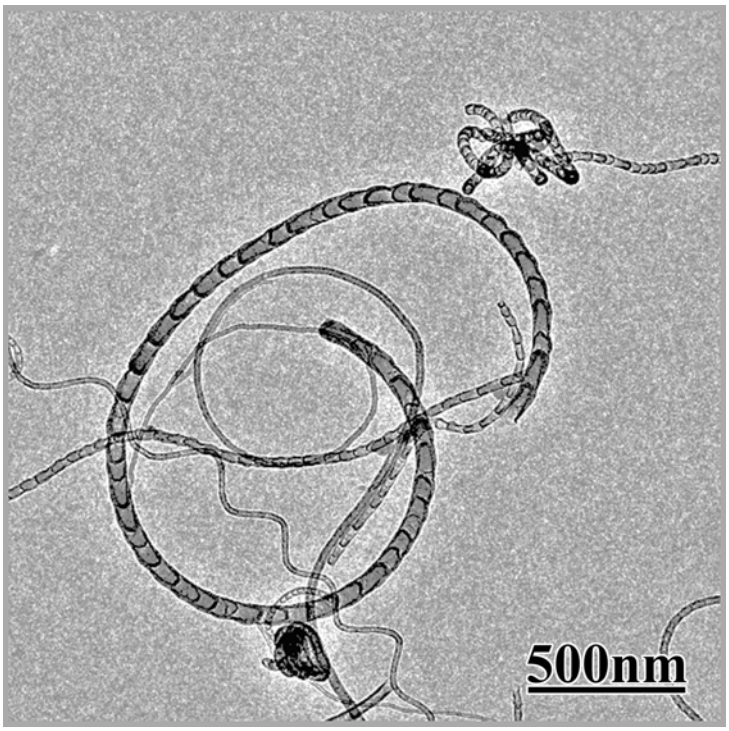

Fig. 4.2.1. TEM image of the BNF´s.

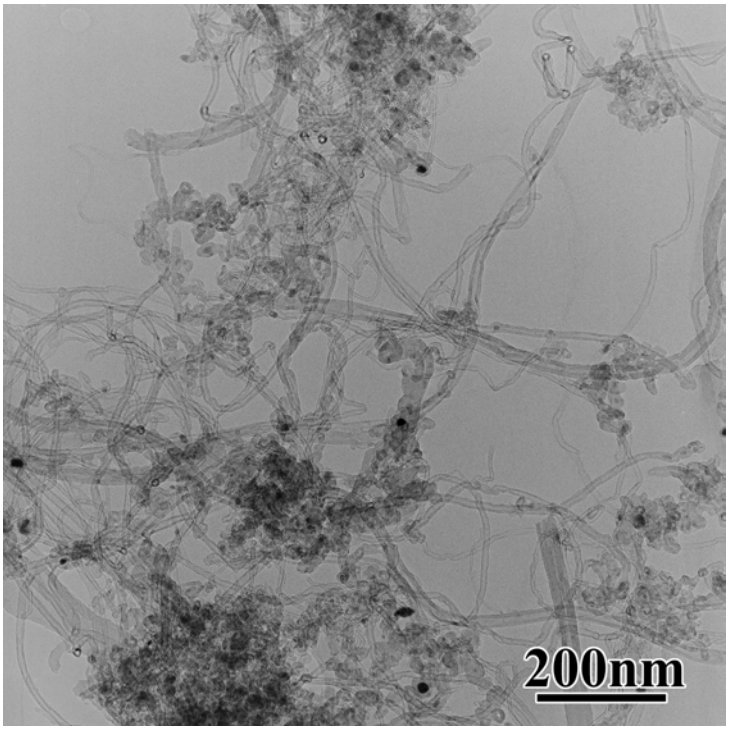

Fig. 4.2.2. TEM image of MWNT´s (ethane decomposition).

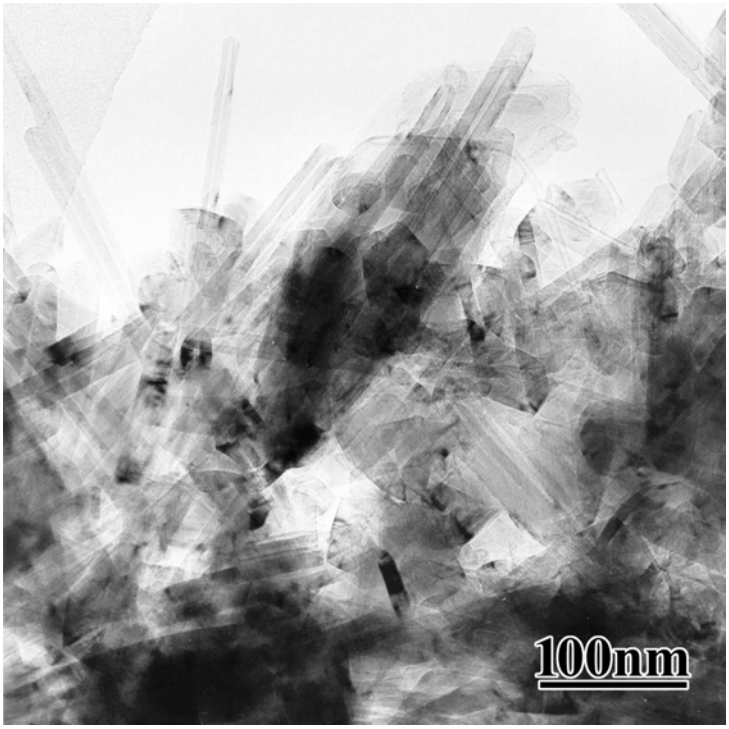

Fig. 4.2.3. TEM image of MWNT´s-A.

The MWNT-A sample prepared by the arc-discharge technique is an example for perfect multiwalled carbon nanotubes. According to TEM, these straight nanotubes consist of cylindrical carbon layers oriented parallel to nanotube axis with an interlayer spacing better comparable to graphite than those of the other nanofilaments and nanotubes (Fig. 4.2.3). The ends of these nanotubes were mainly closed with polyhedral graphite layers. The sample was purified from other carbon forms by centrifugation and subsequent calcination in air, but some graphite pieces and polyhedral carbons still remained (Fig. 4.2.3).

Temperature programmed oxidation (TPO) was used as an integral method which allows one to assess the overall crystallinity of different carbons nanotubes and nanofilaments and to obtain information on the reactivity of carbon as well as on the changes that occur in its nature under the oxidation conditions. It is well known that the less ordered carbons are in general more reactive than well-ordered carbons, *i.e.*

more ordered graphitic structures show higher resistance against oxidation. TPO was monitored by differential weight losses (DTG), differential scanning calorimetry (DSC), and evolved gas analysis (EGA). All samples combust with a single maximum oxidation rate. The maximum oxidation rate of BNF´s was observed at 530°C followed by CNF´s and MWNT´s with the maximum oxidation rates at 615°C and 630°C, respectively. The gasification profile of MWNT´s was significantly broadened in comparison to the other samples, which reflects a contribution of some amorphous material to this carbon catalyst. MWNT´s-A exhibited clearly the highest resistance against oxidation with its maximum oxidation rate at 700°C. MWNT´s-A also exhibited a complex combustion profile, probably due to a mechanism switch to uncontrolled fast combustion.

All these maximum combustion temperatures are significantly lower than that observed for pure natural graphite, which displays its maximum rate of combustion around 780°C under similar conditions [4]. The maximum oxidation rates hence mainly reflect the differences in the crystalline structures of the carbon materials, which have, and this is important in this context, comparable sizes and shapes. Obviously, the nanosize of carbon materials tested, their strong curvature, and their increasingly distorted graphitic structures account for their different combustion temperatures.

Moreover, the evolved CO and CO_2 were recorded with a quadrupole mass spectrometer combined with TPO experiments, and the CO and CO_2 evolution profiles after baseline substraction are shown in Fig. 4.2.5. Different temperatures of the CO and CO_2 release indicate different carbon reactivity with heating under oxidation conditions.

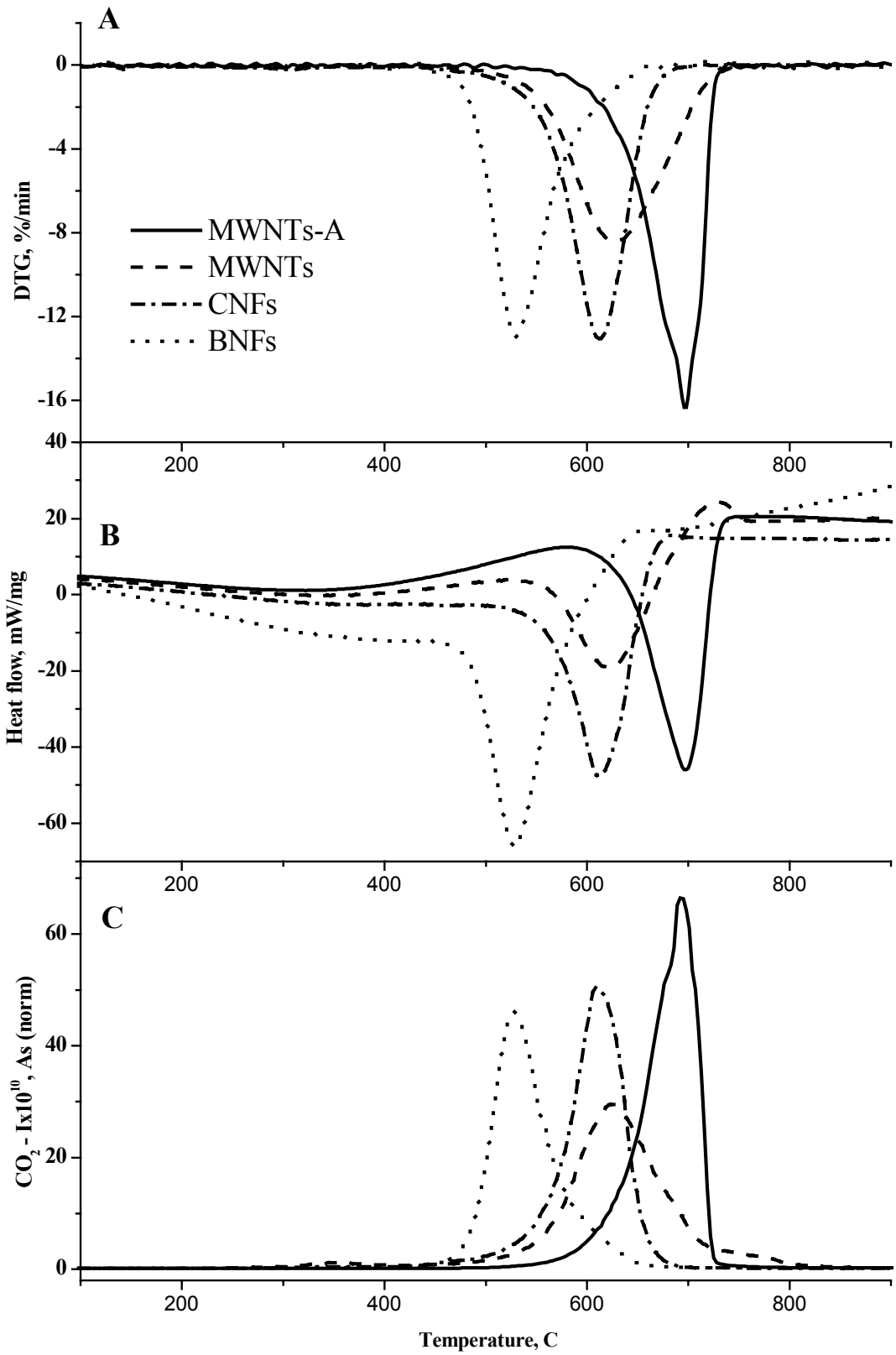

Fig. 4.2.4. TPO of carbon nanofilaments and nanotubes: (A) DTG, (B) DSC, and (C) EGA (CO_2) curves.

The combustion processes began at 550°C for MWNT´s-A, at 475°C for both CNF´s and MWNT´s, and at 450°C for BNF´s (Fig. 4.2.5). Both masses developed simultaneously for all samples. The combustion processes are completed above 725°C for MWNT´s-A, 700°C for CNF´s, 800°C for MWNT´s, and 625°C for BNF´s.

The maximum of the CO_2 and CO releases appeared at different temperatures for different nanofilaments and nanotubes studied (Fig. 4.2.5). The maximum CO and CO_2 formations were observed at about 685°C for MWNT´s-A, at 610°C for CNF´s, 625°C for MWNT´s, and at 525°C for BNF´s. The MWNT´s-A sample has shown a higher temperature of the release of CO_2 and CO due to higher crystallinity and higher resistance to oxidation. The CNF´s and MWNT´s have shown their maximum of CO_2 and CO release 75 and 60°, respectively, lower than that of MWNT´s-A. BNF´s have shown the maximum of CO_2 and CO release 175° lower than MWNT´s-A. These different combustion maximums for the carbon nanofilaments and nanotubes studied can be correlated with their degrees of crystallinity ranging from MWNT´s-A (maximum) to BNF´s (minimum). In the discussion below, it will be shown that degree of crystallinity of the carbon samples has an influence on their catalytic properties in the ODH reaction.

According to literature, there are two types of oxygenated species on the carbon surface: the first one evolves CO_2 upon decomposition and the second evolves CO [5-6]. The CO_2 evolution indicates the decomposition of carboxylic acids, whereas the CO formation points to the decomposition of basic species of a quinoidic character [5,7]. The acidic surface species decompose at lower temperatures, hence are less stable, whereas the basic surface species decompose at higher temperatures and are more stable [5,7].

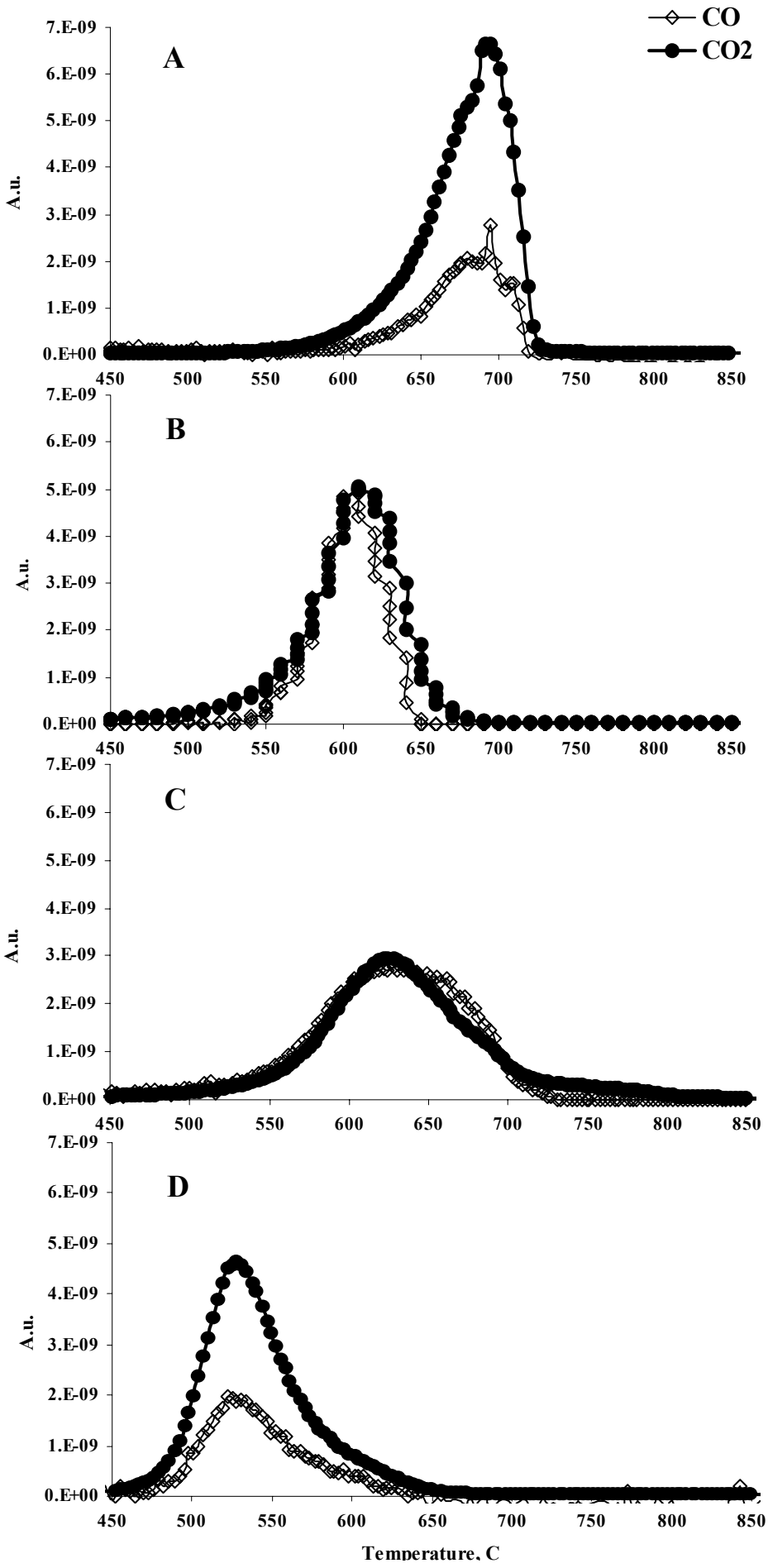

Figure 4.2.5. The CO (◊) and CO_2 (●) release with TPO experiments with (A) MWNT´s-A, (B) CNF´s, (C) MWNT´s, and (D) BNF´s.

Apparently, an increasing amount of surface oxygen with rising temperature during the TPO leads to the formation of both surface oxygenated species, i.e. the acidic and basic functionalities. The coincidence of the maximum temperatures for CO_2 and CO releases in the present TPO experiments seems to be a consequence of the selected analysis parameters (oxygen partial pressure and heating rate) [8].

The amounts of released CO and CO_2 were equal for CNF´s and MWNT´s, while about 3.3 times more CO_2 than CO was evolved at the combustion maximum for MWNT´s-A and about 2.5 times more for BNF´s. The asymmetry of the CO_2 and CO peaks evidences that the experimental curve can be deconvoluted at least on two peaks. The inhomogeneity of combustion, i.e. assymmetric peak shapes for CO_2 and CO releases, could be a sequence of mass transport limitation at maximum combustion temperature or more complicate mechanism of the combustion with the additional Boudouard equilibrium. The carbon activity in combustion process could also be different to their catalytic activity under reaction conditions because the active sites have different intrinsic activities.

Only negligible amounts of H_2O could be detected for all samples during these TPO experiments proving the absence of CH functionalities on these carbon surfaces.

Figure 4.2.6 shows the specific EB consumption rates (W), selectivities to ST (S_s) and ST yields (R_s) obtained over carbon nanofilaments and nanotubes as a function of time on stream. CNF´s displayed an induction period of about 3 hours and then a stable state with a specific EB consumption rate $W = 2.0 \cdot 10^{-7}$ $mol \cdot m^{-2} \cdot s^{-1}$, a selectivity to ST $S_s = 4.6 \cdot 10^{-7}$ $mol \cdot m^{-2} \cdot s^{-1}$, and a ST yield $R_s = 2.0 \cdot 10^{-7}$ $mol \cdot m^{-2} \cdot s^{-1}$ (Fig. 4.2.5).

The structure of CNF´s is shown in Figures 4.1.2 and 4.1.3 and described in

detail in the previous chapter. The oxidation of the outer amorphous layers led to the exposure of the herring-bone graphene structure to the reaction mixture, which were also oxidised with the formation of step edges (Fig. 4.2.3). The formation of these oxidised step edges is suggested to lead to the significant catalytic activity.

The specific EB consumption rates, selectivities and ST yields obtained over BNF´s and MWNT´s were very low during all time on stream. The BNF's did show a specific EB consumption rate $W = 0.34 \cdot 10^{-7}$ mol·m^{-2}·s^{-1}, a selectivity to ST $S_s = 0.26 \cdot 10^{-7}$ mol·m^{-2}·s^{-1} and a ST yield $R_s = 0.43 \cdot 10^{-7}$ mol·m^{-2}·s^{-1}. The activity of MWNT's was close to that of BNF´s with $W = 0.18 \cdot 10^{-7}$ mol·m^{-2}·s^{-1}, $S_s = 0.43 \cdot 10^{-7}$ mol·m^{-2}·s^{-1}, and $R_s = 0.23 \cdot 10^{-7}$ mol · m^{-2}·s^{-1} (Fig. 4.2.6).

MWNT's-A showed a long induction period, after which a stable catalytic performance was reached with an activity much higher than those over the other samples tested. MWNT's-A showed $W = 2.9 \cdot 10^{-7}$ mol·m^{-2}·s^{-1}, $S_s = 5.35 \cdot 10^{-7}$ mol·m^{-2}·s^{-1}, and $R_s = 4.15 \cdot 10^{-7}$ mol·m^{-2}·s^{-1} under steady state (Fig. 4.2.6).

The specific EB consumption rates, selectivities to ST and ST yields over BNF´s and MWNT´s were several times lower than those over CNF´s and MWNT´s-A. Obviously, such different catalytic activity is a sequence of the different density of active sites located on the surfaces of these carbon nanostructures. The density of active sites per square unit of BNF´s and MWNT´s surfaces was several times lower than that for CNF´s or MWNT´s-A.

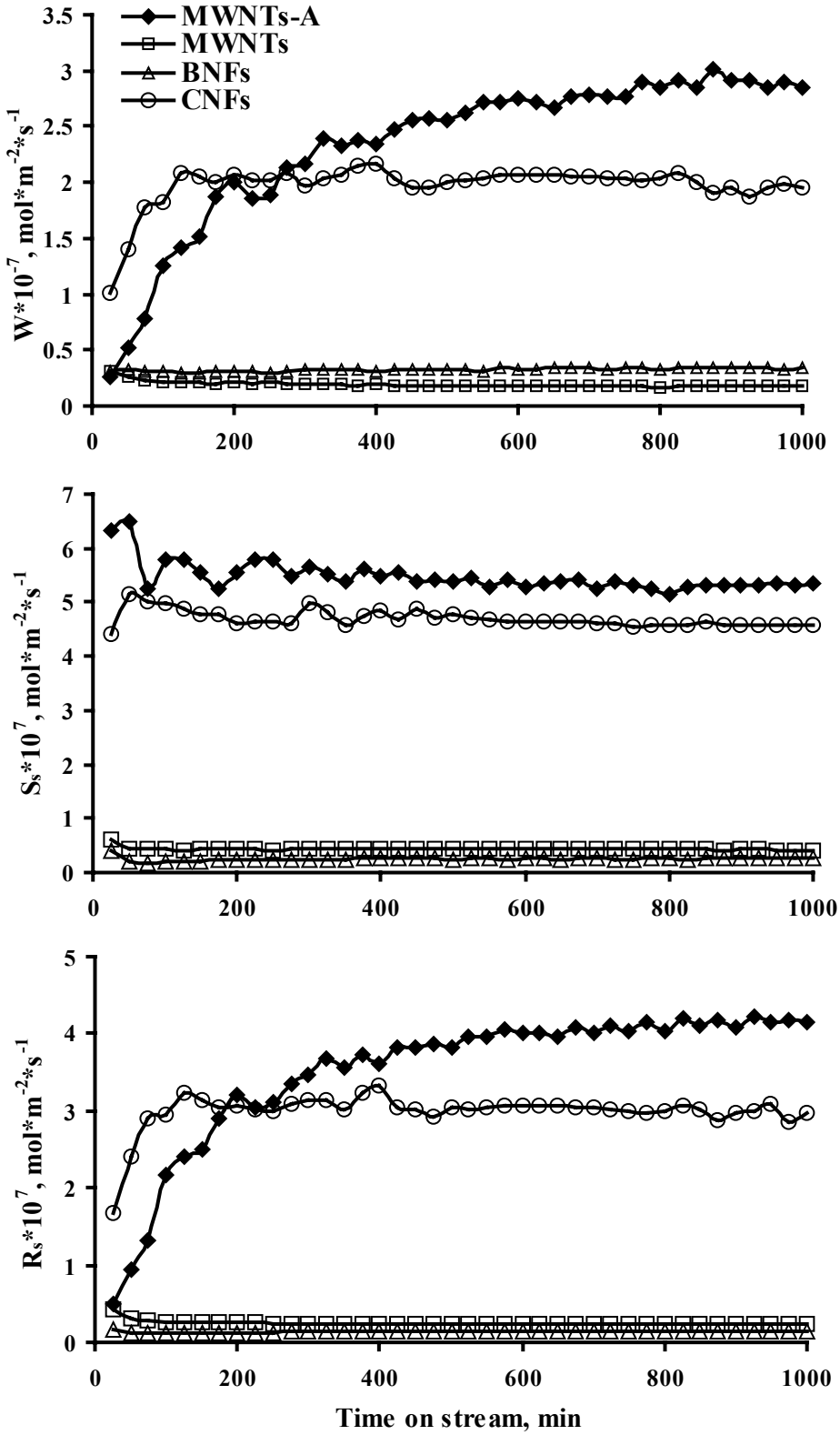

Fig. 4.2.6. The reaction rates (W), specific selectivities to ST (S_s), and specific ST yields (R_s) over carbon nanofilaments and nanotubes in ODH of EB to ST at 520°C.

According to TEM and TPO, the BNF´s and MWNT´s structures are more amorphous than those of CNF´s and MWNT´s-A. According to TEM, fresh MWNT´s-A are characterized by a well crystallised graphitic structure with a large abundance of basal planes combined with very small number of prismatic faces. After the catalytic reaction, the formation of step edges within the basal planes was observed, which led to an increase of the amount of exposed prismatic planes. The active and selective sites for oxidative EB dehydrogenation seem to be located at these step edges. The formation of step edges during reaction leads to an increase of the density of active sites with time on stream. But, it is a very slow process due to the high resistance of these nanotubes toward oxidation compared to the other nanofilaments and nanotubes tested (Fig. 4.2.4).

From the steady state product distributions over carbon nanofilaments and nanotubes presented in Table 4.2.2, it can be seen that the lowest ST formation took place over BNF´s, and it was accompanied by accordingly higher CO and CO_2 formations. A higher amount of ST and accordingly lower amounts of CO and CO_2 were observed over CNF´s and MWNT´s formations. The highest ST formation and hence the lowest CO and CO_2 formations were observed over MWNT´s-A formations. This fact confirms that the structure of MWNT´s-A results in a higher selectivity to ST formation than those of other carbons, *i.e.* the structure of MWNT´s-A seems to have the optimum structure.

Table 4.2.2.

Product distributions of EB ODH over carbon nanofilaments and nanotubes at steady state.

Sample	Ethene %	Benzene %	Toluene %	ST, %	CO, %	CO_2, %	EB conversion,%
CNF´s	0.00	4.3	1.71.53	42.3	1.9	10.45	65
BNF´s	0.04	1.07	0.06	19.40	2.27	31.63	55
MWNT´s	0.13	0.70	0.12	28.71	2.44	22.10	55
MWNT´s-A	0.06	1.04	0.54	56.00	9.85	11.70	70

The amounts of CO formed over CNF´s, BNF´s, and MWNT´s was several times lower than those of CO_2 formations. However, in the case of MWNT´s-A, the amount of CO was close to CO_2 (Tab. 4.2.2) formations. These observations could possibly be explained by the chemical nature of the surface of the MWNT´s-A, being of higher crystallinity, which changes under reaction conditions. Consequently, the higher formation of CO over MWNT´s-A could be related to the higher concentration of basic surface groups relative to the other carbons tested. Obviously, such a process depends on the availability of active sites, which can be regenerated by decomposition to CO. Further aspects of the acidity and basicity of the functional groups formed are discussed later in Chapter 5.1.

Figure 4.2.7 shows the product distribution over MWNT´s-A as a function of time on stream. In the beginning, a low formation of CO_2 and CO was observed formations. The CO_2 and CO yields being close to zero in the beginning increased at the same time to 13 and 9%, respectively. The increasing formations of CO_2 and CO with time on stream is suggested to be related to an increasing combustion of carbonaceous deposits reflecting the surface changes under reaction conditions. This

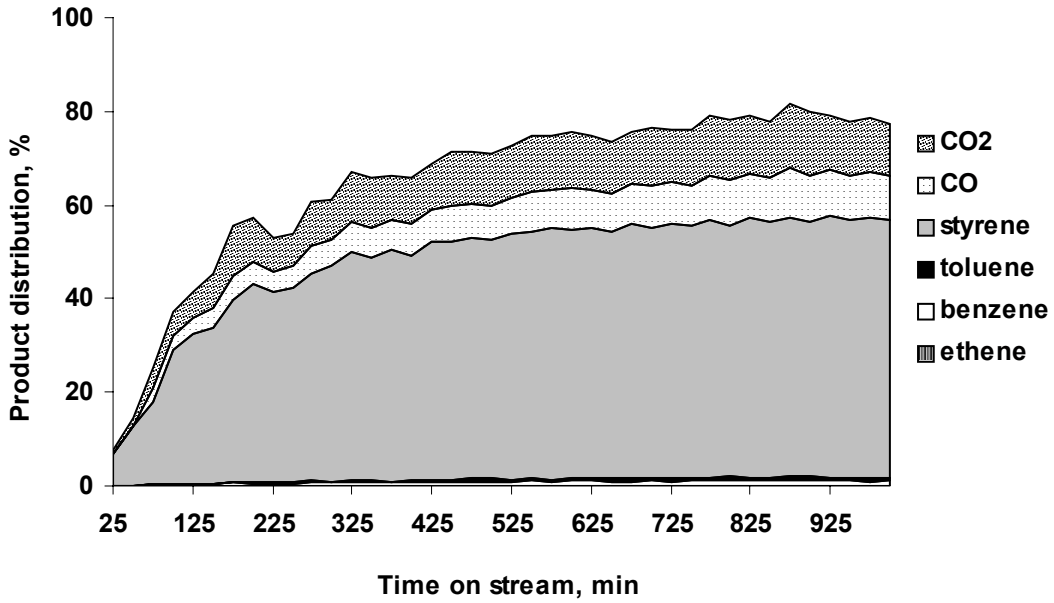

Fig. 4.2.7. Product distribution in ODH of EB at 520°C over MWNT´s-A as a function of time on stream.

is also in the good agreement with the increasing oxygen consumption. These changes of the surface might also lead to a change of the reaction paths and reaction kinetics. Kinetic aspects of the ODH reaction are discussed in more detail further in Chapter 5.2.

The low initial activity of MWNT´s-A is thought to be a consequence of the abundance of basal planes on the fresh surface. Under reaction conditions, defects and step edges are increasingly formed via a surface oxidation (TEM), and hence, prismatic planes increasingly developed. The increasing number of prismatic faces relative to the basal planes considerably enhanced the catalytic activity. It is suggested that these prismatic planes of well-crystallized nanocarbons are responsible for their catalytic reactivity.

4. 3. Onion-Like Carbon

Onion-like carbons (OLC) consist of several almost spherical shells (Fig. 4.3.1) and constitute a highly interesting new type of carbon nanoparticles. Although these carbon shapes are not crystals in the strict sense, they do possess some symmetry and their building units (B.U.) are crystalline graphene sheets. The outer shells are formed by spherical tiling of small graphitic domains [9]. The distance between the shells is comparable to that of the graphite spacing (0.34 nm). The BET specific surface area of OLC was measured to be 456 m^2/g. These closed spherical carbon shells could possess interesting catalytic properties due to the almost perfect

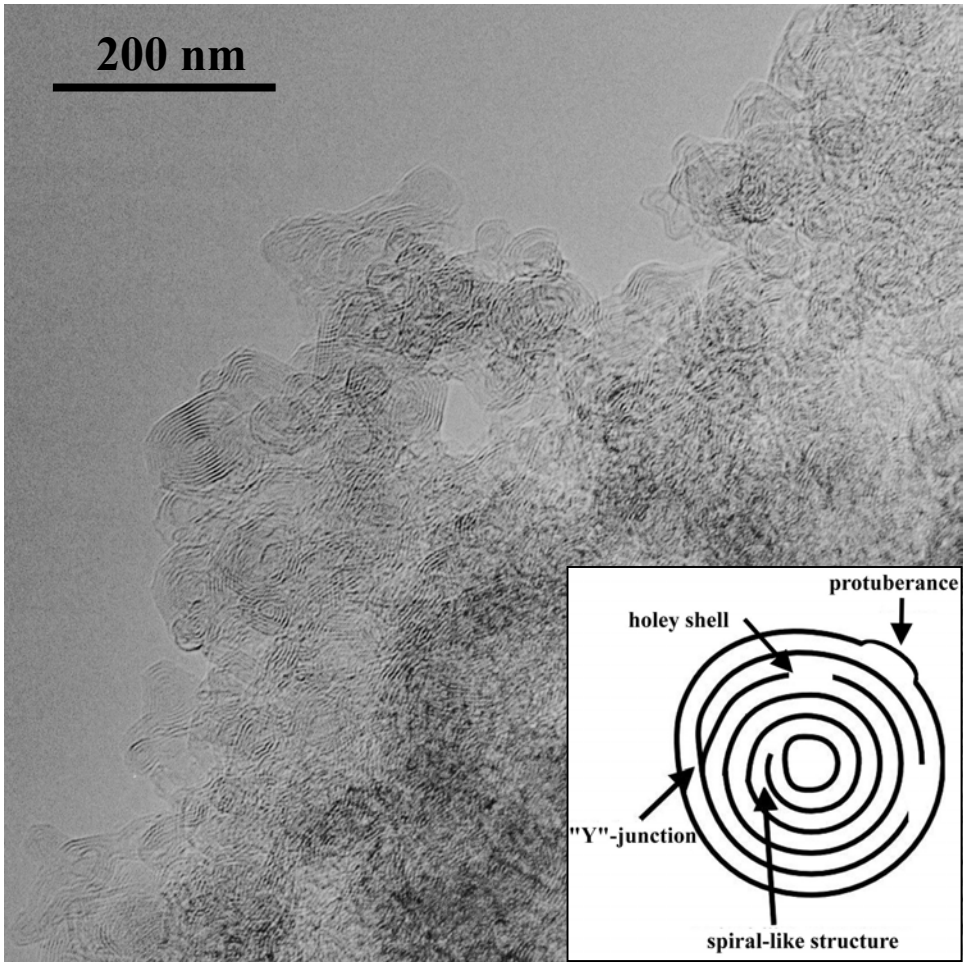

Fig. 4.3.1. TEM image of the OLC sample and schematic drawing of an OLC particle with possible defects (inset).

graphitic network with a high degree of curvature and their high BET surface area.

The porosity of carbon materials so far seems to play a negative role in the ODH of EB by hindering the ST desorption, which limits the EB conversion and leads to non-selective, consecutive reactions [10]. Due to the absence of inner particle porosity, OLC are valuable candidates for the study of this reaction as compared to other forms of sp^2 carbon materials.

Figure 4.3.2 displays the catalytic behavior of the OLC material on a mass referenced basis in the ODH of EB to ST at 515°C. For comparison, the steady state yields obtained over the industrial $K_2Fe_{22}O_{34}$ catalyst (K-Fe) at 680°C and other forms of carbons at 550°C (Chapter 4.1) are also shown. The OLC catalyst exhibited a very low initial activity with 19% EB conversion and a predominant ST formation, developing into conversion levels of 92% after an activation period of about 2 hours on stream. The yields of ST and all by-products increased during this induction period and ST yields of 62% with a ST selectivity of 68% were reached at the steady state.

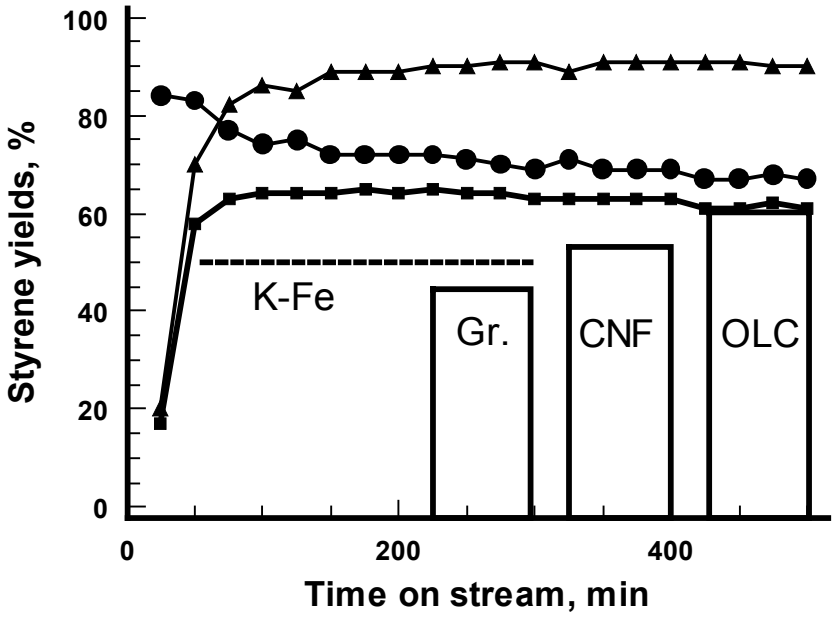

Fig. 4.3.2. Performance of OLC in the ODH of EB at 515°C with time on stream: EB conversion (7), selectivity to ST (●) and ST yield (■).

The product distribution under steady state is 0.06% ethane, 2% benzene, 1.2% toluene, and 14% CO and CO_2 each. A carbon balance estimated for the first measured point was as high as 200%. Subsequently, it decreased during the induction period and reached 80% at the steady state. The changing carbon balance indicates an initial oxidation of the OLC, *i.e.* formation of step edges, during induction period, which decreased, and carbon deposition at steady state.

During the induction period, the EB conversion increased 4.5 times and the ST yield increased 3.5 times. Such radical increase of the catalytic activity accompanied with changes in carbon balance seems to be a consequence of some surface reformations leading to the generation of the finally active carbon surface during the first 2 hours in stream.

The specific EB consumption rate increased during the induction period and was close to $W = 0.1 \cdot 10^{-7}$ $mol \cdot m^{-2} \cdot s^{-1}$ at steady state. This rate is 20 times lower than that of MWNT's-A (Fig. 4.2.5). This low specific EB consumption rate over OLC hints a very low concentration of active centers, which are highly diluted on this high surface area material.

High resolution transmission electron microscopy of fresh OLC (Figure 4.3.3 A, a) showed clean, multi-shell particles with an interlayer distance close to 0.35 nm, typical for sp^2 carbon structures. The inset of Fig. 4.3.3A a shows the magnification of a single, intact OLC. The arrows indicate blurred regions of less ordered structure. A TEM image of the OLC sample after the reaction is shown in Figure 4.3.3A b. The difference in contrast as compared to the image prior to catalysis confirmed the formation of ill-defined carbon during the reaction.

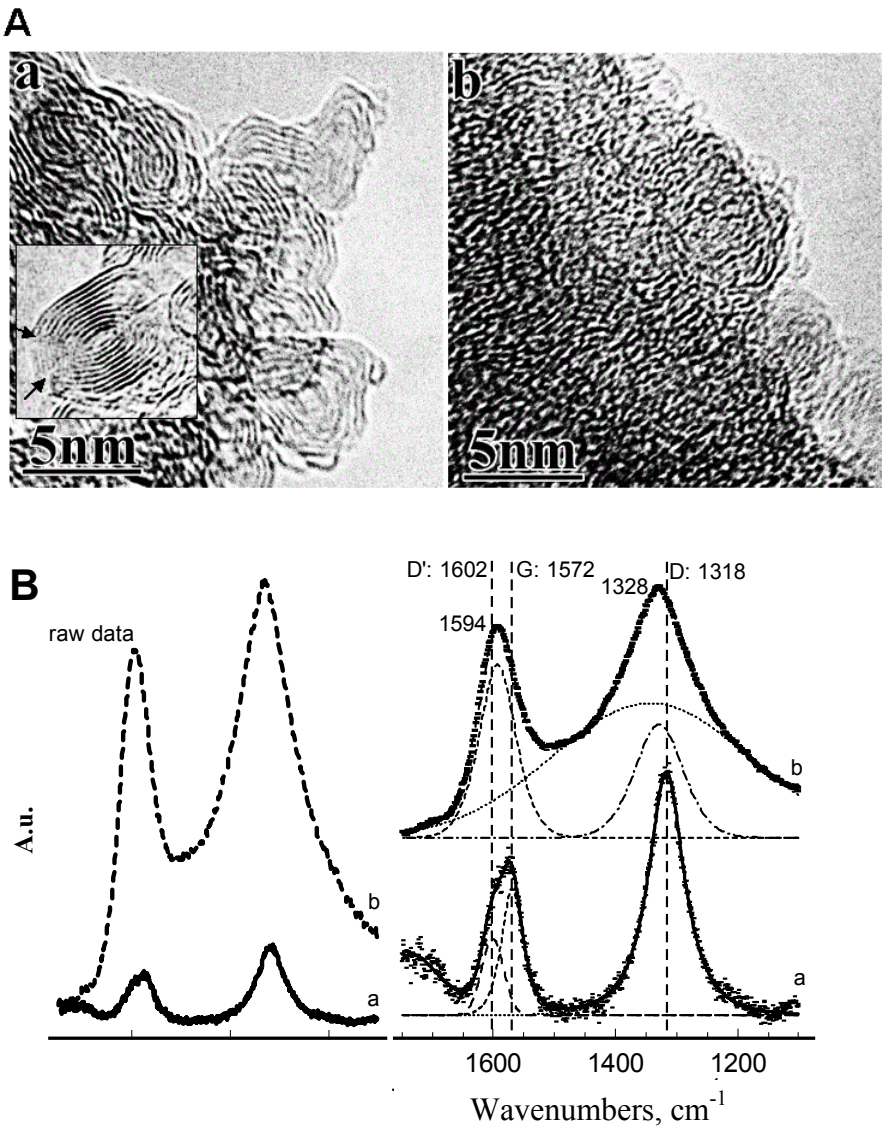

Fig. 4.3.3 **A.** High resolution TEM images of OLC (a) before and (b) after ODH of EB. **B.** Left side: original Raman spectra of OLC (a) before and (b) after the reaction. Right side: deconvolution of the Raman spectra (a) before and (b) after the reaction.

Raman spectroscopy revealed the nature of this ill-defined carbon. Figure 4.3.3 B shows the experimental spectra obtained from the fresh (spectrum a) and used (spectrum b) OLC on its left side. The Raman spectrum of fresh OLC (Fig. 4.3.3 B, spectrum a) exhibits the Raman bands characteristic for disordered (D: 1318 cm^{-1}, and

D': 1594 cm^{-1}) and ordered (G: 1573 cm^{-1}) graphene structures [11-13]. The theoretical positions of reflections of graphite (G) and diamond (D) are shown for comparison. This Raman spectrum is in agreement with the high resolution TEM analysis, which revealed intact graphene layers and ill-defined structures at the curvatures of OLC (Fig. 4.3.3 A, image a). The intense Raman signature of the D (1328 cm^{-1}) and D' (1594 cm^{-1}) bands of the catalyst subsequent to reaction, completely overwhelming the G band at 1573 cm^{-1}, clearly evidenced a pronounced presence of disordered carbon structures after the catalytic test. The intensity increase of the two D and D' Raman signals was accompanied by a broadening and a slight shift of the D band. The deconvolution additionally revealed a very broad background contribution to this band due to C-H, C-C deformations [14].

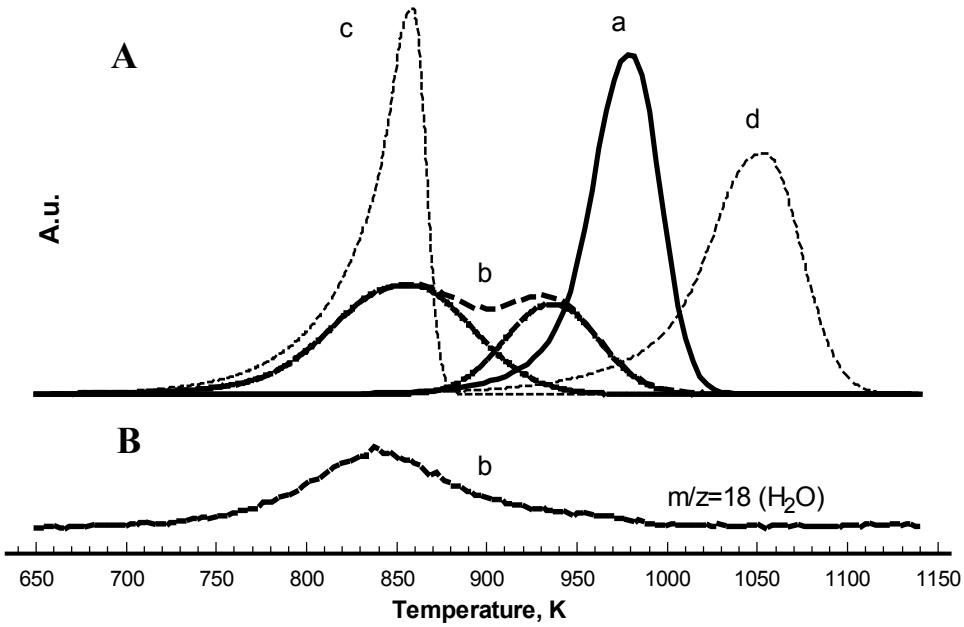

Fig. 4.3.4. Differential Thermal Gravimetry of the temperature-programmed combustion of OLC. **A.** (a) before, (b) after ODH of EB, (c) amorphous carbon (Norit A, Aldrich), and (d) graphite (SFG6, Timcal AG). **B.** Mass spectrometer trace of water formed during the combustion of OLC subsequent to the reaction.

In addition to Raman spectroscopy, temperature-programmed combustion confirmed the presence of two carbon species (Figure 4.3.4). As compared to the fresh, well-organized sp^2-bonded OLC (a), the used active catalyst displayed a composite signal (b), which evidenced disordered sp^2-/sp^3-carbon with a maximum combustion rate at around 580°C, in agreement with the reference, amorphous activated charcoal. The contribution to combustion at higher temperatures assigned to remaining ordered sp^2 carbon structures. The water release simultaneous to the low temperature combustion peak confirmed the presence of hydrogen atoms in the highly disordered carbon.

Fig. 4.3.4 shows the O1s and C1s XP spectra obtained for the fresh and used OLC material. X-ray photoemission spectroscopy proved that the almost oxygen-free

carbon surface of the fresh OLC (solid line, Fig. 4.3.4 A) was transformed after reaction into an oxygen-containing surface (open circles, Fig. 4.3.5 A). The deconvolution into two contributions with a binding energy (B.E.) of 531.1 and 533.4 eV is shown too. The O1s spectrum after reaction can also be deconvoluted into two signals. The first is due to chinoidic carbonyl functions with B.E. of 530.9 eV [1] similar to spectra reported for other active carbon catalysts [11,15]. The dehydrogenating power of the catalyst thus seems to be linked to the generation of these strongly basic sites during activation. The second contribution with a B.E. of 533.4 eV arises from water adsorbed during transport through air.

The C1s spectra (Fig. 4.3.5, B) indicated the presence of oxidized carbon by an increased intensity at the high energy wing of the C1s signal. The inset of Fig. 4.3.5, B shows the difference spectrum of used (full line) and fresh OLC (dotted line). Its deconvolution confirmed the presence of two contributions at 288.2 eV, indicative for basic, chinoidic surface groups, and 286.0 eV due to C-O groups. Additionally, the graphitic C1s line at 284.4 eV was considerably broadened after catalysis proving the presence of structurally ill-defined carbon in line with Raman, XRD and TG-TPO.

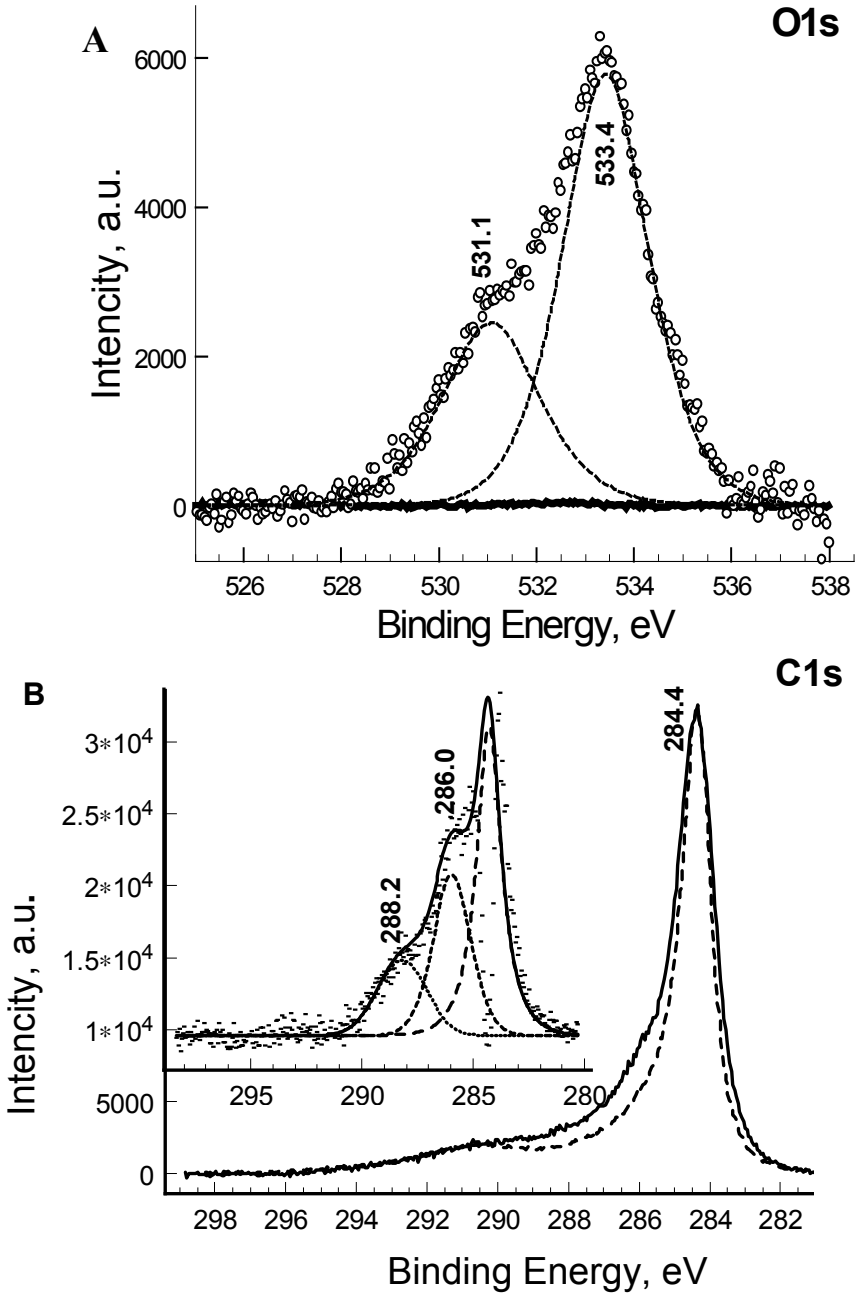

Fig. 4.3.5. **A.** O1s XP spectra of the OLC before (solid line) and after (open circles) to ODH of EB to ST. **B.** C1s XP spectra of OLC before (dashed line) and after (full line) the reaction. The inset shows the deconvolution of the difference C1s spectrum into three contributions with B.E. of 288.2, 286.0 and 284.4 eV.

The structural characterization reveals that the function of the OLC carbon as ODH catalyst is uniquely related to its microstructure. The starting material, intact

OLC with a large surface abundance of graphitic (0001) facets combined with a small abundance of edge/kink sites where the bending of the graphene layers occurs (blurred contrast in the TEM), is characterized by the complete absence of surface oxygen functionalities. In addition, the catalytic test revealed that this material does not show initial catalytic activity. Catalytic activity develops with time on stream. XPS characterization proves the generation of strongly basic, chinoidic surface functionalities on the active carbon catalyst. It is suggested that these basic dehydrogenating surface groups are generated as the resonance stabilized C=O surface terminations of the edge/kink regions of OLC. This oxidation of the edge/kink sites is also seen as being responsible for the disintegration of the OLC during catalysis. The catalytic activity develops with increasing formation of these basic functionalities and accordingly increasing OLC disintegration. Hence, it may be questioned whether OLC are catalytically active at all.

The fact that carbon derived from OLC is superior in its performance on a mass referenced basis compared to other forms of carbons [3] evidences that this type of carbon contains a higher number of active sites per unit weight at steady state. This superior performance is also related to the optimized distribution of the sites required for oxygen activation (basal planes) and Broensted basic centers (prismatic planes) on this type of nanocarbon.

The presence of disordered, sp^2 and sp^3 polymeric carbon resulting from unwanted styrene polymerization is characteristic of all catalytic systems tested so far [16-17]. Its voluminous and defective character makes it, however, particularly susceptible to oxidation *in situ* as evidenced by the data in Figure 4.3.4. A large difference in specific reactivity of the soft coke [18] to the carbon catalyst is a prerequisite for stable operation as the formation of coke cannot be completely

avoided. By reducing the basic sites required for polymerization to the minimum necessary for activating the EB substrate, the tendency for coke formation is smaller on carbon than on (potassium promoted) metal oxide systems.

The present data reveal that a significant potential for catalytic application lies in unpromoted nanocarbon materials if their microstructure can be tailored to support the optimum distribution of electron donating and proton activating functions. The chemical simplicity of carbon and the unique property that deactivated surfaces gasify themselves in ODH reactions not only renders them well-suited model systems but also allow for realistic expectations of a technical application in heterogeneous catalysis. Research on onion-like carbons is confined to the development of synthesis methods and to the description of physical and chemical properties [19]. The synthetic limitations of the present OLC model system may be overcome by tailoring other more abundant forms of carbon into the desired target structure by synthetic and post-synthetic thermochemical procedures [4].

4.4. Ultra-Dispersed Diamonds

The influence of the nature of different types of carbons on their performances in ODH of EB to ST was further investigated by comparing the activities, selectivities and ST yields of non-planar sp^3- and sp^2-hydridized nanocarbons.

Ultra-dispersed diamond (UDD) was chosen as the reference for sp^3-hybridized carbon because of its comparable nanometer particle sizes. Differently heat-pretreated UDD samples were used, this thermal annealing inducing a gradual transition to OLC, in order to study the formation of active sites on sp^3- and sp^2-hybridized carbon surfaces.

4.4.1. Catalytic performance of sp^3-hybridized carbon in ODH of EB to ST

The catalytic test over the UDD sample was conducted under the same reaction conditions as over nanotubes, nanofilaments and OLC (Chapters 4.2 and 4.3). An initial conversion of EB of 92% was accompanied with a selectivity to ST being as low as 25% and, hence, a ST yield of 25% (Fig. 4.4.1). The amounts of ethene and toluene formed were low with 0.7 and 1.9%, respectively. The high initial benzene formation of 33% was unexpected that was not observed over other carbons tested. The yields of CO and CO_2 were 4% of 30%, respectively, under such conditions. An induction period of 3 hours was observed, during which both the selectivity to ST and the ST yield increased to 50 and 44%, respectively, but the EB conversion slightly decreased to 90%. After the induction period, the ST yield and the selectivity to ST decreased, until the steady state was reached with a selectivity to ST of 48% and a ST yield of 38%. Both benzene and CO_2 yields decreased during this induction period to

8 and 23%, respectively. The yields of other by-products remained constant at their initial levels. The EB conversion further decreased slowly to the conversion level of about 80% after 15 hours on stream.

The carbon balance estimated at the first measured point was 62%. Then, it increased and reached 99% after 2 h on stream. Subsequently, the carbon balance slowly decreased again to 80% to become stable. The carbon balance behavior indicates the deposition of carbonaceous material on the catalyst from the EB source in the very beginning of reaction and under steady state. The alterations of the carbon balance during the induction period might hint some reorganization of the carbon surface. The changing carbon balance together with the changing product distribution suggests a change of the reaction mechanism during the induction period.

The estimated specific EB consumption rate slightly decreased during the induction period, after that it was stable at $0.165 \cdot 10^{-7}$ $mol \cdot m^{-2} \cdot s^{-1}$. This value was comparable with the specific EB consumption rate over OLC. But the completely different catalytic activities of UDD and OLC samples, evidenced by different product distributions, allow one to suggest different reaction processes taking place over these carbon materials under identical reaction conditions.

A characteristic TEM image of the fresh UDD sample is shown in Fig. 4.4.2, a. The carbon layers within the UDD particles show interplanar distances of 0.206 nm that is characteristic for sp^3-hybridized carbon. Some UDD particles seem to be enclosed by a very thin amorphous overlayer (~1 carbon layer).

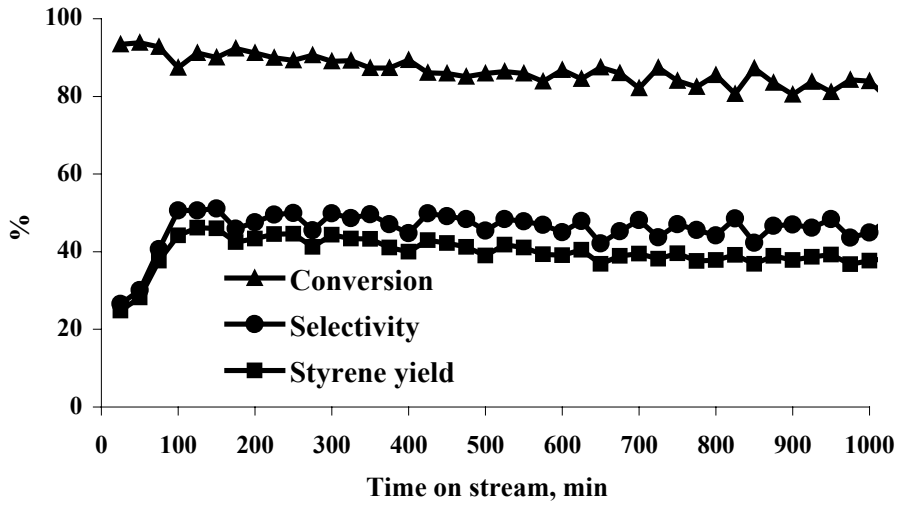

Fig. 4.4.1. Catalytic behaviour of UDD in the ODH of EB to ST.

In comparison to the fresh sample, the amorphous overlayers on the UDD particles after 24 h time on stream were considerably thicker with up to 5 carbon layers (Fig. 4.4.2, b). These disordered carbon overlayers show interplanar distances close to 0.35 nm being characteristic for sp^2-hybridized carbon.

A high rate of benzene formation was observed during the time on stream experiments over UDD. A comparison of the benzene to ST ratios as a function of time on stream for sp^3- and different sp^2-hybridized carbons is shown in Figure 4.4.3. The initial rate of the benzene formation was two times higher than the initial ST formation rate over the fresh sp^3-hybridized carbon surface. However, the benzene formation decreased during the first 3 h on stream simultaneously with an increase of the ST formation (Fig. 4.4.3). Presumably, the decrease of the benzene formation occurred parallel to the observed formation of the sp^2-carbon overlayers. Hence, the observed switch of the reaction pathway from the initially predominant benzene formation to the predominant ST formation at steady state can be explained by the formation of this overlayer (Fig. 4.4.2, b). The still significant benzene formation rate at steady state (~8 % yield) might be explained by an incomplete coverage of the

UDD particles with sp^2- carbon. According to the result obtained over UDD and from the negligible benzene to ST ratios over all the tested sp^2- carbons, it can be concluded that the sp^3- carbon surface is not selective for the ST formation in the ODH of EB.

The determined specific catalytic activities confirm the completely different catalytic behaviours of the OLC and UDD samples with time on stream (Table 4.4.1). The rate of the EB conversion over OLC was low in the beginning, and then it increased several times during an induction period. In the contrary, the rate of the EB

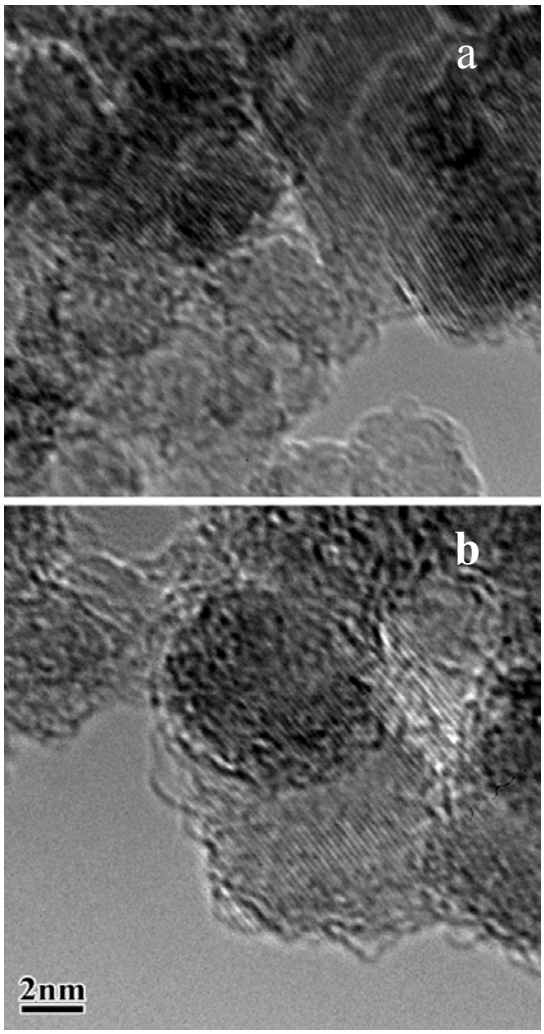

Fig. 4.4.2. TEM image of the UDD sample (a) before and (b) after the catalytic test.

conversion over the UDD sample was significant in the beginning, and then it slightly decreased with time on stream. Under steady state, the specific catalytic activity of the OLC sample was superior to that of UDD. As seen from Table 4.4.1, the specific BET

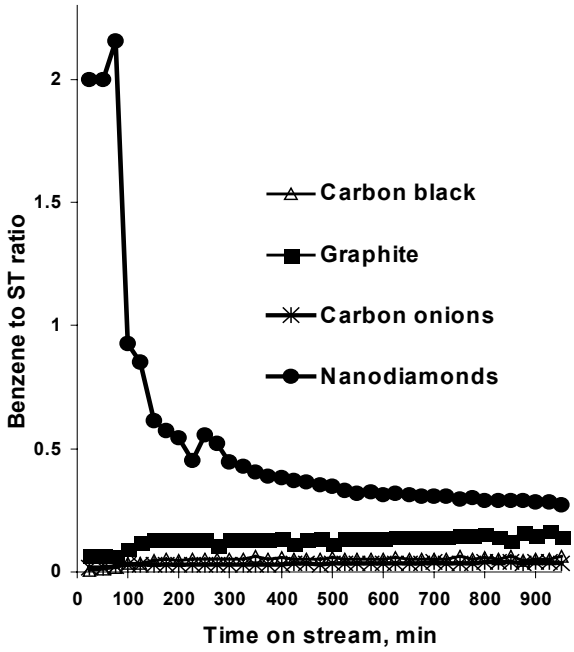

Fig. 4.4.3. The benzene to ST ratio as a function of time on stream over carbon black, graphite, OLC and UDD samples.

surface area decreased during the reaction for both, the OLC and UDD samples.

Table 4.4.1.
Comparison of the specific catalytic activities and specific surface areas before and after the ODH of EB over OLC and UDD.

Sample	Initial EB reaction rate mol/(m^2·s)	Steady state EB reaction rate, mol/(m^2·s)	BET before reaction, m^2/g	BET after reaction, m^2/g
OLC	$0.25 \cdot 10^{-7}$	$1.2 \cdot 10^{-7}$	456	276
UDD	$1.12 \cdot 10^{-7}$	$0.99 \cdot 10^{-7}$	297	199

These textural changes prove the filling of micropores with soft coke deposited during the reaction (HRTEM).

In order to characterise the surface changes of the UDD sample during the catalytic reaction, an XPS analysis was performed of the samples before and after the reaction. A comparison of the C1s XP spectra of the UDD sample before and after the reaction is shown in Fig. 4.4.4. Generally, the main C1s peak of the carbon samples appears at 284.6 eV (dashed line). However, charging of the insulating UDD sample uncontrollably affects the measured kinetic energies of the photoelectrons and leads to a shift of C1s peak from its regular position. A fresh UDD sample shows a symmetric C1s peak with its maximum at 288.5 eV assigned to sp^3-hybridized carbon. The C1s peak after the reaction is less shifted from its regular position and it has an asymmetric shape (Fig. 4.4.4). This asymmetric C1s peak with its visible shoulder was deconvoluted on the basis of two components: the first one at 288 eV corresponds to sp^3-hybridized carbon (dashed line), the second one at 286.5 eV corresponds to sp^2-hybridized carbon (dotted line). Obviously, the C1s core level spectrum of the UDD sample after reaction reflects the presence of two kinds of carbon, the sp^3- and sp^2-carbon on the sample surface. The presence of these two carbons on the UDD's surface after the reaction reflects the deposition of the sp^2-carbon during time on stream. From the peak integrals, it can be estimated that the relative surface concentration of the sp^2-hybridized carbon is 2.45 times higher than that of the sp^3-hybridized carbon (Fig. 4.4.4).

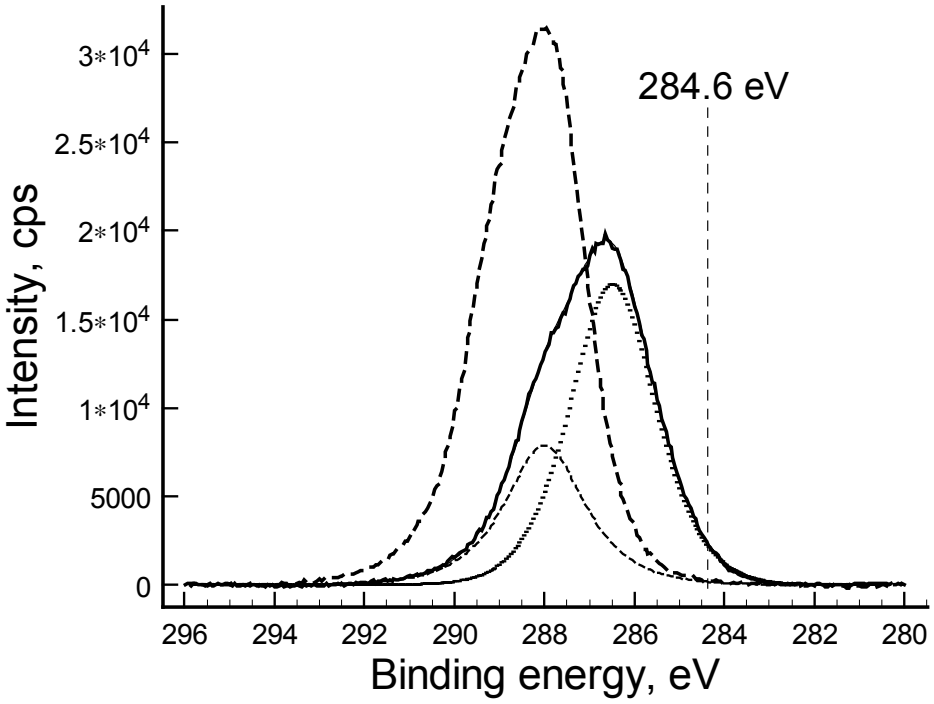

Fig. 4.4.4. C1s core level spectra of UDD before (dashed line) and after catalytic test (solid line). The latter is deconvoluted into its two contributions (dashed and dotted lines).

In order to clarify the nature of the functional groups present on the UDD surface and to characterise the surface changes under reaction conditions, an IR spectroscopic analysis was performed. Figure 4.4.5 shows the IR spectra of the UDD sample before and after reaction. The IR spectrum of the fresh sample (solid line) shows a strong absorbance at 1787 cm^{-1}. Further absorbance bands are detected at 1626 cm^{-1}. The IR spectrum of the sample after reaction exhibits a shoulder at 1711 cm^{-1} of the peak at 1626 cm^{-1} instead of the band at 1787 cm^{-1}. The disappearance of both bands at 1787 and 1262 cm^{-1} after reaction suggests that these bands arise from the same surface group, the carboxylic acid group [6, 20]. The band at 1626 cm^{-1} was detected for both the fresh and used UDD surface and corresponds to adsorbed water. This band was modified and became broader after the reaction. The peak at 1400 cm^{-1} with a weak shoulder at 1386 cm^{-1} was present on the UDD surface before and after

the reaction and remained unaffected (Fig. 4.4.5). This band is assigned to bending vibrations of –O-H surface groups. The adsorption maximum at 1106 cm^{-1} is situated in the spectral region corresponding to C-O stretching vibrations of ether type groups [21]. This broad peak has a shoulder at 1053 cm^{-1}, which is attributed to C-O bonds present in alcohols and ethers [22]. After the reaction, the peak at 1106 cm^{-1} has vanished, and the shoulder at 1053 cm^{-1} was transformed to the strong symmetric peak at 1013 cm^{-1}.

Hence, the IR analysis confirmed changes of the sp^3-carbon surface, *i.e.* the disappearance of carboxyl and phenol surface groups and the appearance of C=O, alcohol and ether groups under reaction conditions. Thus, the nature of the sp^3-carbon surface changed from acidic to basic during reaction. Hence, it can be suggested that the catalytic activity of UDD in the ST formation increased due to the formation of basic surface groups with dehydrogenating properties.

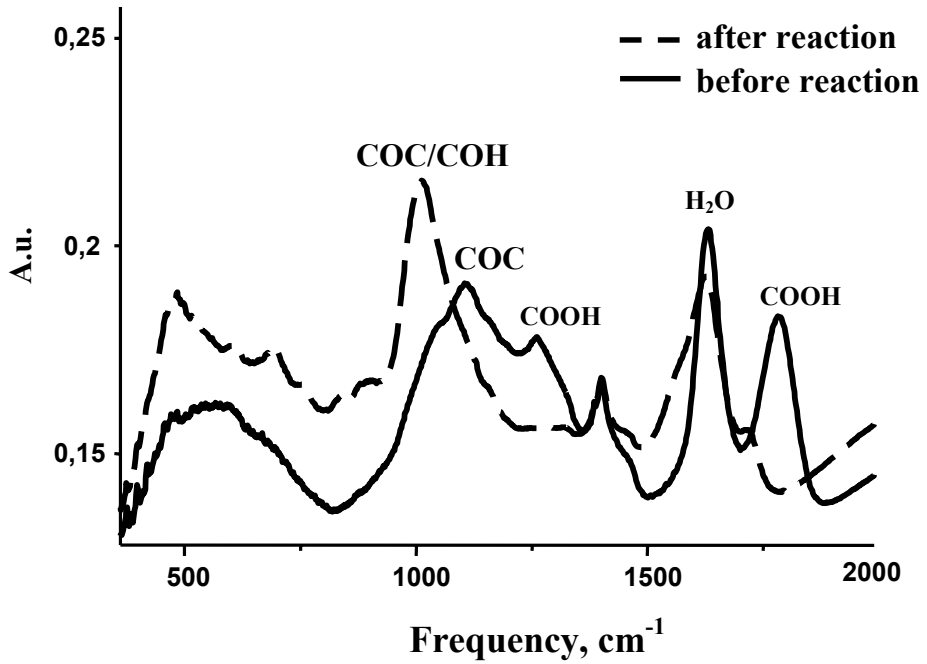

Fig.4.4.5. IR spectra of the UDD sample before and after the reaction.

4.4.2. Catalytic tests of OLC and UDD samples pretreated in helium, hydrogen and oxygen.

The catalytic tests over the differently pretreated OLC and UDD samples were done in order to find a relation between the nature of the carbon surfaces and the catalytic activities of sp^2- and sp^3-hybridized carbons. The OLC and UDD samples were pretreated in flowing helium, hydrogen, and oxygen in the catalytic test reactors prior to catalysis. After the pretreatments, the catalytic tests immediately started.

The OLC and UDD samples were pretreated in three different ways: (i) in pure helium at 600°C for 3 h; (ii) in a mixture of 10% hydrogen in He at 570°C for 3 h; and (iii) in a mixture of 2% oxygen in He at 570°C for 3 h.

Figure 4.4.6 shows a comparison of the EB conversions with time on stream over the pretreated (a) UDD and (b) OLC samples. After the pretreatments in helium and hydrogen, the EB conversions over UDD were as high as 88 and 91 mol%, respectively (Fig. 4.4.6, a). The conversion over the UDD sample pretreated in oxygen was 73 mol% at the first point. With time on stream, the EB conversions slowly decreased to 70 and 72 mol%, respectively, for the helium and hydrogen pretreated catalysts and to 45 mol% in the case of the oxygen pretreatment (Fig. 4.4.6, a).

An induction period was observed over the OLC sample pretreated in helium and hydrogen, after that steady states were achieved with conversions of about 85 mol% (Fig. 4.4.6, b). After the pretreatment in oxygen, the EB conversion was as high as 80 mol% in the very beginning of reaction. Then it increased slightly during approximately 6 h and reached 85 mol% in the steady state.

Figure 4.4.7 shows a comparison of the ST selectivities with time on stream over the pretreated (a) UDD and (b) OLC samples. For all differently pretreated UDD

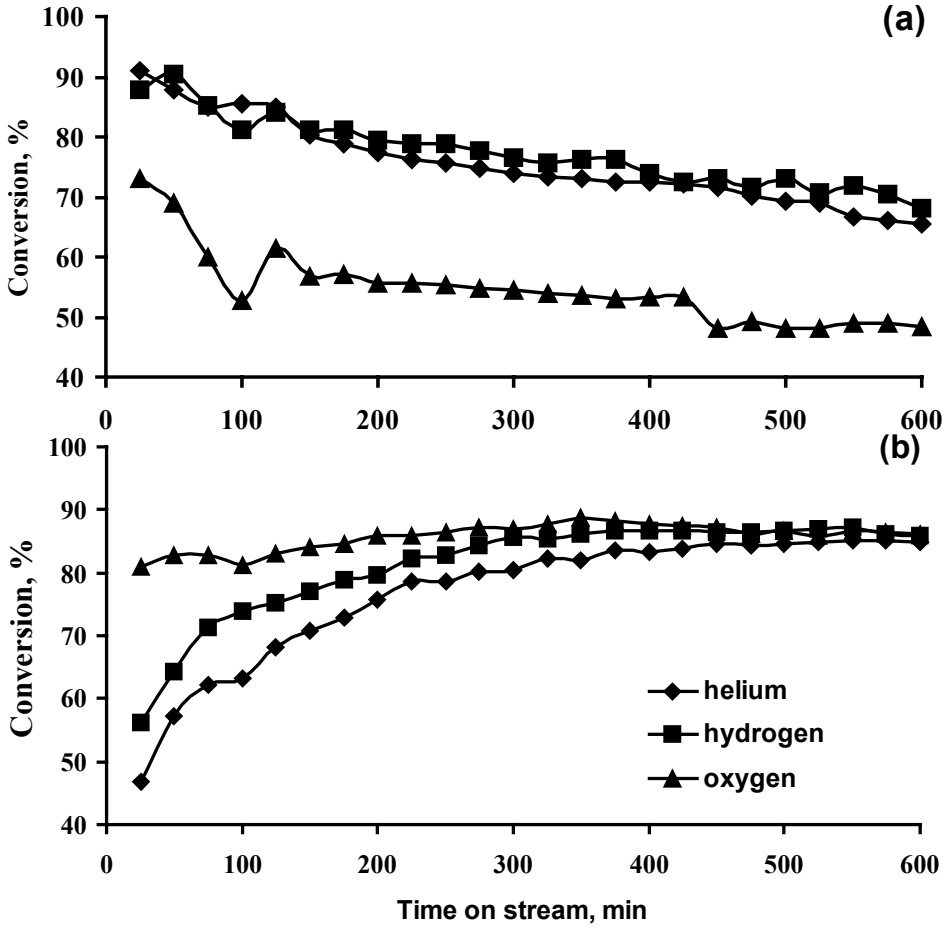

Fig. 4.4.6. Conversions of EB obtained over the pretreated (a) OLC and (b) UDD samples in helium, hydrogen, and oxygen.

samples, a stabilization period was observed during the first 2 hours, after which the ST selectivities of 55 mol% were almost stable (Fig. 4.4.7, a). The ST selectivities over the OLC samples pretreated in helium, hydrogen, and oxygen were almost identical during all time on stream. They were as high as 85 mol% in the first point and slightly decreased to 75 mol% during 10 hours on stream (Fig. 4.4.7, b).

Figure 4.4.8 shows the ST yields obtained over the (a) UDD and (b) OLC samples pretreated in helium, hydrogen, and oxygen. A stabilization of the ST yields was observed during first 2 hours (Fig. 4.4.8, a) for all pretreated UDD samples. After stabilization, a ST yield of 48 mol% was achieved for the hydrogen pretreatment, a ST yield of 42 mol% was observed after the helium pretreatment, and a ST yield of

only 31 mol% was observed after the oxygen pretreatment. Subsequently, the ST yields slightly decreased with time on stream to 35 and 37 mol%, respectively, for the helium and hydrogen pretreated samples, and to 26 mol% for the oxygen pretreatment (Fig. 4.4.8, a).

From the results obtained, it can be seen that the catalytic performance over the UDD sample was dramatically reduced after the oxygen pretreatment. The UDD surface seemed to be cleaned under oxygen atmosphere at 570°C, and only the pure sp^3-carbon surface was accessible to the reaction mixture. Obviously, the sp^3-hybridized carbon surface has a low capacity for the formation of the stable and active species, which are necessary for the ST formation.

Completely different catalytic behaviours, *i.e.* ST yields, were observed over the OLC samples after the different pretreatments (Fig. 4.4.8, b). After the helium and hydrogen pretreatments, induction periods of about 5 h were observed, after which ST yields of about 42% were reached. In the case of oxygen pretreatment, the induction period was not observed at all. The ST yield was as high as 68 mol% from the very beginning, and it was stable with time on stream (Fig. 4.4.8, b).

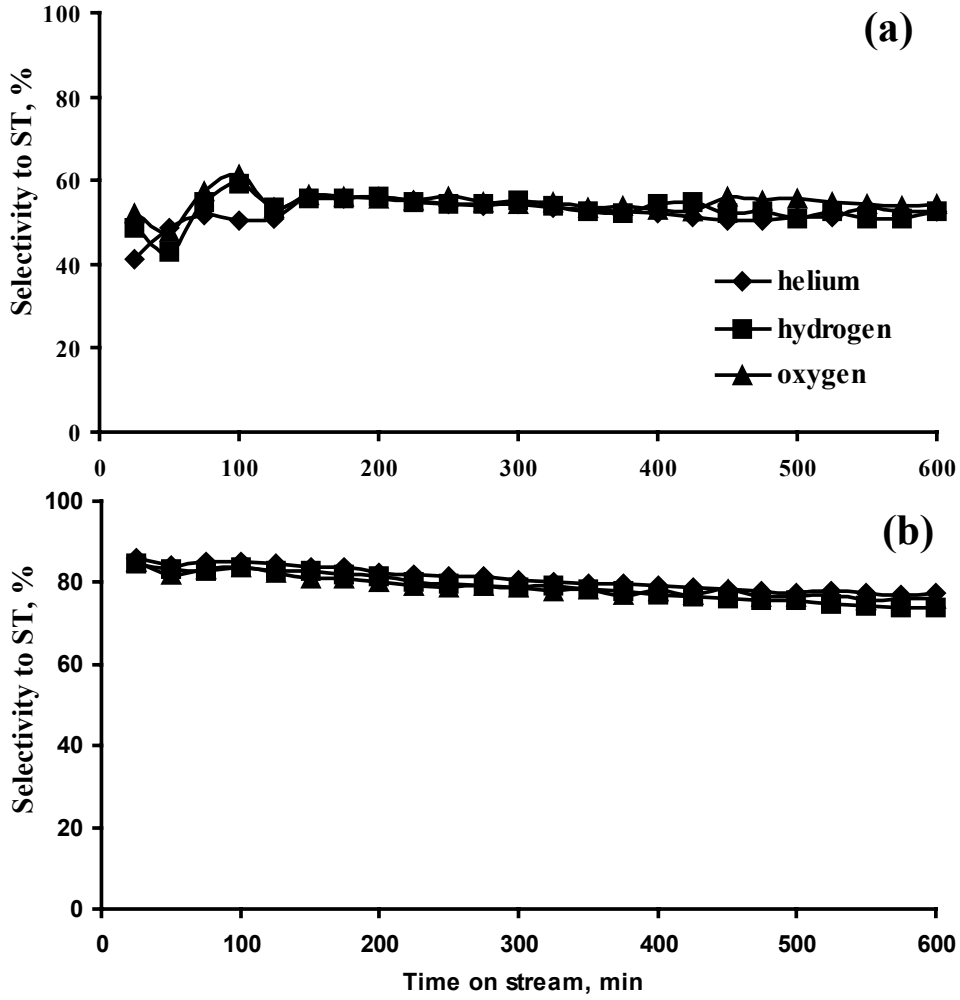

Fig. 4.4.7. Selectivities to ST obtained over the (a) OLC and (b) UDD samples pretreated in helium, hydrogen, and oxygen.

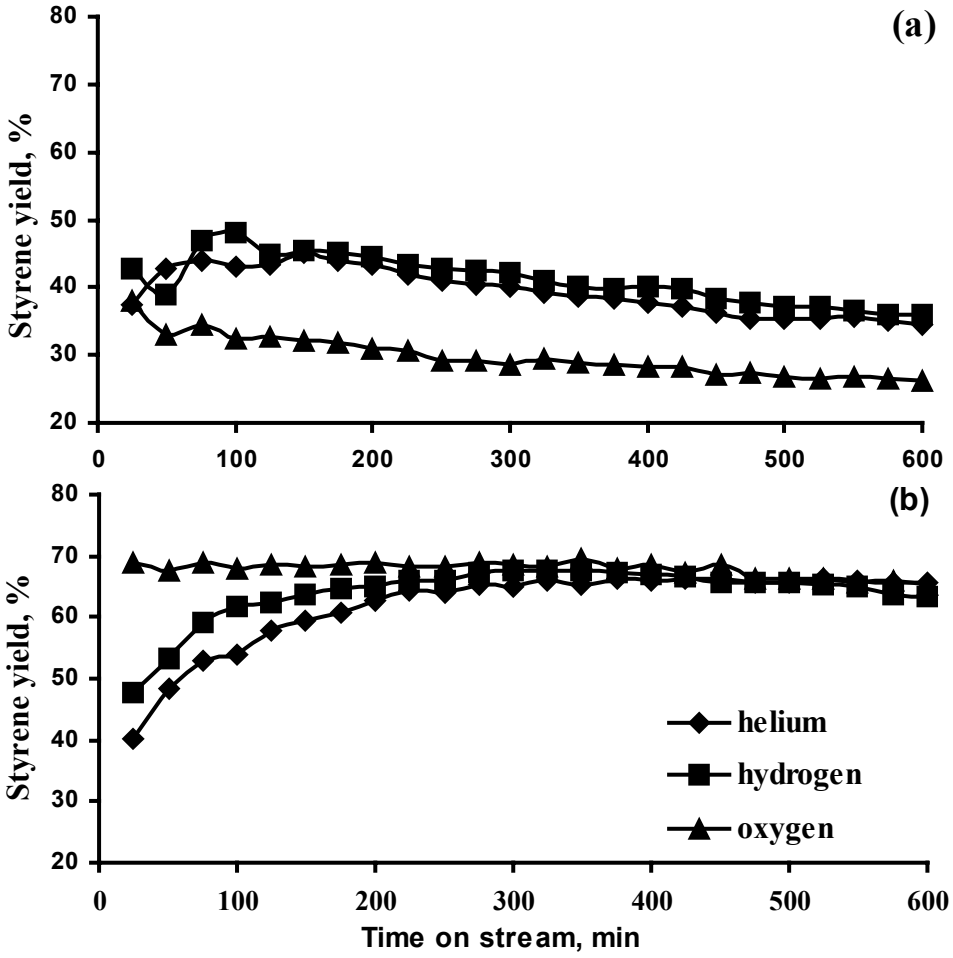

Fig. 4.4.8. Yields of ST obtained over the (a) OLC and (b) UDD samples pretreated in helium, hydrogen, and oxygen.

Figure 4.4.9 shows a comparison of the EB conversions, selectivities to ST, and ST yields as a function of time on stream over the OLC sample pretreated in oxygen at 520 and 570°C both for 3 hours. An induction period of about 3 h was observed after the oxygen pretreatment at 520°C, during which the EB conversion increased from 10 to 70 mol% (Fig. 4.4.9, a). At the same time, the selectivity to ST increased from 42 to 84 mol%, and the ST yields rised from 3 to 60 mol% (Fig. 4.4.9, b and c).

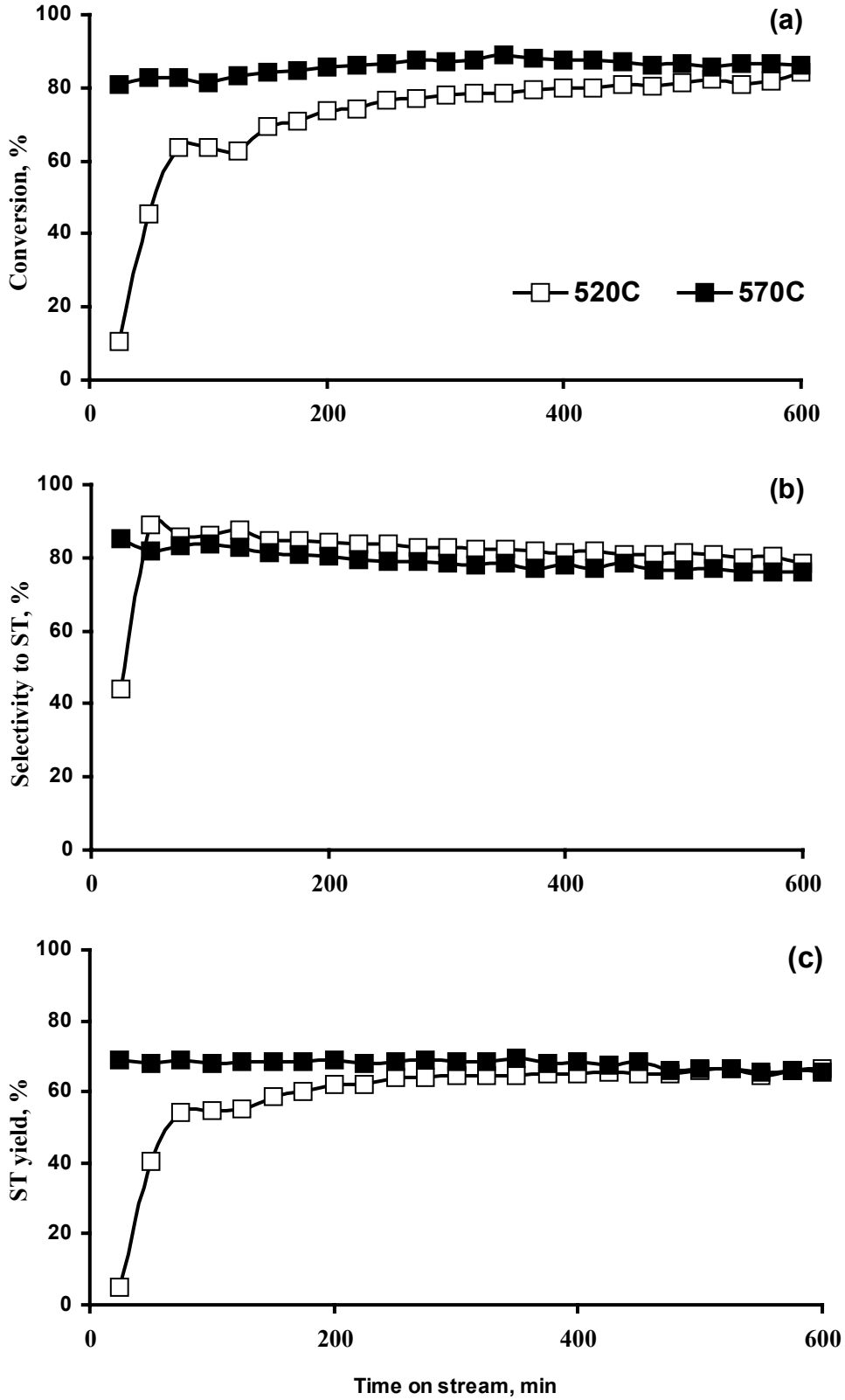

Fig. 4.4.9. EB conversions (a), selectivities to ST (b), and ST yields (c) with time on stream obtained over OLC samples pretreated in oxygen at 520 and 570°C.

The oxygen pretreatment at 570°C leads to a completely different catalytic behaviour of the OLC sample (Fig. 4.4.9, a-b). The induction period was absent, and the EB conversion higher than 80 mol%. Selectivities to ST of about 80 mol%, and ST yields of 68 mol% were observed during all times on stream (Fig. 4.4.9, a-b).

These differences in the initial catalytic behaviours clearly prove the destruction / creation of functional groups on the OLC surface during the reductive (H_2, He) or oxidative pretreatment at 570°C, respectively. These findings are in full agreement with the suggested mechanism (see following Chapter 5.2), in which basic, chinoidic surface groups play a fundamental role in the oxidative dehydrogenation of EB to ST.

References

[1] Ago H., Kugler T., Cacialli F., Salaneck W.R., Shaffer M.S.P., Windle A.H., Friend R.H., J.Phys.Chem. B 103 (1999) 8116.

[2] Guerrero-Ruiz A., Rodriguez-Ramos I. Carbon 32 (1994) 23.

[3] Mestl G., Maksimova N.I., Keller N., Roddatis V.V., Schlögl R. Angew. Chem. 113(11) (2001) 2122; Angew. Chem. Int. Ed. 40 (11) (2001) 2066.

[4] Keller N., Maksimova N.I., Roddatis V.V., Schur M., Mestl G., Kuznetsov V.L. Schlögl R.. Angew. Chem. 41 (11) (2002) 1885.

[5] Boehm H.P. Carbon 32 (1994) 759.

[6] Atamny F., Blöcker J., Dübotzky A., Kurt H., Timpe O., Loose G., Mahdi W., Schlögl R. Molec. Phys. 76 (1992) 851.

[7] Rodrigues-Reinoso F. Carbon 36 (1998) 159.

[8] Li C., Minh C.L., Brown T.C. J.Catal. 178 (1998) 275.

[9] Zwanger M.S., Banhart F., Seeger A. Journal of Crystal Growth 163 (1996) 445-454.

[10] Pereira M.F.R., Orfao J.J.M, Figueiredo J.L. Appl. Catal. A: General 184 (1999) 153.

[11] Vidano R.P., Fishbach D.B., Willis L.J., Loehr T.M. Solid State Commun. 39 (1981) 423.

[12] Dresselhaus M.S., Dresselhaus G. Adv. Phys. 30 (1981) 139.

[13] Kawashima Y., Katagiri G. Phys. Rev. B 52 (1995) 10053.

[14] Espinat D., Dexpert H., Freund E., Martino G., Couzi M., Lespade P., Cruege F. Appl. Catal. 16 (1985) 343.

[15] Pham-Huu C., Keller N., Roddatis V.V., Mestl G., Schlögl R., Ledoux M.J. Phys. Chem.-Chem. Phys 4(3) (2002) 514.

[16] Cavani F., Trifiro F. Appl. Catal. A: General 133 (1995) 219.

[17] Vrieland G.E. J. Catal. 111 (1988) 14.

[18] Schlögl R. in Handbook of Heterogeneous Catalysis, Vol. 1 (Eds.: G. Ertl, H. Knözinger, J. Weitkamp), Wiley-VCH, Weinheim, 1997, pp.138-191.

[19] Ugarte D. Carbon 33(7) (1995) 989.

[20] Jiang T., Xu K. Carbon 33 (1995) 1663.

[21] O'Reilly J.M., Mosher R.A.. Carbon 21 (1983) 47.

[22] Fanning P.E., Vannice M.A. Carbon 31(1993) 721.

Chapter 5. Kinetics and Reaction Mechanism of the Oxidative Dehydrogenation of Ethylbenzene to Styrene

5.1. Surface Functional Groups

The carbon surface is essentially composed of elemental carbon associated with various elements mainly oxygen and hydrogen. All sp^2-hybridized carbon materials have in common the same basic lamellar structure, which consists of polycondensed hexagonal rings (Fig. 5.1). Their surface is also composed of aromatic lamellae of various sizes, which constitute the basal planes. At the ends of basal planes, different types of defects can be present, i.e. imperfections like vacancies, dislocations, edges, and steps forming the prismatic planes. This strong anisotropy of graphite leads to its anisotropic electronic and chemical properties [1].

The surface chemistry of carbons has been extensively studied, and two approaches have been considered. The first one is "a solid state chemistry" approach developed on carbons of sufficient crystalline ordering [2]. The second one emphasizes the organic character of the surface groups and applies more to the

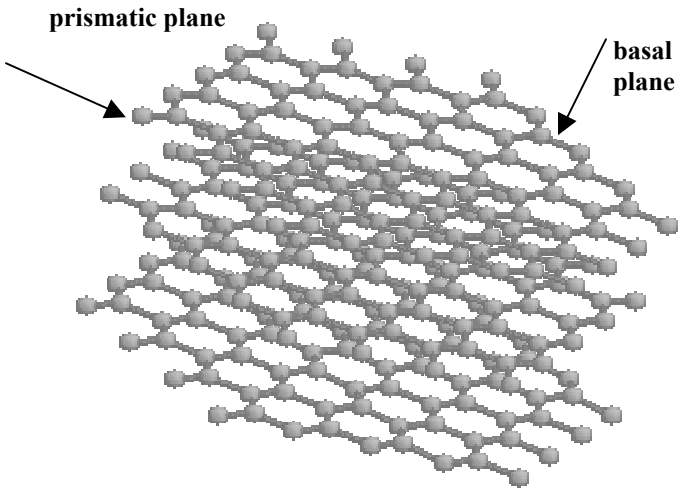

Fig. 5.1. Scheme of the basal and prismatic planes in carbon.

description of the surface properties of less ordered carbon [3].

In the “solid state chemistry” approach, the defects on the aromatic basal planes are considered as “active sites” of the carbon surface [1]. In fact, the carbon atoms located on the edges of basal planes are more reactive than carbon atoms of the basal planes. The extent of the active surface area depends on the structural properties of the carbon and also on its surrounding conditions. For the less ordered carbon materials, such as carbon black, the ratio of prismatic to basal planes is higher and the surface is more heterogeneous. Consequently, such carbon surfaces contain higher amounts of active sites, i.e. their active surface areas are more developed.

The “organic surface groups” approach deals with the nature and the functionality of surface complexes of oxygen and other compounds chemisorbed at the surface defects (Fig. 5.2). According to this approach, the surface functionality of carbons mainly depends on the nature of these groups / complexes [3]. It is clear that neither the “solid state chemistry” approach nor the “organic surface groups” approach alone can completely describe the reactivity of carbon materials. Only a

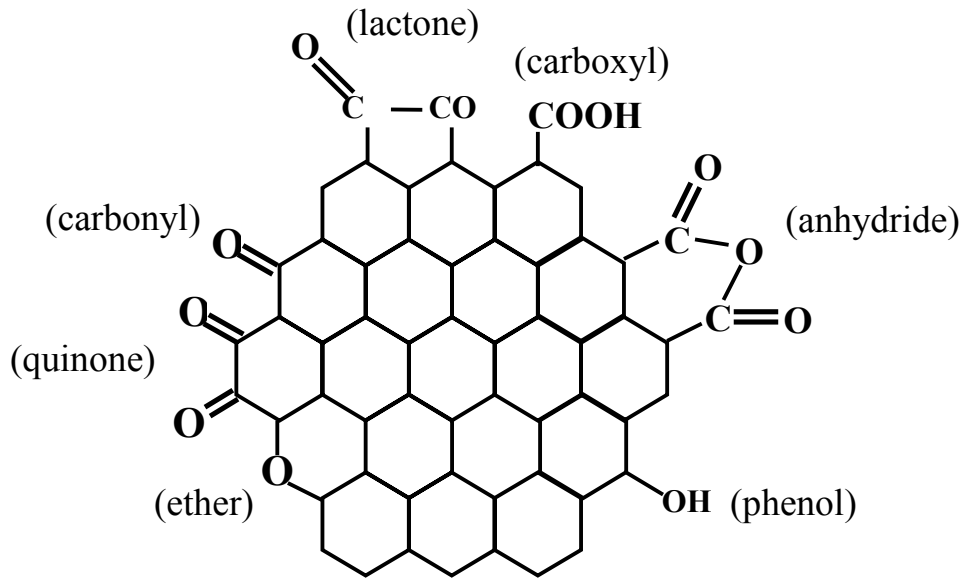

Fig. 5.2. Surface functional groups on an oxidized carbon surface.

combination of both approaches leads to a deeper insight in the real processes taking place on the carbon surface especially under reaction conditions.

Carbon materials have a surface composition consisting of appreciable amounts of oxygen and traces of nitrogen and hydrogen in dependence of the manufacture process. Oxygen is the most common foreign element present on the carbon surface [1]. Functional oxygen groups can have a significant influence on the surface properties of carbons. Due to the absence of a technique allowing the direct characterization of surface oxygen under reaction conditions, the chemical state of oxygen on the carbon surface is still under debate [1].

Some models of the oxygen activation on the carbon surface have been suggested. According to the most recent model [4], the activation of molecular oxygen is a sequence of molecular chemisorption, reduction to a peroxide-like species by carbon π-electrons, and the following dissociation into two O^- species. The O^- species formed migrate on the defect-free graphene layer of the surface until they reach a point defect or a step edge of the well-ordered patch where they are reduced to O^{2-}, form covalent bonds to the carbon and give back the initial π-electrons to the conduction electron system of the well-ordered graphene layer [4]. Obviously, this suggested mechanism of oxygen activation can lead to a turnover mechanism, in which the active oxygenated species, if consumed by an additional reaction, can be regenerated cycle by cycle.

For a full understanding of the activity of the carbon surface in ODH of EB to ST, the acidity and/or basicity of oxygen surface groups should also be taken into account. According to literature [4], two types of surface sites have been identified, i.e. (i) low temperature desorbing surface complexes of acidic character and (ii) high temperature desorbing surface complexes of basic character. Both acidic and basic

groups can simultaneously be present on the carbon surface. It is well accepted that the acidic or basic character of a given carbon is developed as a result of surface oxidation and depends on the history of its formation, i.e. the oxidation temperature. The most important surface groups of acidic character are carboxyl, lactone, and anhydride groups (Fig. 5.2). Ether, phenol, carbonyl and quinone groups are considered as being of basic character.

The fundamental idea of using carbon as an oxidation catalyst is to couple a second reaction to the oxygen activation-fixation reaction by co-adsorbing an organic acceptor for the activated oxygen [5], which consumes these active species. Sp^2-carbon substrates should react with the active oxygen and the products might desorb easier from the surface as in the case of more conventional oxidation catalysts such as oxides and metals. The role of stable carbon – oxygen surface groups additionally present could be beneficial for chemisorption (polarity) and activation (acid-base character of OH-functions) of the organic substances.

Oxygenated functions of basic character were proposed to be responsible for the adsorption of acids by carbons. If a carbon is treated over 700°C, it acquires a basic character after cooling in inert atmosphere and reexposure to oxygen at room temperature. Further, protons can adsorb on the carbon basal planes due to the π electron system and, consequently, such carbon surfaces show basic character [4].

This concept is in good agreement with XPS results obtained for sp^2-hybridized carbon materials tested as catalysts in the ODH of EB. XPS proved that the OLC surface, being oxygen-free before the reaction (Chapter 4.3), contained surface oxygen groups of a basic character after the reaction. Chinoidic carbonyl groups with strongly basic character seemed to be generated during the activation period of the catalytic reaction. A comparison of the performance of OLC and the formation of

chinoidic carbonyl groups under reaction conditions indicates the dehydrogenating function of these groups for the catalytic process.

5.2. Reaction Kinetics

The determination of an empirical rate equation allows one to quantify the influence of temperature, reactant concentrations and other factors, such as amount of catalyst, on the ST formation reaction.

For the determination of a form of the rate equation, the reaction orders with respect to each reactant were estimated for the used reaction conditions. The reaction order relatively to EB was found from experiments, in which the EB concentration in the feed was varied, while all other parameters were kept constant. The relation of the reaction rate vs. the EB partial pressure in the feed is shown in Fig. 5.3. Because the

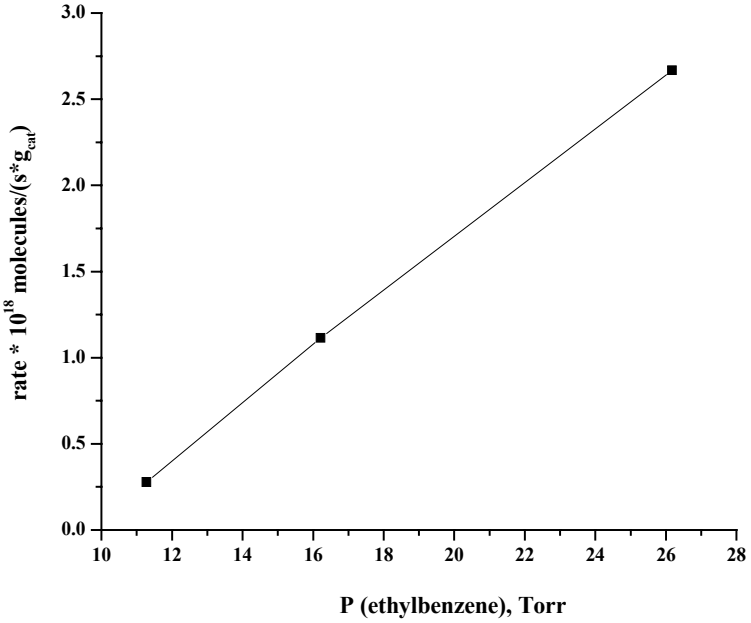

Fig. 5.3. Reaction rate vs. the partial pressure of EB.

functional relationship between the reaction rate and EB partial pressure is linear, the ODH reaction is of the first order with respect to EB at the chosen reaction conditions.

In a twice-stoichiometric excess of oxygen used, the catalytic reaction is independent on the oxygen content. Therefore, the ODH reaction is of zero order

relatively to oxygen, and the reaction order is determined by the EB partial pressure in the feed under the used conditions. The reaction mechanism involves the dehydrogenation of EB molecule, i.e. the breakage of two C-H bonds. Hence, the ODH of EB to ST over carbon materials is of the first order with the following reaction rate law:

$$r = k\,[F_{EB}]^1[F_{O2}]^0 \qquad (5.1)$$

or

$$r = k\,[F_{EB}] \qquad (5.2)$$

The reaction constant k can be determined from the Arrhenius equation [7]:

$$k = A * \exp\,[-E_a / (RT)], \qquad (5.3)$$

with A being the pre-exponential factor, E_a the apparent activation energy, $J \cdot mol^{-1}$, R the universal gas constant, $J \cdot mol^{-1} \cdot K^{-1}$, T the temperature, K, and k being defined as the reaction rate constant, $mol \cdot s^{-1} \cdot m^{-2}$.

The reaction rate is a function of temperature, pressure and the concentrations of reactants. The determination of the reaction constant k was conducted at atmospheric pressure. The reaction rate was varied only with temperature, and the concentrations of all reactants were chosen to be constant. The reaction rate was estimated from the area-specific EB consumption:

$$r = \frac{\Delta C_{EB}}{\tau \times S}, \quad mol \cdot s^{-1} \cdot m^{-2} \qquad (5.4)$$

where ΔC_{EB} is the EB consumption, mol; τ is the contact time, s^{-1}; S is the specific surface area of catalyst, m^2.

If the logarithm of k plotted vs. the reciprocal temperature, i.e. the Arrhenius plot, is linear, it is indicated the absence of heat and mass transfer limitations to the reaction rate and of changes in the reaction mechanism in the chosen temperature

region. In such case, the reaction constant k can be evaluated from the dependency (5.4), and the apparent activation energy E_a is the slope to the Arrhenius plot.

All kinetics experiments were conducted at atmospheric pressure in the temperature region of 500 - 525°C with the same concentrations of reactants. The high contact time τ of 4.5 h^{-1} allowed one to escape the heat and mass transfer limitations. Under these conditions, the total concentration of by-products formed via side reactions did not exceed of 1%. Hence, the formation of by-products could be disregarded for the calculation of the kinetic parameters. The catalytic tests were done for every measured point of the Arrhenius plot with a fresh catalyst sample and conducted for the same time on stream (~10 h) to get a steady state of the catalytic performance.

It can be expected that the reaction rates of the ODH reaction over the different carbon materials might vary as a function of the carbon microstructures. To pronounce this dependency on the carbon microstructure, the determination of the kinetics of the ODH of EB were conducted over the less active carbons on one side - i.e., carbon black - and the more active carbons on the other - i.e., carbon onions and nanotubes MWNT's-A.

As observed earlier, carbon black was not stable with time on stream under severe reaction conditions. The complete combustion of carbon black was observed at increased contact time with time on stream. This resulted in a rapid catalyst weight loss, and hence a high experimental error in the estimation of the reaction rate. Accordingly, these results are not further discussed.

The carbon nanostructures with high degree of crystallinity, i.e. carbon nanotubes and onions, were stable under the same specified reaction conditions as expected. The dependency of the logarithm k and reciprocal temperature obtained over carbon nanotubes and onions was linear for both carbons in the temperature region of 500-525°C (Fig. 5.4, a and b). From these results, the E_a for MWNT´s-A is estimated to be 122 $kJ \cdot mol^{-1}$ (Fig. 5.4, a). The E_a for OLC was significantly higher than for MWNT´s-A being 196 $kJ \cdot mol^{-1}$ (Fig. 5.4, b). Obviously, the carbon nanostructure directly affects the ODH of EB as suggested above. The higher activation energy over OLC clearly evidences that this nanocarbon material is less effective for the ODH reaction than MWNT´s-A under the experimental conditions chosen.

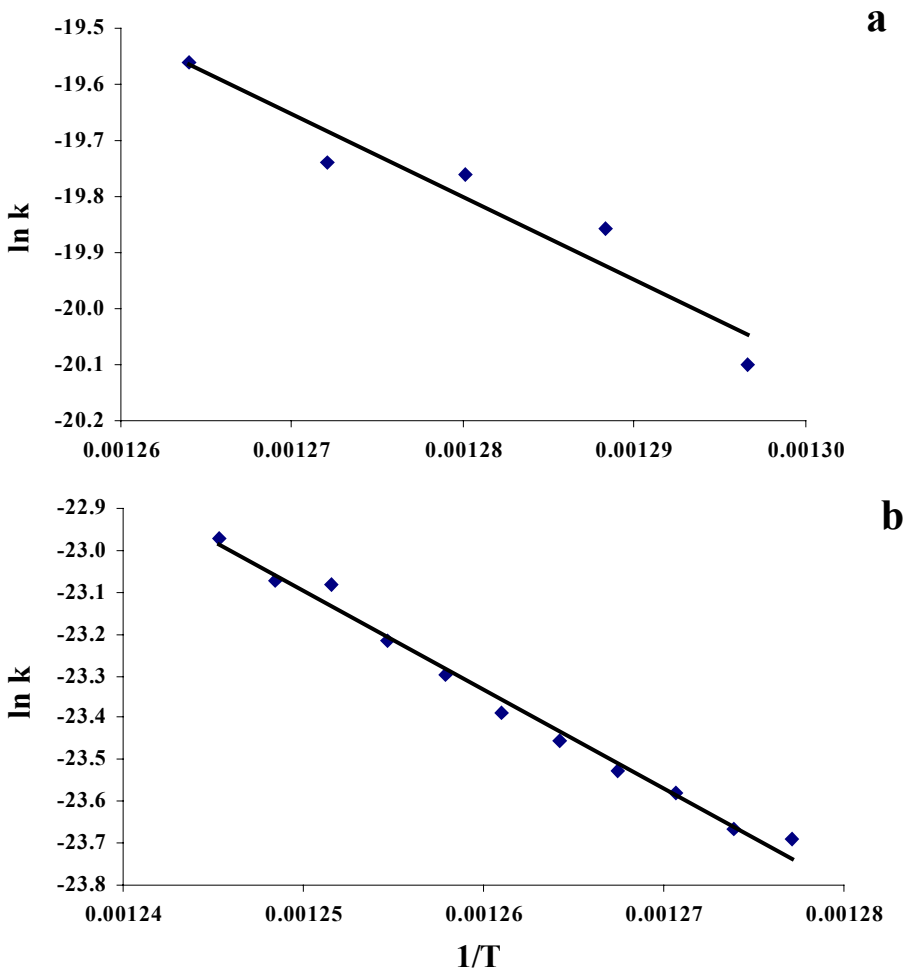

Fig. 5.4. The Arrhenius plots obtained over (a) MWNT´s-A and (b) OLC in the temperature region of 500-525°C.

From a comparison of the Arrhenius plots for MWNT´s-A and OLC (Fig. 5.4), it can be seen that the density of active centres is higher for OLC than for MWNT´s-A, which could be expected from the TEM characterization. But, the lower Ea for MWNT´s-A indicates that the reaction proceeds faster over MWNT´s-A than that over OLC. The high difference in reactivity with respect to activation energies estimated indicates that the rate-limiting step can be different for MWNT´s-A and OLC. Hence, the microstructure of MWNT´s-A is more effective for the ODH reaction. Because the surface structure of both samples is more or less similar, and the only difference is in a higher crystallinity of the nanotubes, it can be concluded that the degree of crystallinity is an important factor influencing the carbon activity. Earlier, the dependence of the carbon crystallinity on its catalytic activity was also observed in the case of partial oxidation of methanol over different carbonaceous materials [6]. Obviously, the degree of crystallinity of carbon nanostructures has a strong influence on their dehydrogenating power. It can be expected that the oxygen activation also strongly depends on the carbon crystallinity since it occurs at the perfectly crystallized basal planes (Chapter 4.2) [7]. However, the oxygen activation cannot affect the determined reaction rate due to the zero reaction order relatively to oxygen. Hence, the role of the carbon microstructure in the ODH of EB to ST can be deduced from the results obtained.

The first reaction order relative to EB at the used reaction conditions implies that the reaction rate depends on the EB content in the feed. It was suggested that the dehydrogenation of EB depends on the basicity of the hydroxyl/quinoidic structures, which depends on the electronic resonance stabilisation of carbon-oxygen bonds and hence the details of the local electronic structure. In particular, the formation of localized C=C bonds vs. the availability of an aromatic π-electronic system will

strongly affect the basicity of C=O groups. The delocalisation of π-electrons of the quinone groups has to be higher on MWNT´s-A than that on OLC due to the higher crystallinity of the former. Hence, the basicity and, consequently, the activity of MWNT´s-A are higher.

The kinetics results obtained allow one to further substantiate an optimum carbon structure as catalyst for the ST production processes: highly crystalline multiwalled carbon nanotubes seem to have optimum properties for this reaction.

5.3. Model of the Reaction Mechanism

The mechanisms of heterogeneous catalytic reactions at the atomic level are still unknown, except in a few cases, e.g. the oxidation of CO on Pt. In most cases, however, the reaction mechanisms can only be described making assumptions and correlations with suggested models.

The mechanism of the ODH of EB to ST over carbon materials is very complex due to the inhomogeneity of the carbon surface, which might give rise to parallel reactions leading to by-products. The nature and density of the activated species adsorbed on the catalyst surface or of the active centers are also unknown. A determination of the unknown mechanism of the ODH of EB to ST over carbon catalysts requires a special study. In this thesis, a possible model for the ODH of EB over the sp^2-carbon surface is suggested on the basis of some obtained results.

The catalytic tests over UDD (Chapter 4.4) have shown that the reaction over the fresh sp^3-bound carbon proceeds via the side chain combustion of the EB molecule to benzene and CO_2. Obviously, the ST formation is favoured only over sp^2-bound carbon. This fact was proven by a high selectivity to ST over all sp^2 carbon materials tested (Chapters 4-1-4.3). Because all sp^2-carbon catalysts follow the same trend of the ST formation, the mechanism of the ODH of EB over these carbons might be identical.

Catalytic reactions taking place on heterogeneous surfaces can often be described by the Langmuir-Hinshelwood (LH) mechanism involving several stages, i.e. (i) adsorption of the reactants, (ii) surface reaction, and (iii) desorption of the products. According to this model, two reacting species are first chemisorbed on the catalyst surface. Then, the reaction between the chemisorbed species takes place, after that the products are desorbed from the catalyst surface.

It was suggested that a kinetic model for the ODH of EB to ST over sp^2 - carbon materials can follow a Langmuir-Hinshelwood mechanism, in which both adsorbed EB and adsorbed O-species play an important role. The reaction could occur via the following elementary steps (Fig. 5.6):

1.) EB is adsorbed on the graphite step edges, i.e. prismatic graphene planes;

2.) EB reacts with the oxygenated species also located at the prismatic planes leading to the dehydrogenation of EB to ST (which could either be a sequence of two C-H bond scissions or a concerted reaction step, in which both C-H bonds are broken simultaneously);

3.) the dehydrogenating oxygen species transform to hydroxyl groups, which remain on the graphite edges;

4.) the ST formed desorbs from the carbon surface;

5.) gas-phase oxygen activation on the basal planes of the graphene layers, which is indeed a sequence of elementary reactions, i.e. O_2- adsorption, activation and dissociation [4];

6.) the dissociated oxygen diffuses over the basal plane to the prismatic planes with the hydroxyl groups [4];

7.) the activated oxygen reacts with the hydroxyl groups to re-form the basic, chinoidic oxygen functionalities and to give water, which subsequently desorbs.

The oxygenated species re-formed from the hydroxyl groups remain on the prismatic planes (Fig. 5.5). These oxygenated species have a strongly basic, adjacent chinoidal nature. In the present model, the ODH reaction passes these steps cycle by cycle [6].

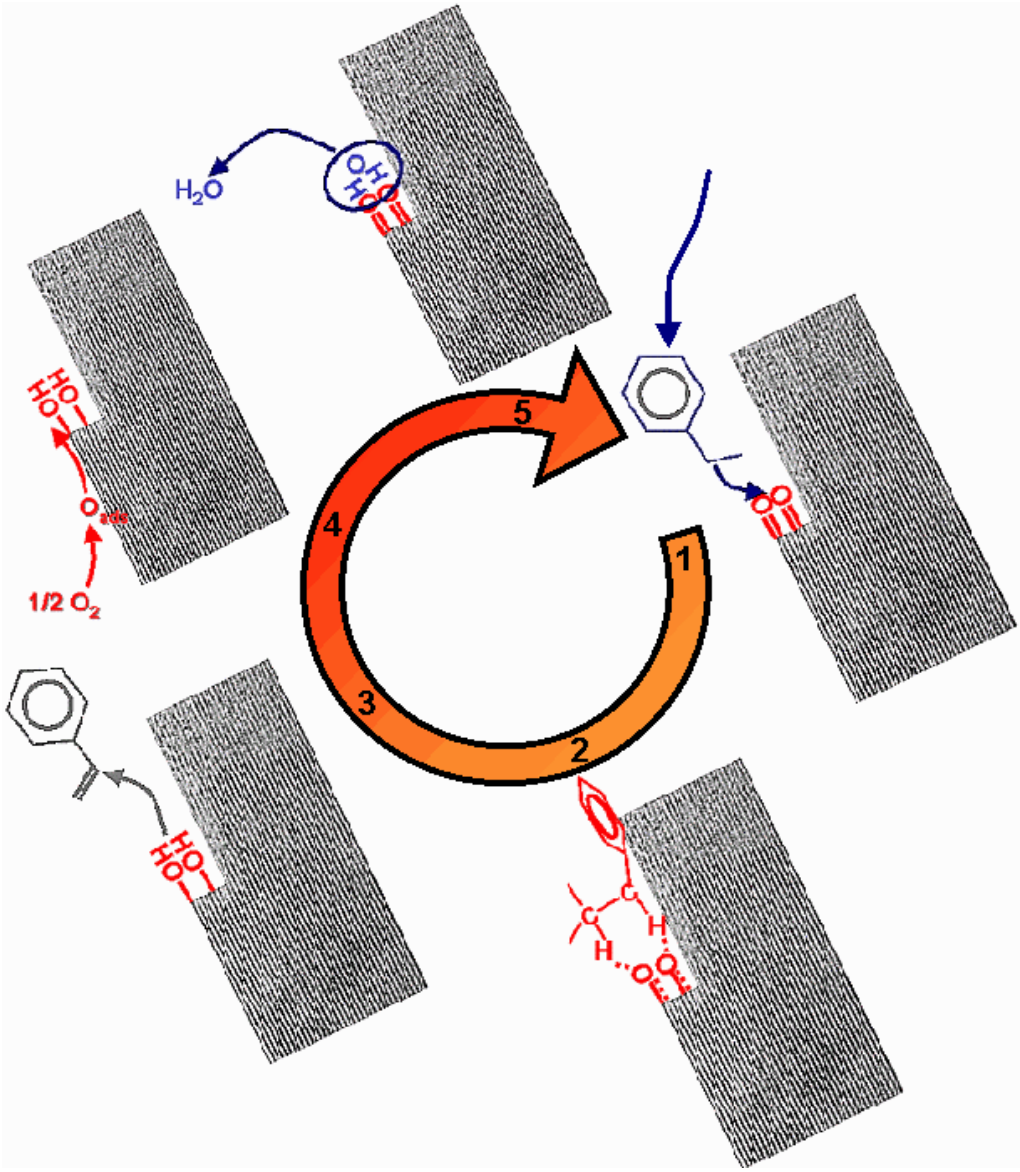

Fig. 5.5. Schematic drawing of the catalytic oxidative dehydrogenation over carbon nanofilaments, 1 - adsorption of ethylbenzene, 2 - dehydrogenation at basic centres, 3 - desorption of styrene, 4 - adsorption of oxygen and reaction with OH groups, 5 - desorption of water.

The Mars - van Krevelen mechanism (MvK) is often used as an alternative mechanism to explain partial oxidation reactions. Briefly, it is suggested in the MvK

mechanism that the organic substrate is oxidized by the so called “lattice oxygen”. This “lattice oxygen” is in turn replenished by oxygen diffusion from the bulk to the surface. Reoxidation of the catalyst is suggested to take place at a site different form the catalytically active centre.

First of all, the mathematical formalism of the MvK mechnism is identical to that of the LH mechanism, which itself poses serious doubts about the generality of the MvK mechanism. Secondly, carbon does not form a solid oxide, hence oxidation through “lattice” oxygen and its replenishing through bulk oxygen diffusion is simply impossible. Therefore, the MvK mechanism can be completely ruled out in case of carbon catalysts and, hence, is not generally applicable for partial oxidation reactions.

Special catalytic testes confirmed the operation of the ODH mechanism. The reaction was carried out over graphite by the usual way, but without the presence of oxygen (Fig. 5.6, a). It can be seen that there was some activity in the beginning, but it decreased rapidly with time on stream. The initial activity was observed due to the presence of oxygenated species on the fresh surface of graphite. The consumption of these oxygenated species in the ODH reaction led to the fast loss of activity (Fig. 5.6, a). When oxygen was added to the stream, the ST yield and EB conversion rapidly increased (Fig. 5.6, b). These catalytic tests confirmed that the surface oxygen is involved in the reaction, and that the reoxidation of the carbon surface regenerates the active sites. The pre-treatment experiments of OLC with oxygen at 520 and 570° (Chapter 4.4.2) demonstrated that the formation of active oxygenated species requires a high temperature. The fact that the oxygenated species are formed at high temperatures gives an indirect proof of their basic character.

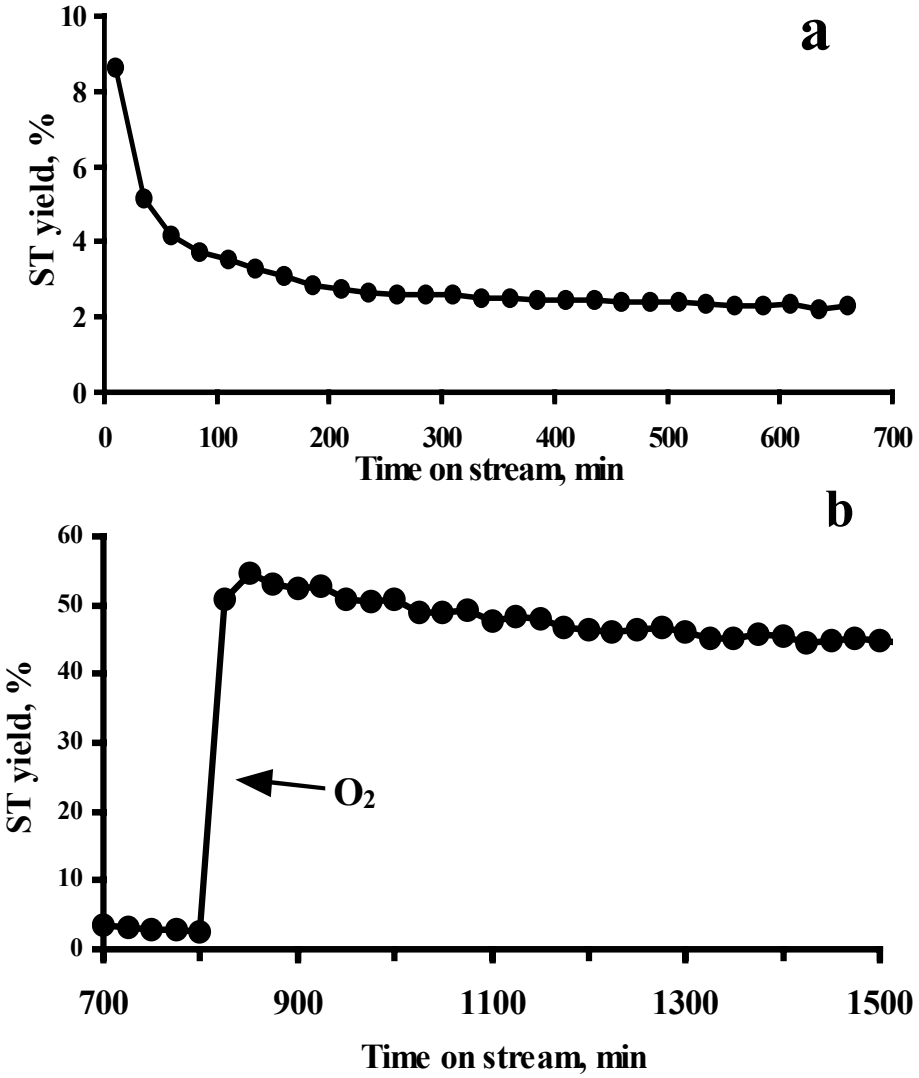

Fig. 5.6. Dehydrogenation of EB over graphite without O_2 (a) and dehydrogenation of EB over graphite without O_2 and then with O_2 (b).

The ODH of EB over different carbons was also accompanied by parallel reactions leading to the formation of by-products, mainly benzene, toluene, CO and CO_2 (Tab. 5.1). For carbons with characteristic induction period, the yields of by-products increased also during the initial stage. Ethene was formed in negligible amounts over all carbons (Tab. 5.1).

Benzene and toluene were both produced in essential amounts, but benzene at a more significant production rate than toluene. A benzene formation in the region of 2-4% was also observed over graphite, CNF´s and OLC. The benzene yield was as high as 14% over UDD under steady state. Toluene was formed in amounts not

exceeding 2%, with the exception of UDD, over which 2.7% of toluene yield was detected. The significant benzene and toluene formations indicate that the side chain oxidation of EB also takes place under the reaction conditions.

The CO and CO_2 yields, both of about 11-13%, were observed over carbon black and OLC, while CO and CO_2 yields of both 2% were observed over graphite. The CO_2/CO ratio was as high as 6 over CNF´s, 1.4 over MWNT´s-A, and about 7 over UDD. The higher CO and CO_2 formations relative to benzene and toluene seems to be due to the additional combustion of soft coke deposited during the reaction. Under steady state, it is assumed that the coke formation from the unavoidable styrene polymerisation reaction is balanced by the coke combustion. This soft coke is much easier combusted as the well crystallized sp^2-carbon, which leads to a "self-cleaning" of the reactive catalyst surface.

Table 5.1.

Product distribution obtained in the ODH of EB over different carbon materials in 7 hours of time on stream.

Carbon material	EB conversion,%	ST yield, %	Ethene, %	Benzene, %	Toluene, %	CO, %	CO_2, %
Carbon Black	81.6	56.27	0	0.75	0.41	12.86	11.34
Graphite	52.7	43.47	0	3.76	1.56	2	2.1
CNFs	64.7	47.46	0	4.29	1.86	1.59	9.52
MWNT´s-A	68.7	50.76	0.06	0.71	0.41	6.96	9.82
OLC	91.2	61.62	0.07	2.1	1.1	12.97	13.39
UDD	90.4	37.6	0.57	13.98	2.7	4.41	31.2

The fact that carbon materials of different structures have shown different catalytic activities indicates that the carbon activity is influenced by some structural factors. Carbon nanofilaments and nanotubes of comparable dimensions and with similar structural element shapes, however, exhibited different activities in the ODH reaction (Chapter 4.2). The suggested reaction mechanism proposes that basal planes play an important role for the oxygen activation, while prismatic planes are important for the location of the active oxygenated species. For all carbon materials tested, the presence of oxygen in the reaction mixture at elevated temperatures caused changes in the surface microstructure. Probably, the optimised ratio of basal planes (required for oxygen activation) and prismatic planes (stabilizing basic, quinoid centres) is adjusted under reaction conditions during the observed activation periods. The highest catalytic activity observed for MWNT´s-A seems to be related to not only high degree of crystallinity, but also to their optimised distribution of basal and prismatic planes as shown by TEM (Chapter 4.2). Obviously, basal planes should have a pronounced metallic character for optimum oxygen activation.

A high degree of crystallinity not only provides the oxygen activation but also high stability toward oxidation. Obviously, less perfect carbon nanostructures (carbon black, BNF`s) can not provide: a) enough sites for oxygen activation, necessary for an improved surface OH group reoxidation, and b) enough stability toward oxidation. A low activity of the high surface area graphite used for the present study seems to be a consequence of low density of the basic chinoidic groups presented on this “perfectly” crystallized surface.

The effect of the curvature of the structural elements, i.e. nanotube radius, on the activity of carbon nanostructures in the ODH reaction is still under discussion. Carbon nanostructures of higher curvatures should exhibit better oxygen activation

properties relative to strictly plane carbons. Indeed, it was observed in the present study that the curved carbon nanostructures, i.e. nanofilaments, nanotubes and onions, were more active than graphite, but a clear determination of the curvature effect requires further special investigations.

References

[1] Design and Control of the Structure of Advanced Carbon Materials for Enhanced Performance. Ed. by B. Rand, S.P. Appleyard and M.F. Yardim. NATO Science Series. Series E: Applied Sciences – Vol. 374, Kluwer Academic Publishers 2001.

[2] Nanostructured Carbon for Advanced Applications. Ed. by Bedenek G., Milani P., Ralchenko V.G. NATO Science Series. Series II: Mathematics, Physics and Chemistry – Vol. 24, Kluwer Academic Publishers 2001.

[3] Garten V.A., Weiss D.E. Aust. J. Chem. 10 (1957) 309.

[4] Atamny F., Blöcker J., Dübotzky A., Kurt H., Timpe O., Loose G., Mahdi W., Schlögl R. Molecular Physics 76 (4) (1992) 851.

[5] Emig G., Hofmann H. J. Catal. 84 (1983) 15.

[6] The role of lattice defects in the catalytic oxidation of methanol over graphite catalyst. Sanchez-Cortezon E. PhD Thesis, Technical University, Berlin 2001.

[7] Marsh H., Warburton A.B. J. Appl. Chem. 20 (1970) 133.

Conclusions

In the present work, the different nanostructures, i.e. carbon black, graphite, nanofilaments, nanotubes, onions, ultra-dispersed diamonds, were tested as catalysts for the oxidative dehydrogenation of ethylbenzene to styrene. The comparative characterizations of carbons before and after catalytic tests with TEM, XPS, Raman- and IR-spectroscopy, TG/DTA, and BET surface area techniques allowed us to develop a structure-activity relationship and to propose a model of the reaction mechanism.

The determination of the conditions, under which carbon catalysts develop their activity maximum, was done with Experimental Design. A screening of the experimental parameters was conducted with the theoretically lowest possible number of experiments according to the Box-Behnken Plan and Simplex method. The optimum reaction conditions for all carbons tested lied at the temperature range of 495-515°C. The oxygen content in the feed was found to be an insignificant parameter in the accessible mass flow rates and the chosen temperature region.

It was found that sp^2-bound carbon is required for the selective styrene formation, since sp^3-bound carbon led to the production of benzene instead of styrene. It has been shown that the microstructure of sp^2-bound carbon materials is of paramount importance in order to obtain high and stable efficiencies. Carbon nanofilaments have shown the highest styrene yields at the highest ethylbenzene conversions as compared to carbon black and graphite. The comparative study of carbon nanofilaments and nanotubes of different structure has shown that more perfect carbon nanotubes produced by the arc-discharge technique are the most active catalysts in terms of reaction rates. The onion-like carbon was found to be the most

efficient catalyst for the oxidative dehydrogenation reaction on a mass-referenced basis.

XPS results revealed that the surface of onion-like carbon, being oxygen-free before the reaction, contained surface oxygen groups after the reaction. The experiments with oxygen pretreatment confirmed the creation of functional groups on the onion-like carbon surface at 570°C. Due to the high formation temperature and the XPS binding energy of the oxygenated species, it was proposed that chinoidic carbonyl groups of strongly basic character are generated during the reaction.

The reaction model suggested for the oxidative dehydrogenation of ethylbenzene to styrene over sp^2 - carbon materials follows a Langmuir-Hinshelwood mechanism, in which both adsorbed ethylbenzene and adsorbed oxygen-species play an important role. According to this model, the reaction might occur via i) ethylbenzene adsorption at the graphite step edges, ii) ethylbenzene reaction with the oxygenated species also located at the graphite step edges leading to the dehydrogenation of ethylbenzene to styrene, iii) the simultaneous transformation of the dehydrogenating oxygen species to hydroxyl groups, which remain at the graphite edges, iv) the styrene desorption from the carbon surface, v) gas-phase oxygen activation on the basal planes of the graphene layers, vi) oxygen diffusion to the prismatic planes with the hydroxyl groups, vii) reformation of the basic, chinoidic oxygen functionalities from the activated oxygen and the hydroxyl groups, iix) water desorption. The catalytic reaction passes these steps cycle by cycle.

The establishment of structure-activity relation by the catalytic tests and the characterisation of different carbon nanostructures allowed one to determine carbon nanostructure stable under oxidative reaction conditions. Carbon nanotubes and onions have shown a high and stable efficiency in the ODH reaction.

A radius of curvature of the basic structural element of carbon nanotubes and onions and also their high aspect ratio seem to provide a high density of functional surface groups under reaction conditions. The perfectness of these carbon nanostructures provides also enough stability toward oxidation and is essential for gas phase oxygen activation. The simplicity of carbon and its unique property that deactivated surfaces gasify themselves in oxidative dehydrogenation reactions not only renders them well-suited model systems but also allow for realistic expectations for a technical application.

APPENDIX

Abbreviations

- **BET** **Brunauer-Emmett-Teller method for the specific surface area determination**
- **BNF´s** **Bamboo-like nanofilaments**
- **CNF's** **Carbon nanofilaments**
- **DTG** **Differential thermogravimetry**
- **EB** **Ethylbenzene**
- **FWHM** **Full width at half maximum**
- **HSAG** **High surface area graphite**
- **GHSV** **Gas-hourly-space velocity**
- **LH** **Langmuir-Hinshelwood mechanism**
- **MvK** **Mars - van Krevelen mechanism**
- **MWNF's** **Multi-walled nanofilaments**
- **MWNT's** **Multi-walled nanotubes obtained by hydrocarbon decomposition**
- **MWNTs-A** **Multi-walled nanotubes obtained by arc-discharge**
- **ODH** **Oxidative dehydrogenation**
- **ST** **Styrene**
- **TG** **Thermogravimetry**
- **TEM** **Transmission electron microscopy**
- **TPO** **Temperature programmed oxidation**
- **XPS** **X-ray photoelectron spectroscopy**

Kurzzusammenfassung

Seit der Entdeckung der Fullerene 1985 erfährt die Chemie sp^2-hybridisierter, nanostrukturierter Kohlenstoffe zunehmendes Interesse, zum einen aus fundamentaler Sicht, zum anderen wegen potentieller Anwendungen. Inzwischen wurde eine Vielzahl neuer Fulleren-verwandter Materialien (Riesenfullerene, Nanoröhren, Nanokugeln, Nanokonen, Nanobündel, zwiebelähnlicher Kohlenstoff, etc.) synthetisiert. Die einzigartigen chemischen und physikalischen Eigenschaften dieser Verbindungen ermöglichen neue Anwendungen. Diese Kohlenstoffnanomaterialien besitzen wegen ihrer nahezu perfekten graphitischen und trotzdem stark gespannten Strukturen auch neue interessante katalytische Eigenschaften.

Eine gravierende Einschränkung erfährt die direkte Dehydrogenierung von Kohlenwasserstoffen wegen des endothermen Charakters dieser Reaktion. Dehalb sucht man intensiv nach alternativen Syntheseverfahren. Für die Styrolsynthese, einer der zehn wichtigsten Industrieprozesse, ist die exotherme, oxidative Dehydrogenierung von Ethylbenzol eine elegante und vielversprechende Alternativreaktion, in der Kohlenstoffkatalysatoren bereits ihre Effizienz gezeigt haben. Die begrenzte oxidative Stabilität oberflächenreicher Kohlenstoffe und deren Porosität wirkt sich jedoch negativ auf die katalytische Wirksamkeit aus.

Jedoch scheint die katalytische oxidative Dehydrierung über Kohlenstoffkatalysatoren mit guten Ausbeuten möglich zu sein. Kohlenstoffnanofilamente und Kohlenstoffnanoröhren zeichnen sich hierbei besonders durch ihre hohe Oxidationsstabilität aus. Die verbesserte Leistungsfähigkeit der Kohlenstoffnanofilamente und Kohlenstoffnanoröhren im Vergleich zu anderen Kohlenstoffformen ist ebenfalls auf eine optimierte Verteilung der Basalflächen und der Prismaflächen bei diesen Typen von Nanokohlenstoff zurückzuführen. Rationale Experimentplanung auf Grund einer funktionalen Analyse technischer Katalysatoren mit Hilfe oberflächenphysikalischer Methoden führte in kürzester Zeit gezielt zu einem hochtemperaturstabilen, aktiven und selektiven Katalysator für die oxidative Dehydrierung von Ethylbenzol.

Danksagung

Mein Dank gilt an erster Stelle Herrn Prof. Dr. R. Schlögl, Direktor der Abteilung Anorganische Chemie des Fritz-Haber-Institutes. Weiterer Dank geht an Herrn Dr. G. Mestl, Leiter der Arbeitsgruppe „Heterogene Katalyse“. Beide haben durch Anregungen und konstruktive Kritik sowie die Bereitstellung hervorragender Arbeitsbedingungen sehr zum Gelingen dieser Arbeit beigetragen.

Sämtlichen Mitarbeitern der Arbeitsgruppen “Heterogene Katalyse” und “Elektronenmikroskopie” möchte ich für unzählige anregende Diskussionen and die gute Zusammenarbeit danken. Auch der Arbeitsgruppe “Modellkatalyse” danke ich für motivierende Gespräche. Besonderer Dank geht an Dr. Wolfgang Ranke. Allen Mitarbeitern der Abteilung Anorganische Chemie danke ich für die angenehme, freundliche Arbeitsatmosphäre.

Den stets hilfsbereiten Mitarbeitern der Bibliothek, des Elektroniklabors, des Rechenzentrums und PP&B sei ebenfalls gedankt.

Meiner Familie danke ich für die Unterstützung in allen Lebenslagen und für ihre Geduld.

LEBENSLAUF

11. Februar 1966	Geburt in Novosibirsk, Russland (Staatsangehörigkeit: russisch)
ab 1973	Schulbesuch (bis 1979 Schule 158, dann Schule 102)
1984	Abitur Studium der Geochemie an der Staats Universität Novosibirsk
1990-1996	Studium der Chemie an der Moskau Staats Akademie der Leichtindustrie
1996	Diplomprüfung mit Abschluss
1996-1999	Wissenschaftliche Mitarbeiterin am Boreskov Institut für Katalytischen Chemie der Akademie der Wissenschaften Russland, Novosibirsk
Seit Juli 1999	Doktorandin am Fritz-Haber-Institut der Max-Planck-Gesellschaft, Berlin

PUBLIKATIONSLISTE

1. Maksimova N.I., Krivoruchko O.P., Sidelnikov V.N. Study of liquid and solid products of thermo- and thermocatalytic decomposition of polyethylene, polyvinyl alcohol and polystyrene. Russian J. Appl. Chem. 71 (1998) 1315-1320.

2. Maksimova N.I., Krivoruchko O.P. Study of thermocatalytic decomposition of polyethylene and polyvinyl alcohol in the presence of an unsteady-state Fe-containing catalyst. Chem. Eng. Sci. 54 (1999) 4351-4357.

3. Maksimova N.I., Krivoruchko O.P., Chuvilin A.L., Plyasova L.M. Preparation of nanoscale thin-walled carbon tubules from a polyethylene precursor. Carbon 37 (1999) 1657-1661.

4. Krivoruchko O.P., Maksimova N.I., Zaikovskii V.I., Salanov A.N. Study of multiwalled graphite nanotubes and filaments formation from carbonized products of polyvinyl alcohol via catalytic graphitization at 600-800°C in nitrogen atmosphere. Carbon 38 (2000) 1075-1082.

5. Maksimova N.I., Krivoruchko O.P., Mestl G., Zaikovskii V.I., Chuvilin A.L. Salanov A.N., Burgina E.B. Catalytic synthesis of carbon nanostructures from polymer precursors J. Mol. Catal. A-Chem 158 (2000) 301-307.

6. Maksimova N.I., Roddatis V.V., Mestl G., Ledoux M., Schlögl R. Oxidative dehydrogenation of ethylbenzene to starene over carbonaceous materials. Eurasian ChemTech. J. 2 (2000) 231-236.

7. Mestl G., Maksimova N.I., Keller N., Roddatis V.V., Schlögl R. Kohlenstoffnanofilamente in der heterogenen Katalyse: eine technische Anwendung für neue Kohlenstoffmaterialien? Angew. Chemie 113 (11) (2001) 2122-2125.

8. Maksimova N.I., Mestl G., Schlögl R. Catalytic activity of carbon nanotubes and other carbon materials for oxidative dehydrogenation of ethylbenzene to styrene. Studies in Surface Science and Catalysis 133, Elsevier Science 2001, p. 383-389.

9. Keller N., Maksimova N.I., Roddatis V.V., Schur M., Mestl G., Yu.V. Butenko, Kuznetsov V.V., Schlögl R. Zwiebelförmige Kohlenstoffe als Katalysatoren in der Styrolsynthese durch oxidative Dehydrierung von Ethylbenzol. Angew. Chemie 114 (11) (2002) 1962-1966.